MONTHLY NOTICES

OF THE

ROYAL ASTRONOMICAL SOCIETY

Vol. 114 No. 5 1954

Published and Sold by the
ROYAL ASTRONOMICAL SOCIETY
BURLINGTON HOUSE
LONDON, W. 1

Price Thirteen Shillings and Sixpence

NOTICE TO AUTHORS

1. *Communications.*—Papers must be communicated to the Society by a Fellow. They should be accompanied by a summary at the *beginning* of the paper conveying briefly the content of the paper, and drawing attention to important new information and to the main conclusions. The summary should be intelligible in itself, without reference to the paper, to a reader with some knowledge of the subject; it should not normally exceed 200 words in length. **Authors are requested to submit MSS. in duplicate. These should be typed using double spacing and leaving a margin of not less than one inch on the left-hand side. Corrections to the MSS. should be made in the text and not in the margin.** Unless a paper reaches the Secretaries more than seven days before a Council meeting it will not normally be considered at that meeting. By Council decision, MSS. of accepted papers are retained by the Society for one year after publication; unless their return is then requested by the author, they are destroyed.

2. *Presentation.*—Authors are allowed considerable latitude, but they are requested to follow the general style and arrangement of *Monthly Notices*. References to literature should be given in the standard form, including a date, for printing either as footnotes or in a numbered list at the end of the paper. Each reference should give the **name and initials** of the author cited, irrespective of the occurrence of the name in the text (some latitude being permissible, however, in the case of an author referring to his own work). The following examples indicate the style of reference appropriate for a paper and a book, respectively :—

A. Corlin, *Zs. f. Astrophys.*, **15**, 239, 1938.
H. Jeffreys, *Theory of Probability*, 2nd edn., section 5.45, p. 258, Oxford, 1948.

3. *Notation.*—For technical astronomical terms, authors should conform closely to the recommendations of Commission 3 of the International Astronomical Union (*Trans. I.A.U.*, Vol. VI, p. 345, 1938). Council has decided to adopt the I.A.U. 3-letter abbreviations for constellations where contraction is desirable (Vol. IV, p. 221, 1932). In general matters, authors should follow the recommendations in *Symbols, Signs and Abbreviations* (London : Royal Society, 1951) except where these conflict with I.A.U. practice.

4. *Diagrams.*—**These should be designed to appear upright on the page, drawn about twice the size required in print and prepared for direct photographic reproduction except for the lettering, which should be inserted in pencil. Legends should be given in the manuscript indicating where in the text the figure should appear.** Blocks are retained by the Society for 10 years; unless the author requires them before the end of this period they are then destroyed.

5. *Tables.*—**These should be arranged so that they can be printed upright on the page.**

6. *Proofs.*—Costs of alterations exceeding 5 per cent of composition must be borne by the author. Fellows are warned that such costs have risen sharply in recent years, and it is in their own and the Society's interests to seek the maximum conciseness and simplification of symbols and equations consistent with clarity.

7. *Revised Manuscripts.*—When papers are submitted in revised form it is especially requested that they be accompanied by the original MSS.

Reading of Papers at Meetings

8. When submitting papers authors are requested to indicate whether they will be willing and able to read the paper at the next or some subsequent meeting, and approximately how long they would like to be allotted for speaking.

9. Postcards giving the programme of each meeting are issued some days before the meeting concerned. Fellows wishing to receive such cards whether for Ordinary Meetings or for the Geophysical Discussions or both should notify the Assistant Secretary.

MONTHLY NOTICES

OF THE

ROYAL ASTRONOMICAL SOCIETY

Vol. 114 No. 5

MEETING OF 1954 MAY 14

Dr J. Jackson, President, in the Chair

The election by the Council of the following Fellows was duly confirmed :—

Helmut Arthur Abt, Yerkes Observatory, Williams Bay, Wisconsin, U.S.A. (proposed by S. Chandrasekhar);

Peter John Allender, B.A., B.Sc., Ph.D., 104 Somerset Road, Erdington, Birmingham, 23 (proposed by F. J. Wright);

Raymond Cooper, Royal Fort, The University, Bristol (proposed by C. R. Burch);

Fazli Hussain, Pakistan Military Academy, Kakul, N.W.F.P., Pakistan (proposed by A. Hunter);

Gerald Edward Kron, M.S., Ph.D., Lick Observatory, Mount Hamilton, California, U.S.A. (proposed by J. Stebbins);

Edward Ronald Niblett, M.A., Department of Geodesy and Geophysics, Downing Place, Cambridge (proposed by S. K. Runcorn);

John Beverley Oke, Ph.D., David Dunlap Observatory, Richmond Hill, Ontario, Canada (proposed by L. Spitzer);

Harry Seddon, B.Sc., Royal Observatory, Edinburgh (proposed by W. M. H. Greaves);

Charles Donald Shane, Ph.D., Lick Observatory, Mount Hamilton, California (proposed by H. M. Jeffers);

David Colin Smith, Royal Greenwich Observatory, Abinger Common, Dorking, Surrey (proposed by H. Spencer Jones); and

Henry Tompkins, 6 Crescent Road, Crouch End, London, N.8 (proposed by P. A. Moore).

Ninety-four presents were announced as having been received since the last meeting, including :—

H. Alan Lloyd, *Horology and meteorology* (presented by the author); and

V. A. Hughes and E. E. Treadwell, *A form of equatorial drive for controlling an altazimuth mounted radio-telescope* (presented by the Central Radio Bureau, Ministry of Supply).

The President gave a brief address on the award of the Gold Medal, after which the Medal was handed to Mr Chester E. Beaman, Chief of Protocol, United States Embassy, for transmission to Dr Walter Baade, to whom it had

been awarded for his observational work on galactic and extra-galactic objects. The President said :

" Before proceeding to the reading of papers it is my pleasure to welcome here today Mr Chester Beaman from the United States Embassy. He has come to receive on behalf of Dr Walter Baade, of the Mount Wilson and Palomar Observatories, the Gold Medal of the Society awarded to him. At the Anniversary Meeting in February an Address was given on Dr Baade's work (see p. 370), and so it is unnecessary today for me to say more than that the award was for outstanding researches on galactic and extra-galactic objects. But for Mr Beaman's information I would like to say that the Gold Medal is the highest award of the Society. It is usually bestowed once a year and in selecting its medallist the Council is not restricted by nationality or in any other way. It is no new thing for the Medal to be awarded to an astronomer working in California. There you have excellent atmospheric conditions for making observations, and there you have erected magnificent telescopes. But the Medal is not awarded to Dr Baade because of the superb conditions under which he works but for the superb use he has made of his opportunities—opportunities which were offered to him as a result of his earlier work. Mr Beaman, in forwarding this Medal to Dr Baade we would like you to convey to him not only our admiration for the work he has already done but our hope that he shall be able to continue and extend it with the great 200-inch Hale telescope on Mount Palomar."

MEETING OF 1954 OCTOBER 8

Dr J. Jackson, President, in the Chair

The election by the Council of the following Fellows was duly confirmed :—

William Ross Hossack, M.A., Ph.D., David Dunlap Observatory, Richmond Hill, Ontario, Canada (proposed by C. A. Chant); and

Patrick Aloysius O'Brien, M.Sc., Ph.D., Department of Physics, University of Natal, Durban, South Africa (proposed by G. Burbidge).

Two hundred and fifty-one presents were announced as having been received since the last meeting, including :—

H. Alfvén, *On the origin of the solar system* (presented by the Association of Special Libraries and Information Bureaux);

G. van den Bergh, *Eclipses in the second millennium B.C. and how to compute them in a few minutes* (presented by the author);

N. O. Bergquist, *The Moon puzzle* (presented by C. Hamburgers Bogtrykkeri);

F. Chemla-Lamech, *Carte topographique de la Lune* (presented by the executors of the late Mr M. E. J. Gheury de Bray);

S. G. Hacker, *Arithmetical view-points—an introduction to mathematical thinking* (presented by the author);

S. G. Hacker, *Theoretical astrophysics. Parts I and II* (presented by the author);

International Union of Geodesy and Geophysics, *Photographic atlas of auroral forms* (bequeathed by the late R. L. T. Clarkson); and

L. Rudaux, *Sur les autres mondes* (presented by the executors of the late Mr M. E. J. Gheury de Bray).

PHOTOELECTRIC INVESTIGATIONS OF SOLAR CORPUSCULAR RADIATION, II

M. J. Smyth

(Communicated by the Astronomer Royal for Scotland)

(Received 1954 August 13)

Summary

Photoelectric measurements of the solar *K*-line in 1951 and 1953, with improved equipment, confirm the conclusion of a previous paper that absorption in the violet wing, corresponding to particles approaching with speeds between 750–1150 km/sec, does not exceed one-half per cent at any time following moderately intense flares. There is also little evidence of absorption of this magnitude associated with sequences of recurrent geomagnetic storms.

---

1. *Introduction.*—A previous paper (**1**)* gave an account of some observations in 1949–50 intended to detect or set an upper limit to anomalous absorption in the violet wing of the solar *K*-line due to approaching corpuscles associated with flares. These observations failed to reveal in most cases any absorption exceeding 0·5 per cent corresponding to particles with velocities in the range 650–1500 km/sec.

Further series of observations have been made at the Royal Observatory, Edinburgh, during 1951 and again during 1953, with an improved apparatus. As flare activity declined, 27-day sequences of geomagnetic disturbance became prominent, and it was hoped that improved instrumental stability would make it possible to investigate also any absorption effect associated with recurrent magnetic sequences. The solar source of these sequences is still obscure, despite many inconclusive attempts to correlate them with various solar features (**2**). In the absence of evidence to the contrary, however, persistent corpuscular streams from unidentified "M-regions" are usually regarded as responsible for recurrent geomagnetic activity. It might then conceivably be possible to detect a recurrent absorption effect.

2. *Apparatus.*—A six-inch object-glass by Steinheil provided a solar image 21 mm in diameter. For the 1951 observations a coelostat was used, so that the spectrograph slit, restricted to 4 mm in length, fell centrally and roughly in a North–South orientation on the non-rotating 21 mm solar image. In 1953, the coelostat being required for other purposes, the equipment was transferred to a site using a siderostat, so that the image now rotated slowly during the course of the day. This was of no consequence in looking for a corpuscular cloud or stream which might be expected to cover the Sun's disk.

With a solar image of this size, conduction by the slit jaws was sufficient to prevent overheating, and no heat filter was required.

* Referred to as Paper I in the text.

The Cooke spectrograph was of conventional design, with separate collimator and camera, and an 80 mm × 50 mm aluminized plane grating, forming a first-order spectrum with dispersion 9·7 angstroms/mm. In the focal plane was a set of fixed exit-slits, as indicated in Fig. 1 and described later. The slits were all cut on a Dumoulin dividing engine in the emulsion of a single fully fogged and developed process plate, so that stability of their dimensions and relative positions was assured. Light from any one of the slits *V*, *X*, *Y*, *R*, chosen by means of shutters, passed through a field lens to a selected 931-A photomultiplier. A weak prism deflected the light from the "Hg" slit, after passing through the field lens, to a second 931-A.

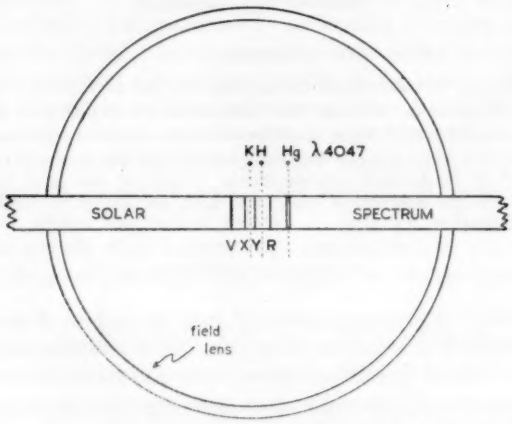

FIG. 1.—*Exit-slits in focal plane of spectrograph. X and Y lie in the wings of the K-line, V and R determine the continuum, while Hg is centred on the mercury line λ 4047 as wave-length reference and also serves for compensation of seeing in the solar spectrum.*

The photomultipliers were fed from a divider network in the usual manner, voltage being obtained initially from dry batteries and later from a stabilized mains power unit. The photocurrents went to two calibrated taut-suspension galvanometers, side by side and indicating on the same scale, so that they could be read simultaneously. Thus with each reading for one of the *V*, *X*, *Y*, *R* slits a simultaneous reading of "Hg" (in the continuous spectrum) was obtained. This enabled the intensity ratios *V*:*X*:*Y*:*R* to be determined with great reduction in the error arising from changes in sky transparency, and an estimated accuracy of $0^{m}\cdot003$ (0·3 per cent) for a single ratio was usually attained. In practice, each "observation" involved the average of three or four readings for each ratio.

3. *Wave-length adjustment and reduction of observations.*—In the Cambridge apparatus (Paper I) the appropriate wave-lengths were brought on to the exit-slits by using the solar *K*-line itself as reference, adjusting to equality a further pair of exit-slits placed symmetrically close to the centre of the line. It was found that this method of wave-length adjustment produced a small systematic shift depending on the "slope" of the spectrum and the consequent distortion of the *K*-line profile. So for the present observations a laboratory wave-length reference was used. The slits were arranged so that *V*, *X*, *Y*, *R* fell in their correct positions when the line λ 4046·7 of a mercury lamp was centred on the double "Hg" slit. This was really a single slit with a central opaque bar corresponding to the width (0·15 mm) of the primary slit. The line was correctly centred when its image fell

on the opaque bar and the only light passing was due to ghosts, scattered light, etc. Very sharp "tuning" was possible by obtaining the minimum deflection on the second galvanometer by means of the wave-length adjustment.

This adjustment was made for each set of observations, so that the main exit-slits were always set on their correct wave-lengths, determined approximately by measurement as follows:—

V: λ 3870·6 to λ 3880·7
X: λ 3918·8 to λ 3924·0
Y: λ 3942·8 to λ 3948·0
R: λ 3990·1 to λ 3993·1

The primary slit-width of about 0·15 mm corresponded to 1·9 angstroms in the focal plane.

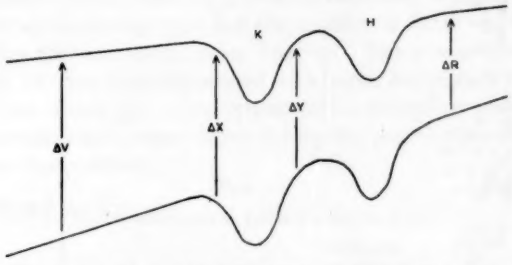

FIG. 2.—*Positions of exit-slits relative to the H and K-lines, showing effect of variation of "slope" of spectrum with solar altitude.*

Fig. 2 shows the positions of these slits relative to the H and K profiles. V and R, placed symmetrically about the K-line, served to determine the continuum; X corresponded to absorption by approaching Ca II (K) ions with velocities between 750–1150 km/sec, the expected range of particle velocities, while Y, similarly placed in the red wing, acted as a control. It will be noted that Y corresponded also to Ca II (H) ions with approach velocities between 1500–1900 km/sec, but we do not expect such high particle velocities to be associated with minor flares or M-regions. The different widths of the slits were chosen to give approximately equal photomultiplier responses.

In estimating possible extra absorption at X or Y it was now necessary to allow for the effect of changing atmospheric extinction. Fig. 2 illustrates schematically the changes in intensity ΔV, ΔX, ΔY, ΔR corresponding to a change of solar altitude. For each observation, using a logarithmic calibration table for the galvanometer readings, the quantities* $\frac{5}{2}\log(X/R)$, $\frac{5}{2}\log(Y/R)$, $\frac{5}{2}\log(V/R)$ were formed. In Paper I it was shown that as the solar altitude varies the changes in these observed quantities should be proportional, provided that the solar spectrum itself is undisturbed. Therefore linear formulae were assumed:

$$\tfrac{5}{2}\log(X/R) = A + B\{\tfrac{5}{2}\log(V/R)\},$$
$$\tfrac{5}{2}\log(Y/R) = C + D\{\tfrac{5}{2}\log(V/R)\}.$$

The values of the constants A, B, C, D were determined by the method of least squares, using a whole year's observations in each case. This procedure was preferred to using theoretical values for B, D derived from the Rayleigh λ^{-4}

* All logarithms are to base 10.

formula as in Paper I, as it involved no assumption about the "effective" wavelengths of the wide slits. "Undisturbed" values of $\frac{5}{2}\log(X/R)$ and $\frac{5}{2}\log(Y/R)$ were calculated from the above formulae for each observed value of $\frac{5}{2}\log(V/R)$, and subtracted from the observed values of $\frac{5}{2}\log(X/R)$ and $\frac{5}{2}\log(Y/R)$. Any significant negative X- or Y-residual would then indicate excess absorption (in magnitudes) in the corresponding wing of the K-line.

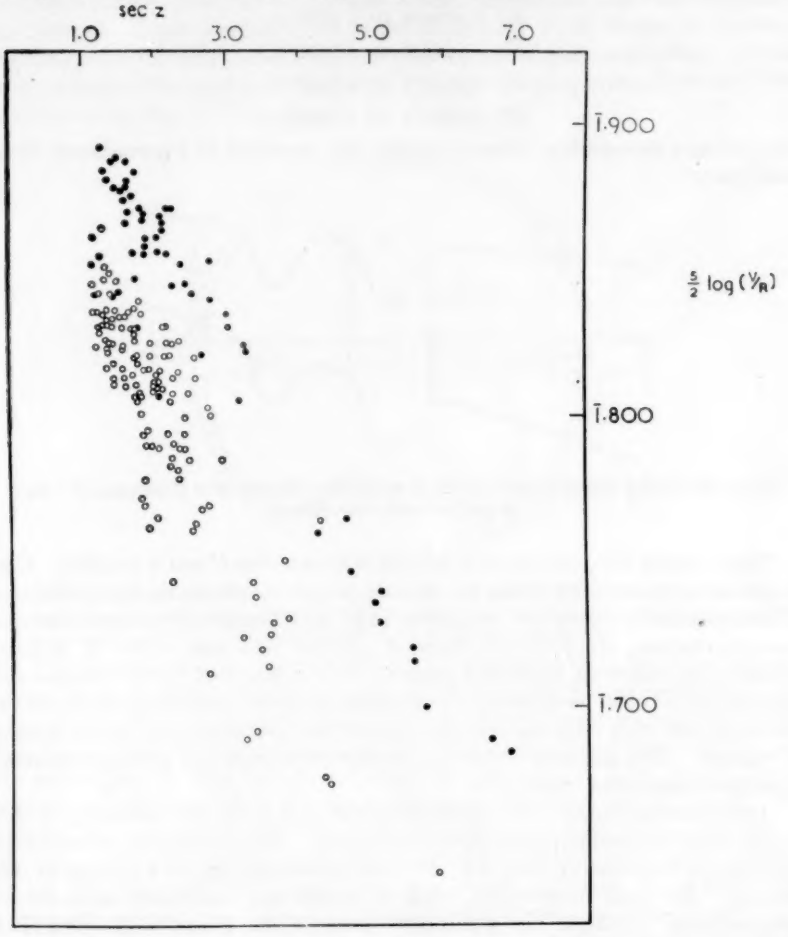

FIG. 3.—*Correlation of atmospheric reddening with sec z for Sun, 1953 observations. V and R are continuous-spectrum intensities at two points about 60 angstroms to the violet and red respectively of the K-line, so that lower values of* $\frac{5}{2}\log(V/R)$ *indicate increased reddening.*

Open circles : observations before June 21.
Filled circles : observations after June 21.

As a matter of interest, a plot was made (Fig. 3) of the relation of $\frac{5}{2}\log(V/R)$, which is a measure of the local reddening of the continuous spectrum, to the secant of the Sun's zenith distance. It will be seen that there is considerable scatter, showing that zenith distance is not a sufficient criterion for atmospheric reddening. Further, the scatter is greater and the reddening generally stronger

for the observations before midsummer (open circles, Fig. 3). This seems to be an indication of the greater water droplet content of the atmosphere during spring and early summer which is a familiar feature of the Edinburgh climate.

Before discussing the results, comment should be made on the use of a laboratory source as wave-length standard. The geocentric radial velocity of the Sun has the maximum absolute value $e(1-e^2)^{-1/2}$ times the mean orbital velocity, or 0·50 km/sec, attained in April and October. Also the Earth's horizontal rotation velocity at the latitude of Edinburgh is 0·26 km/sec. Hence the maximum relative velocity between laboratory source and Sun, at sunset in April or sunrise in October, is $\pm 0{\cdot}76$ km/sec, corresponding to a Doppler shift of 0·01 angstrom, or 1 micron in the focal plane. This would scarcely be detectable, and is not revealed by any systematic trend in the readings. Thus the use of a terrestrial wave-length standard is justified in this application.

4. *Observations following flares, 1951.*—After declining in the latter half of 1950, solar activity rose again during 1951, but the number of flares was of course much lower than during the maximum years 1947–9. There was considerable geomagnetic activity, in some cases associated with flares, but mainly of the recurrent type with indefinite onset (3). Few opportunities therefore arose for detecting corpuscular emission from intense flares during the period 1951 June–December covered by these observations.

TABLE I

K-line observations following flares, 1951

Date	Class	r/R	Interval	Delayed geomagnetic effect	Observed absorption
1951					
June $18^d\,08^h\,28^m$	1	0·22(E)	?	SC June $18^d\,23^h\,14^m$	No absorption at 14^h.
June $19^d\,13^h\,05^m$	2	0·31(W)	...	...	Absorption $<0{\cdot}6$ per cent 5^m after flare, zero after 1^h (see Fig. 4).
June $22^d\,10^h\,40^m$	1	0·27(E)	...	...	Absorption $<0{\cdot}3$ per cent 35^m after first flare, $<0{\cdot}5$ per cent 2^h after second flare.
$13^h\,23^m$	1	0·89(W)	...	...	
Sept. $3^d\,13^h\,15^m$	3	0·62(E)	55^h	SC Sept. $5^d\,20^h\,45^m$	No absorption on Sept. 4.
Sept. $7^d\,10^h\,54^m$	1–2	0·36(W)	...	...	No absorption $5\frac{1}{2}^h$ after flare.
Sept. $14^d\,13^h\,43^m$	2	0·55(E)	...	...	Slightly negative readings *preceding* flare !
Sept. $15^d\,15^h\,10^m$	2+	0·12(W)	...	...	Absorption $<0{\cdot}6$ per cent 35^m after flare, zero after 2^h (see Fig. 4).
Oct. $9^d\,08^h\,48^m$	2	0·93(E)	...	...	Absorption $<0{\cdot}8$ per cent 50^m after flare, zero within 2^h (see Fig. 4).
Oct. $17^d\,11^h\,26^m$	1	0·78(W)	...	...	No absorption between 2^h and 4^h after flare.

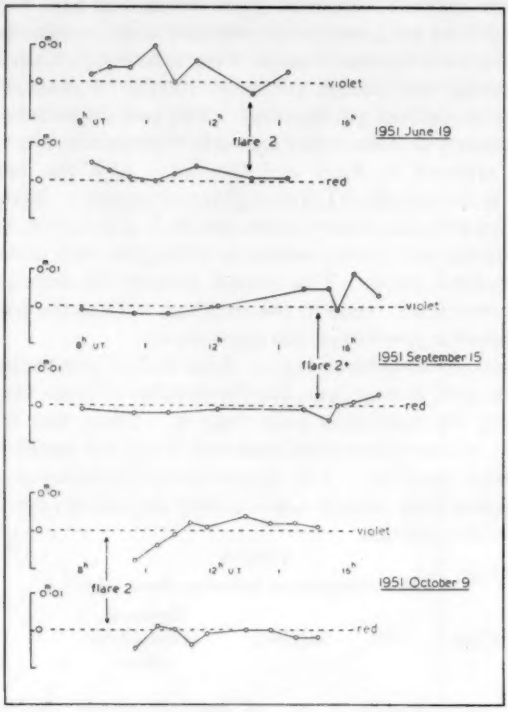

FIG. 4.—*K-line wing residuals following flares, 1951 (negative indicates absorption).*

TABLE

27-day analysis of geomagnetism and K-line residuals for six solar rotations, 1951. For the second gives the daily mean violet-wing residual X and the third the daily mean red-wing

1951 June 15	11	8	14	16	13	4	6	3	2	2	14	6
	...	...	...	+2	+3	+13	...	+5	+7	...	+2	...
	...	...	...	+3	+2	+1	...	0	+2	...	+1	...
July 12	3	3	2	9	10	11	11	6	6	3	12	11
	...	...	...	...	...	...	...	...	...	...	...	...
	...	...	...	...	...	...	...	...	...	...	...	...
Aug. 8	2	6	5	8	9	15	6	10	13	10	2	6
	...	...	−4	...	...	...	...	...	...	...	...	...
	...	...	−2	...	...	...	...	...	...	...	...	...
Sept. 4	3	8	10	8	6	9	12	13	14	13	11	13
	+2	−1	+2	+10	+8	...	...	...	...	...	−3	+2
	0	−2	+2	+2	+1	...	...	...	...	...	−1	−1
Oct. 1	3	7	4	2	2	0	15	16	12	14	9	7
	...	...	...	...	−5	−3	+2	+1	0	...	−4	−8
	...	...	...	...	−2	+2	0	−2	−1	...	0	+1
Oct. 28	19	6	5	0	3	8	12	10	8	11	10	4
	...	...	−2	...	−8	...	−6	...	...	...	...	...
	...	...	+2	...	−3	...	−4	...	...	...	...	...
Averages	6·8	6·3	6·7	7·2	7·2	7·8	10·3	9·8	9·0	9·0	9·7	7·8
	+2	−1	−1	+6	0	+5	−2	+3	+3	...	−2	−3
	0	−2	+1	+2	0	+1	−2	−1	0	...	0	0

A few flares* followed by *K*-line observations are listed in Table I, together with the distance r/R of the flare from the disk centre, any subsequent geomagnetic disturbance†, and the results of the *K*-line observations. Only one flare of importance 3 occurred during the period, and observations at Edinburgh were unfortunately not possible until the following day. Flares of importance 1 are included in the table only when confirmed by ionospheric effects.

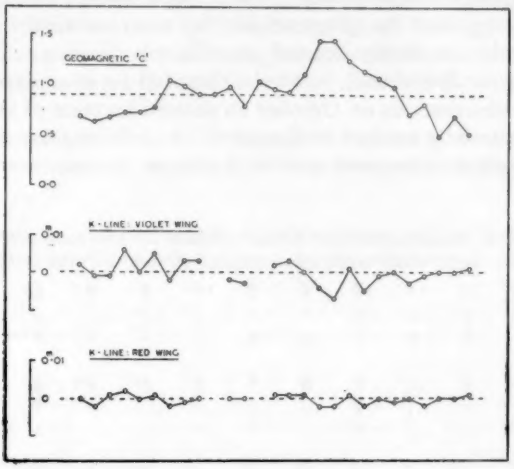

FIG. 5.—*Superposed-epoch analysis of geomagnetic character-figures and K-line wing residuals (negative indicating absorption) for six solar rotations,* 1951 (*see also Table II*).

II

each rotation the first line gives the magnetic character-figures (with decimal point omitted), residual Y (in units of $0^{m}{\cdot}001$, *negative figure denoting absorption).*

8	8	7	6	12	17	12	10	6	7	4	5	8	4	4
...	+4	+6	...	...	...	+1	...	...	...	...	...	...	+6	...
...	+1	+1	...	...	...	+1	...	...	...	...	...	...	0	...
3	8	13	11	13	7	8	14	15	11	5	8	7	6	5
...	...	...	...	...	...	...	...	...	...	...	...	...	...	...
...	...	...	...	...	...	...	...	...	...	...	...	...	...	...
13	16	13	11	10	14	12	12	10	8	6	9	3	1	3
...	+5	+3	+2	...	...	...	...	...	+4	...	...	...	...	+1
...	+1	0	+3	...	...	...	...	...	0	...	...	...	...	+1
17	15	11	17	17	17	16	15	13	18	16	16	6	11	4
...	−3	0	−3	−5	−7	...	...	−1	...	−3	−1	−1	−2	...
...	0	+1	0	−2	−2	...	...	0	...	0	−2	0	+1	...
12	10	7	10	17	14	15	10	8	10	7	1	0	10	5
...	...	...	...	−3	...	...	−5	...	−3	...	...	0	−3	...
...	...	...	...	−3	...	...	−2	...	−2	...	...	0	−1	...
8	0	4	11	16	16	11	6	11	4	4	9	5	9	9
...	...	...	...	...	...	...	...	...	...	...	...	...	...	...
...	...	...	...	...	...	...	...	...	...	...	...	...	...	...
10·2	9·5	9·2	11·0	14·2	14·2	12·3	11·2	10·5	9·7	7·0	8·0	4·8	6·8	5·0
...	+2	+3	0	−4	−7	+1	−5	−1	0	−3	−1	0	0	+1
...	+1	+1	+1	−2	−2	+1	−2	0	−1	0	−2	0	0	+1

* Flare data from the *Quarterly Bulletin of Solar Activity.*

† Geomagnetic data from the *Journal of Geophysical Research.*

It will be seen that there is little evidence of absorption. In Fig. 4, the detailed graphs for the three most important cases where observations were obtained for some time following flares, the violet-wing residuals X do perhaps show some tendency towards low values for an hour or so after the flares, but the effect is not strongly marked and is certainly less than one per cent. The red-wing residuals Y show somewhat less variability. None of these flares preceded a magnetic storm.

The year's greatest magnetic storm, that of 1951 October 28 with range of 545γ in H at Abinger (**3**), had the characteristic SC onset associated with solar flare origin, and stands completely isolated on a Bartels diagram. Nevertheless no flare or ionospheric disturbance had been recorded for nine days preceding the storm. K-line observations on October 26 showed no trace of absorption.

In 1953 solar activity reached minimum values, with long sequences of spotless days. Flares were so infrequent and small that no purpose would be served by

TABLE

27-day analysis of geomagnetism and K-line residuals for nine solar rotations, 1953. For the second gives the daily mean violet-wing residual X and the third the daily mean red-

1953 Apr. 21	13	11	10	5	7	10	5	2	5	6	2	1
	+4	+4	+5	+6	+7	...	...	...	+4	+2	...	+1
	−6	−5	−7	−4	−5	...	...	...	−8	−10	...	−6
May 18	9	11	9	6	8	3	3	2	4	11	4	2
	...	...	+7	...	+7	...	...	...	+8	+2	...	0
	...	...	−8	...	−8	...	...	...	−3	−4	...	−3
June 14	5	2	2	5	2	2	8	7	8	0	4	1
	...	...	...	...	...	+7	...	...	+3	...	+2	0
	...	...	...	...	...	+4	...	...	+1	...	+3	+3
July 11	2	6	8	6	8	0	1	2	2	4	2	4
	...	...	...	...	...	...	...	...	...	...	...	...
	...	...	...	...	...	...	...	...	...	...	...	...
Aug. 7	6	3	10	10	10	14	12	8	6	6	1	2
	...	−1	...	−2	−3	...	...	...	...	...	...	−3
	...	+4	...	+3	+6	...	...	...	...	...	...	+4
Sept. 3	15	17	11	8	8	5	3	6	9	6	5	0
	...	...	...	...	+1	−2	−2	−4	...	−4	−4	−6
	...	...	...	...	+8	+8	+10	+11	...	+6	+8	+7
Sept. 30	5	8	4	3	2	0	2	7	7	5	6	5
	...	...	0	...	−4	−11	...	...	...	...	...	...
	...	...	+11	...	+12	+9	...	...	...	...	...	...
Oct. 27	8	4	6	3	2	4	0	2	1	8	3	2
	−3	0	−6	...	...	...	−4	...	0	...	...	...
	+7	+6	+10	...	...	...	+8	...	+13	...	...	...
Nov. 23	13	7	7	2	3	0	1	0	0	0	2	6
	−2	...	+3	...	...	...	...	...	...	...	...	...
	+5	...	+6	...	...	...	...	...	...	...	...	...
Average	8·4	7·7	7·4	5·3	5·6	4·2	3·9	4·0	4·7	5·1	3·2	2·5
	0	+1	+2	+2	+2	−2	−3	−4	+4	0	−1	−2
	+2	+2	+2	0	+3	+7	+9	+11	+1	−3	+5	+1

attempting to correlate them with the present observations. Magnetic storms were small and of the recurrent variety (4).

5. *Analysis of recurrence tendencies*, 1951.—Since much of the magnetic disturbance during 1951 was of the recurrent type, but still presumably of corpuscular origin, it was important to look for any recurrence tendencies in the observed *K*-line residuals. It had been noted that the *X* (violet-wing) residuals showed rather greater variability, both during the day and from day to day, than did those for the red wing. This was most marked during 1951 September and October, a period of numerous prolonged and overlapping magnetic storms with indefinite onset, but there was no clear relationship between the magnetic activity and these variations.

The daily means of the *X* and *Y* residuals were used in a superposed-epoch analysis in order to detect any 27-day recurrence tendency. Instrumental

III

each rotation the first line gives the magnetic character-figures (with decimal point omitted), wing residual Y (in units of $0^{m}\cdot001$, *negative figure denoting absorption).*

1	1	10	15	11	11	10	6	3	0	0	1	15	18	12
...	+5	+2	+3	+2	+2	−1	...	...	...	...	...	...	+3	...
...	−11	−13	−11	−9	−7	−8	...	...	...	...	...	...	−10	...
2	4	1	15	14	10	10	7	4	1	1	6	5	9	8
...	...	...	...	...	...	+6	+2	+7	+4	+8	...	+3	...	...
...	...	...	...	...	...	−2	−3	−7	−10	−7	...	−8	...	...
0	2	2	15	14	11	11	8	8	6	7	10	8	6	2
...	...	...	...	...	+3	...	+7	...	...	...	...	...	...	...
...	...	...	...	...	+5	...	+11	...	...	...	...	...	...	...
15	8	6	10	14	12	12	10	8	8	6	4	5	4	4
...	...	...	...	...	−5	...	...	−6	−5	...	−4	...	...	−2
...	...	...	...	...	+3	...	...	+4	+1	...	+3	...	...	+5
1	0	0	1	16	16	13	11	15	13	14	15	13	8	9
...	...	...	−4	...	−2	−4	−5	...	0	−8	...	...	−5	−3
...	...	...	+2	...	+1	+7	+6	...	+6	+5	...	...	+2	+8
13	10	7	10	18	14	12	11	14	12	8	5	9	3	2
...	...	...	...	+3	...	...	+3	...	...	...	...	...	−3	0
..	...	...	...	+12	...	...	+15	...	...	...	...	...	+17	+17
2	1	0	16	16	14	15	16	14	10	9	6	7	3	1
...	...	−2	...	...	...	...	−5	...	...	...	...	...	...	...
...	...	+5	...	...	...	...	+4	...	...	...	...	...	...	...
3	0	0	4	11	16	15	16	14	11	9	15	12	7	1
...	...	...	...	...	...	...	...	...	...	...	...	...	...	...
...	...	...	...	...	...	...	...	...	...	...	...	...	...	...
3	4	2	4	6	3	13	10	7	2	4	2	4	2	3
−1	...	...	...	+5	...	...	...	...	...	+1	+6	...	...	...
+6	...	...	...	+8	...	...	...	...	...	+8	+5	...	...	...
4·4	3·3	3·1	10·0	13·3	11·9	12·3	10·6	9·7	7·0	6·4	7·1	8·7	6·7	4·7
−1	+5	0	0	+3	0	0	0	0	0	0	+1	+3	−2	−2
+6	−11	−4	−4	+4	0	−1	+7	−1	−1	+2	+4	−8	+3	+10

stability was important in assessing long-term variations; in the present method of spectrophotometry the principal cause of drift is gradual changes in the transmission of the exit-slits due to the accumulation of dust. It was satisfactory that the daily means of the Y (red-wing) residuals in 1951 were constant within 0·4 per cent for five months. The X (violet-wing) residuals showed greater variability and a systematic downward trend not exceeding one per cent over the same period. This would not be sufficient to obscure any genuine 27-day periodicity.

Table II gives details of daily mean residuals and magnetic character-figures for six solar rotations in the latter half of 1951. The averages, represented graphically in Fig. 5, show a broad peak in the character-figures, indicating a rather poorly defined M-sequence. The average red-wing residuals do not depart significantly from zero. Those for the violet wing show a slight drop a day or two *after* the peak of the magnetic disturbances. This cannot be regarded as significant. The smoothing of the averages for the K-line residuals is evidently poorer than for the magnetic character-figures, since the observations represent only 48 out of the possible 162 days. Thus an upper limit of 0·5 per cent can certainly be set for the average absorption, associated with this M-sequence, by Ca II ions with approach velocities between 750 and 1150 km/sec.

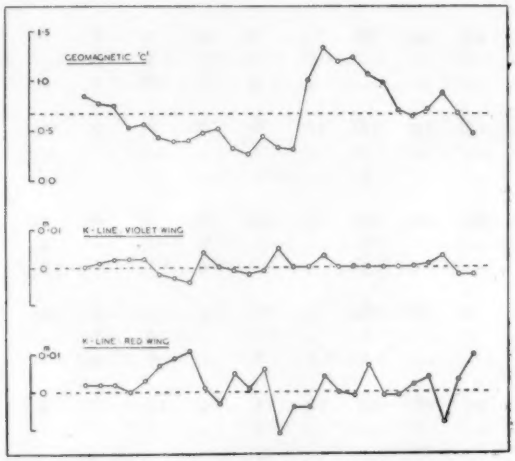

FIG. 6.—*Superposed-epoch analysis of geomagnetic character-figures and K-line wing residuals (negative indicating absorption) for nine solar rotations,* 1953 (*see also Table III*).

6. *Analysis of recurrence tendencies,* 1953.—In 1953 the very low sunspot and flare activity were accompanied by two pronounced M-sequences. The second of these, persisting for nine rotations from May until December, was well covered by K-line observations. A similar superposed-epoch analysis, of which details appear in Table III, shows a pronounced peak in the magnetic character-figures. It will be seen that in 1953 the red-wing residuals showed considerably greater variability than those for the violet wing. This can scarcely be regarded as other than accidental, but is nevertheless surprising. The averaged curves (Fig. 6) show no relation to the magnetic curve. Again the K-line residuals are less fully smoothed since they represent only 76 out of the possible 243 days. There is evidently no trace of absorption in the violet wing connected with the M-sequence.

7. *Conclusion.*—Flare observations presented in this paper support the conclusion of Paper I, that there is no detectable absorption of as much as one-half per cent in the violet wing of the *K*-line following moderately intense flares. This result, as was pointed out, is not in conflict with the minimum particle density required for the generation of a magnetic storm.

The most favourable combination of circumstances, a long series of observations following an intense central flare producing a great magnetic storm, has however not arisen during the course of the investigations described in these papers. A spectrophotometric technique has been developed which may be capable of detecting a borderline effect in such favourable circumstances, and should be worth applying at the next sunspot maximum. It may be that corpuscular absorption rises above the threshold of observability only for a limited time and over a limited area of the Sun's disk, and some experiments have been made with a disk-scanning device for detecting localized *K*-line asymmetry.

It now appears that there is little hope of detecting absorption associated with M-regions while spectrophotometric errors remain of the order of a few thousandths of a magnitude. This is not surprising, since it is well known that recurrent magnetic storms are, as a class, of lower intensity than those associated with flares. It would be desirable in any further investigation to check the exit-slit transmissions frequently, and to attempt the most precise wave-length setting, probably involving temperature control of the spectrograph, in order to ensure optical and mechanical stability consistent with the high precision of the photomultipliers. In addition, the present observations have investigated absorption only by particles in the velocity range 750–1150 km/sec. It has been suggested (**5**) that "slow" corpuscular radiation in the range 350–600 km/sec is responsible for M-sequences, and this would involve absorption closer to the centre of the *K*-line. In any case a more complete survey of variations in the profile will eventually be desirable.

8. *Acknowledgments.*—The paper contains some material from a thesis for which the degree of Doctor of Philosophy was awarded by the University of Cambridge. I am grateful to Professor W. M. H. Greaves who supervised this work. Acknowledgment is made to the Director of the Cambridge Observatories for the loan of equipment and to the Moray Endowment of the University of Edinburgh for an equipment grant.

Royal Observatory,
Edinburgh :
1954 *July* 24.

References

(1) M. J. Smyth, *M.N.*, **114**, 137, 1954.
(2) M. J. Smyth, article in *Vistas in Astronomy*, Vol. 2, London, 1955.
(3) H. W. Newton and H. F. Finch, *The Observatory*, **72**, 44, 1952.
(4) H. W. Newton and H. F. Finch, *The Observatory*, **74**, 44, 1954.
(5) K. O. Kiepenheuer, *J. Geophys. Res.*, **57**, 113, 1952.

RELAXATION OF STELLAR VELOCITIES

R. v. d. R. Woolley

(Received 1954 June 17)

Summary

The stability of truncated Maxwellian velocity distributions is examined by calculating the fraction of stellar encounters in which the exchange of energy lies within a given interval.

1. In a previous paper* the writer examined the distribution of stars in a globular cluster, supposing the velocity distribution to be "truncated Maxwellian", that is to say a Maxwellian distribution with all velocities in excess of a certain value absent. This paper attempts to enquire whether such a distribution, if set up, would have a long life without substantial change.

The exchange of energy between two stars in a gravitational encounter may be calculated in a well-known manner. The calculation is repeated here because the result is wanted in a particular form. There is no exchange of energy when the velocities are measured relative to the centre of gravity of the star pair, but when that centre of gravity moves relative to an origin (such as the centre of a globular cluster) there is, in general, an exchange of energy.

Consider an encounter between two particles of which the first has mass m_c and scalar velocity c, while the second (the field star) has mass m_x and scalar velocity x. Let the velocity of the centre of gravity be g and the initial relative velocity between the stars be v. Further, let $\mu_c = m_c/(m_c+m_x)$ and $\mu_x = m_x/(m_c+m_x)$. Fig. 1 represents the initial velocities. If the angle XOC is θ and the angle OGC is β we have

$$\left.\begin{aligned} 2gv\sin\beta &= 2xc\sin\theta, \\ 2gv\cos\beta &= x^2(1+\mu_x-\mu_c)-c^2(1+\mu_c-\mu_x)+2xc(\mu_c-\mu_x)\cos\theta. \end{aligned}\right\} \qquad (1.1)$$

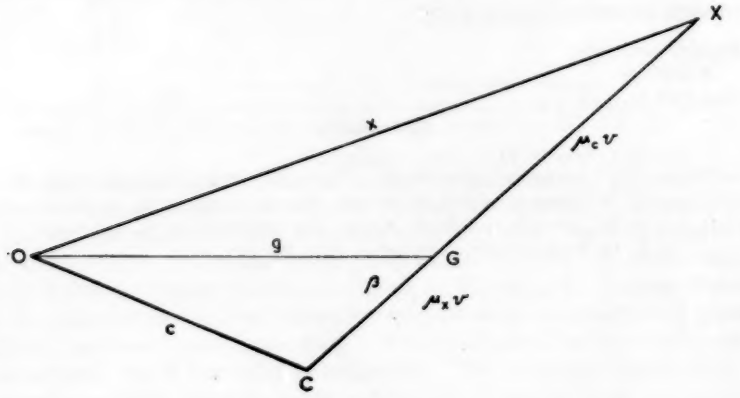

FIG. 1.

* *M.N.*, **114**, 191, 1954.

The plane of Fig. 1 is the plane containing the two vector motions relative to the origin and is not in general the "orbital" plane which is the plane containing the two stars and their relative motion. Fig. 2 represents the celestial sphere on which the great circle C′XBC is the orbital plane and the great circle XOC is the plane of Fig. 1. The two points C and X, 180° apart, are the initial velocities of the stars relative to the motion of the centre of gravity and the point O is the direction of motion of the centre of the cluster relative to the centre of gravity of the star pair. The effect of the encounter is to move the velocity of the C star

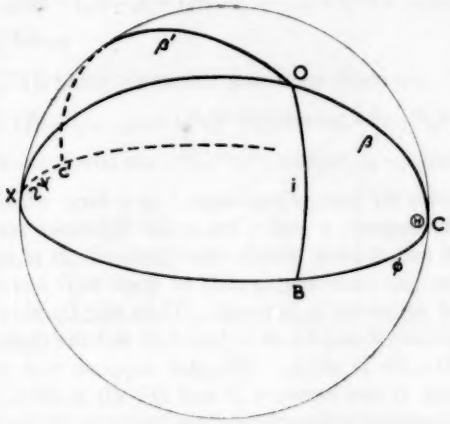

FIG. 2.

in the orbital plane from C to C′, where $XC' = 2\psi$, the angle between the asymptotes of the hyperbolic orbit.

We have $OC = \beta$, as in Fig. 1. Let $OC' = \beta'$. Now

$$c^2 = g^2 + \mu_x{}^2 v^2 - 2\mu_x g v \cos\beta,$$

and if c' is the scalar velocity after the encounter,

$$c'^2 = g^2 + \mu^2{}_x v^2 - 2\mu_x g v \cos\beta',$$

since the scalar values of g and v are the same after the encounter as before it. Hence if the gain of energy by the C star is ΔE,

$$\Delta E = \tfrac{1}{2} m_c (c'^2 - c^2) = m_c \mu_x g v (\cos\beta' - \cos\beta). \qquad (1.2)$$

Now let Θ be the angle OCB in Fig. 2 and drop OB perpendicular to XBC. Let $OB = i$ and $BC = \phi$. Then

$$\left.\begin{aligned} \cos\beta &= \cos\phi \cos i, \\ \cos\beta' &= \cos(\pi + 2\psi - \phi)\cos i, \\ \sin\beta\cos\Theta &= \sin\phi\cos i. \end{aligned}\right\} \qquad (1.3)$$

Combining (1.1), (1.2) and (1.3) we get

$$\Delta E = m_c\mu_c[\cos^2\psi\{x^2(1+\mu_x-\mu_c) - c^2(1+\mu_c-\mu_x) + 2xc(\mu_c-\mu_x)\cos\theta\} + \cos\psi\sin\psi\,.\,2xc\sin\theta\cos\Theta]. \qquad (1.4)$$

Now it can be shown* that if D is the distance at which the stars would pass if there was no deflection, and if Γ is the constant of gravitation,

$$\cos^2\psi = \{1 + D^2v^4/\Gamma^2(m_c+m_x)^2\}^{-1},$$

$$\sin\psi\cos\psi = \{Dv^2/\Gamma(m_c+m_x)\}/\{1 + D^2v^4/\Gamma^2(m_c+m_x)^2\}.$$

Write

$$D^2v^4/\Gamma^2(m_c+m_x)^2 = r^4v^4.$$

Then from (1.4)

$$(1+r^4v^4)\Delta E/m_c\mu_c = x^2(1+\mu_x-\mu_c) - c^2(1+\mu_c-\mu_x) + 2xc(\mu_c-\mu_x)\cos\theta + r^2v^4 \cdot 2xc\sin\theta\cos\Theta.$$

Again, $v^2 = x^2+c^2-2xc\cos\theta$, and using this and writing $\Delta E/\mu_c m_c = z$, we get

$$z = \{1 + r^4(x^2+c^2-2xc\cos\theta)^2\}^{-1}[x^2(1+\mu_x-\mu_c) - c^2(1+\mu_c-\mu_x) + 2xc(\mu_c-\mu_x)\cos\theta + r^2(x^2+c^2-2xc\cos\theta)\,.\,2xc\sin\theta\cos\Theta]. \quad (1.5)$$

Equation (1.5) shows the energy exchange z in a form which is useful because the velocities which appear, x and c, are scalar velocities relative to the origin, while the angles θ and Θ have simple distributions. It is assumed that at any point in the cluster (or other aggregation of stars with which we wish to deal) the distribution of velocities is *isotropic*. Then the fraction of the encounters in which θ lies between θ and $\theta+d\theta$ is $\frac{1}{2}\sin\theta\,d\theta$ and the fraction in which Θ lies between Θ and $\Theta+d\Theta$ is $d\Theta/\pi$. We also suppose that the fraction of the encounters in which D lies between D and $D+dD$ is $2D\,dD/D_0^2$. The nature of the limit D_0 is discussed at length by Chandrasekhar in his *Principles of Stellar Dynamics*, pp. 55–57. We shall follow Chandrasekhar and suppose that D_0 is the average distance between stars.

2. If we write

$$r^2(x^2+c^2-2xc\cos\theta) = y,$$

$$x^2(1+\mu_x-\mu_c) - c^2(1+\mu_c-\mu_x) + 2xc(\mu_c-\mu_x)\cos\theta = a,$$

$$2xc\sin\theta = b,$$

then from (1.5)

$$z = \frac{a + b\cos\Theta\,.\,y}{1+y^2} \quad (2.1)$$

and, for a given x, c and θ, the quantities a and b are constants. We now enquire in what fraction of the encounter does z lie between k and $k+dk$ when x, c and θ have fixed values, while all values of Θ between 0 and π are equally likely.

The method of calculating this is illustrated in Fig. 3. Let the solution of $f(x, y) = h$ be $y = \phi(x, h)$. In the figure the curve ABCD represents $f(x, y) = h+dh$ and the curve EFGH represents $f(x, y) = h$. The variables x and y may have any values between zero and X and between zero and Y respectively, and the fraction of cases in which x lies between x and $x+dx$ is supposed to be $\rho_x(x)\,dx/X$, with a similar supposition about y. Now the fraction of cases in which $f(x, y)$ lies between h and $h+dh$ is the sum of the fractions of cases in which it lies in areas of which BCGF is an example, i.e.

$$\Sigma\,\mathrm{FG}\,.\,\rho_x(\mathrm{OL})\,.\,\mathrm{BF}\rho_y(\mathrm{OP})/XY.$$

* e.g. S. Chandrasekhar, *Principles of Stellar Dynamics*, Appendix 1, Chicago, 1942.

But if $FG = dx$, then

$$BF = dh \Big/ \left(\frac{\partial f(x,y)}{\partial y}\right)_x$$

and the required quantity is

$$\frac{dh}{XY}\int_0^X \rho_x(x) \cdot \rho_y(\phi(x,h)) \cdot dx \Big/ \left(\frac{\partial f(x,y)}{\partial y}\right)_x . \tag{2.2}$$

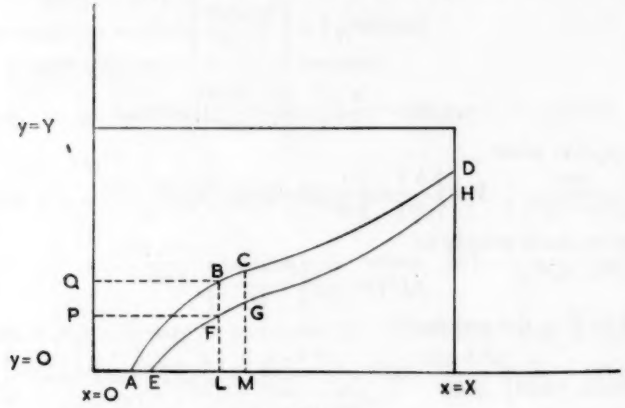

FIG. 3.

We apply this technique to calculate $\rho_z(k)\,dk$, the fraction of the encounters (having a given θ) in which z lies between k and dk. All values of Θ between 0 and π are equally likely, while y lies between 0 and Y, the density being

$$\rho_y(y) = 2y/Y.$$

Before applying (2.2) we examine the limits involved. If $z = k$ then

$$\cos\Theta = \{k(1+y^2) - a\}/by \tag{2.3}$$

or

$$2ky = b\cos\Theta \pm \{b^2\cos^2\Theta - 4k(k-a)\}^{1/2}.$$

No real solution for Θ exists unless $b^2 > 4k(k-a)$, and for $\Theta = 0$ or π,

$$2ky = \pm b \pm \{b^2 - 4k(k-a)\}^{1/2},$$

so that the curve (2.3) cuts the boundaries $\cos\Theta = +1$ and $\cos\Theta = -1$ at four points, in two of which y is positive and two negative (unless $k = 0$). When $k(k-a)$ is positive the two positive points are

$$y_2 = \left|b/2k\right| + \left|\frac{1}{2k}\{b^2 - 4k(k-a)\}^{1/2}\right|,$$

$$y_1 = \left|b/2k\right| - \left|\frac{1}{2k}\{b^2 - 4k(k-a)\}^{1/2}\right|,$$

and both of these points lie on $\cos\Theta = +1$ or both on $\cos\Theta = -1$. When $k(k-a)$ is negative the two positive points are

$$y_2 = \left|b/2k\right| + \left|\frac{1}{2k}\{b^2 - 4k(k-a)\}^{1/2}\right|,$$

$$y_1 = -\left|b/2k\right| + \left|\frac{1}{2k}\{b^2 - 4k(k-a)\}^{1/2}\right|,$$

and one point lies on $\cos\Theta = +1$ and the other on $\cos\Theta = -1$. In all cases $y_2 > y_1$.

Equation (2.2) gives

$$\rho_z(k) = \int_{y_1}^{L} \frac{2y}{\pi Y^2} \frac{dy}{|(\partial z/\partial\Theta)_y|}$$

and the upper limit L is y_2 or Y, whichever is smaller. Since

$$|(\partial z/\partial\Theta)_y| = \left|\frac{by\sin\Theta}{1+y^2}\right|,$$

we have

$$\rho_z(k) = \frac{2}{\pi Y^2}\int_{y_1}^{L} \frac{(1+y^2)\,dy}{|b\sin\Theta|}.$$

When $L = y_2$, i.e. when

$$Y > \left|\frac{b}{2k}\right| + \left|\frac{1}{2k}\{b^2 - 4k(k-a)\}^{1/2}\right|, \tag{2.4}$$

the integration leads simply to

$$\rho_z(k) = \frac{1}{2Y^2}\left|\frac{b^2+2ak}{k^3}\right|, \tag{2.5}$$

whereas, if (2.4) is not satisfied,

$$\rho_z(k) = \frac{1}{\pi Y^2}\left|\frac{b^2+2ak}{2k^3}\cos^{-1}\frac{2lY^2+n}{(m^2-4ln)^{1/2}} - \frac{1}{k^2}(lY^4+mY^2+n)^{1/2}\right|, \tag{2.6}$$

in which $l = -k^2$, $m = b^2 - 2k(k-a)$ and $n = -(a-k)^2$. The inequality (2.4) may also be stated in the form

$$|k| > \left|\frac{a+bY}{1+Y^2}\right|. \tag{2.7}$$

3. The number of encounters which occur in time dt between a star with velocity c and $n(x)\,dx$ stars per unit volume with velocities between x and $x+dx$ is

$$n(x)\,dx\,dt\int_0^{D_0} 2\pi D\,dD\int_0^{\pi}(x^2+c^2-2xc\cos\theta)^{1/2}\,.\,\tfrac{1}{2}\sin\theta\,d\theta$$

$$= n(x)\,dx\,dt\,.\,\pi D_0^{\,2}\times\frac{3x^2+c^2}{3x} \qquad \text{if} \quad x>c \tag{3.11}$$

$$= n(x)\,dx\,dt\,.\,\pi D_0^{\,2}\times\frac{x^2+3c^2}{3c} \qquad \text{if} \quad x<c. \tag{3.12}$$

Similarly the number of encounters $N(k, x, c)\,dx\,dk\,dt$ with energy exchanges between k and $k+dk$ is given by

$$N(k,x,c) = n(x)\,.\,\pi D_0^{\,2}\int_0^{\pi}\tfrac{1}{2}\sin\theta\,.\,(x^2+c^2-2xc\cos\theta)^{1/2}\,.\,\rho_z(k)\,.\,d\theta. \tag{3.13}$$

Since a and b are functions of θ, $\rho_z(k)$ is a function of θ (and k). For simplicity we take, from now on, the case where the stars have equal mass, $\mu_c = \mu_x$. Then

$$a = x^2 - c^2, \qquad b = 2xc\sin\theta,$$

$$y = r^2(x^2+c^2-2xc\cos\theta), \qquad Y = R^2(x^2+c^2-2xc\cos\theta),$$

$$R^2 = D_0/2\Gamma m.$$

The condition $k = \dfrac{a\pm bY}{1+Y^2}$ becomes

$$k = \frac{(x^2-c^2)\pm 2xc\sin\theta\,.\,R^2(x^2+c^2-2xc\cos\theta)}{1+R^4(x^2+c^2-2xc\cos\theta)^2}.$$

When R is large and $x \neq c$ this is

$$k \simeq \frac{\pm 2xc \sin\theta}{R^2(x^2+c^2-2xc\cos\theta)}$$

which has maximal values where $\cos\theta = 2xc/(x^2+c^2)$ and $k = \pm \frac{2xc}{R^2(x^2-c^2)}$, so that if $|k| > \left|\frac{2xc}{R^2(x^2-c^2)}\right|$ equation (2.5) applies. When $x=c$ and $\sin\theta = 0$ the energy exchange is zero.

Using $2\Gamma mR^2 = D_0$ equation (3.13) becomes

$$N(k,x,c) = 4\pi\Gamma^2 m^2 R^4 n(x) \cdot \int_0^\pi \tfrac{1}{2}\sin\theta(x^2+c^2-2xc\cos\theta)^{1/2} \cdot \rho_s(k)\, d\theta.$$

Let

$$N(k,x,c) = \frac{2\pi\Gamma^2 m^2 n(x)}{|k^3|} \times F(k,x,c) \quad \text{when} \quad |k| > \left|\frac{2xc}{R^2(x^2-c^2)}\right| \tag{3.21}$$

$$= \frac{2\pi^2\Gamma m^2 n(x)}{|k^3|} \times G(k,x,c) \quad \text{when} \quad |k| < \left|\frac{2xc}{R^2(x^2-c^2)}\right|. \tag{3.22}$$

The values of $F(k,x,c)$ may be given simply. When $|k| > \left|\frac{2xc}{R^2(x^2-c^2)}\right|$,

$$\rho_s(k) = \frac{1}{2R^4|k^3|} \times \frac{4x^2c^2\sin^2\theta - 2(x^2-c^2)k}{(x^2+c^2-2xc\cos\theta)^2} \quad \text{when} \quad \sin^2\theta > \sin^2\theta_0$$

$$= 0 \quad \text{when} \quad \sin^2\theta < \sin^2\theta_0$$

and $x^2c^2\sin^2\theta_0 = k^2 - k(x^2-c^2)$, with the conventions $0 < \theta_0 < \pi/2$; $\theta_0 = 0$ if $k^2 - k(x^2-c^2)$ is negative; and $\theta_0 = \pi/2$ if $x^2 > k$ and k is positive or if $c^2 > |k|$ and k is negative. These limitations arise through (2.7). Carrying out the integration we have

k negative.—$|k|$ must be less than c^2 as the c star cannot give up more energy than it has.

From $x=0$ to $x^2 = c^2 - |k|$

$$F(k,x,c) = \frac{8x^2-6k}{3c}. \tag{3.31}$$

With $x^2 > c^2 - |k|$

$$F(k,x,c) = \frac{8c^2+2k}{3xc}(c^2+k)^{1/2}. \tag{3.32}$$

k positive.—$F(k,x,c)$ is zero when $k > x^2$ as the x star cannot give up more energy than it has.

From $x^2 = 0$ to $x^2 = k$

$$F(k,x,c) = 0. \tag{3.33}$$

From $x^2 = k$ to $x^2 = c^2 + k$

$$F(k,x,c) = \frac{8x^2-2k}{3xc}(x^2-k)^{1/2}. \tag{3.34}$$

With $x^2 > c^2 + k$

$$F(k,x,c) = \frac{8c^2+6k}{3x}. \tag{3.35}$$

Detailed balancing.—Let the distribution functions for c and x be $c^2 f(c)$ and $x^2 f(x)$, that is to say, let $n(x) = x^2 f(x)$ and let the c stars be the normal field stars.

Then the number of collisions which destroy two velocities c and x and set up two velocities c' and x' (with energy changes $k=c'^2-c^2=x^2-x'^2$) is

$$c^2x^2f(x)\,dcf(x)\,dx\times\frac{1}{|k^3|}\cdot F(k,x,c)\,dk\times 2\pi\Gamma^2m^2$$

per unit area per unit time, when $|k|>|2xc/R^2(x^2-c^2)|$. These arise out of a set of orbits all of which can be described in the opposite sense, destroying c' and x' and setting up c and x, with the energy change $k'=c^2-c'^2=x'^2-x^2$. The number is

$$c'^2x'^2f(c')\,dc'f(x')\,dx'\cdot\frac{1}{|k'^3|}\cdot F(k',x',c')\,dk'\times 2\pi\Gamma^2m^2.$$

The system is conservative if

$$c^2x^2f(c)f(x)\,.\,dc\,dx\,.\,F(k,x,c)\,dk=c'^2x'^2f(c')f(x')\,dc'\,dx'\,.\,F(-k,x',c')\,|dk'|$$

with $dk=c'\,dc'=-x'\,dx'$, $dk'=-c\,dc=x\,dx$ and $dk=-dk'$. Hence

$$xc\,dc\,dx\,dk=x'c'\,dc'\,dx'\,|dk'|$$

and the system is conservative if

$$xcf(c)f(x)F(k,x,c)=x'c'f(c')f(x')\,.\,F(-k,x',c'). \tag{3.4}$$

Consider for example k positive and $x^2>c^2+k$. Then $F(k,x,c)=(8c^2+6k)/3x$. by (3.35). In the reverse exchange k is negative and $x'^2>c'^2-k$ so that

$$\begin{aligned}F(-k,x',c')&=\frac{8c'^2-2k}{3x'c'}(c'^2-k)^{1/2}\quad\text{by (3.32)}\\&=\frac{8c^2+6k}{3x'c'}\times c\\&=F(k,x,c)\times\frac{xc}{x'c'}.\end{aligned}$$

Hence (3.4) gives $$f(c)f(x)=f(c')f(x'),$$

which is of course satisfied by Maxwell's distribution $f(y)=e^{-j^2v^2}$, since

$$c^2+x^2=c'^2+x'^2.$$

Detailed balancing is therefore satisfied. It may be verified in the other cases that

$$xcF(k,x,c)=x'c'F(-k,x',c'),$$

provided $c'^2=c^2+k$ and $x'^2=x^2-k$. It is clear that we must also have

$$xcG(k,x,c)=x'c'G(-k,x',c').$$

4. Now suppose that the velocity distribution is truncated Maxwellian, or

$$\left.\begin{aligned}n(x)=N'x^2e^{-j^2x^2}\quad&\text{when}\quad x<x_0\\=0\qquad\qquad&\text{when}\quad x>x_0\end{aligned}\right\} \tag{4.1}$$

and $$N'=N\Big/\int_0^{x_0}x^2e^{-j^2x^2}\,dx.$$

Let $jx_0=J$. We suppose that e^{-J^2} is a small number, so that $N'=4j^3\pi^{-1/2}N$.

The number of stars removed from the class c, dc by collisions x, dx : k, dk in unit volume in time dt is

$$n(c)\,dc\,dt\,n(x)\,dx\,\frac{dk}{|k^3|}\times 2\pi\Gamma^2m^2H(k,x,c), \tag{4.2}$$

where

$$H(k,x,c)=F(k,x,c) \quad \text{if} \quad k>k_0$$
$$=G(k,x,c) \quad \text{if} \quad k<k_0$$

and $k_0 \simeq |2xc/R^2(x^2-c^2)|$.

In full equilibrium this removal is exactly balanced by the gain to c, dc

$$n(c')\,dc'n(x')\,dx'\,\frac{dk}{|k^3|}\,2\pi\Gamma^2m^2H(-k,x',c'), \tag{4.3}$$

where $c'\,dc'=c\,dc$, $x'\,dx'=x\,dx$, $c'^2=c^2+k$ and $x'^2=x^2-k$ and k may be positive or negative.

Under condition (4.1) certain unbalances occur. The net effect on the population $n(c)$ can be calculated by counting those transitions which do *not* occur as a result of the cut-off. These result in a gain, or no change, or a loss, to the population $n(c)$, as the case may be, as follows:—

If all four states in the transition $c, c' : x, x'$ are of lower energy than the cut-off x_0, then the c and c' transitions both occur, and balance, giving no net change in $n(c)$. If two or more states are of greater energy than x_0 the process and its reversal are both cut off, giving no net change in $n(c)$.

If however *one only* of the four states $c, c' : x, x'$ is of greater energy than the cut-off, a net change does occur. Since $c^2>x_0^2$ is forbidden *ex hypothesi* there are three cases to be considered, namely (1) $x^2>x_0^2$, (2) $x'^2>x_0^2$ and (3) $c'^2>x_0^2$. In case (1) the transition but not its reversal is forbidden, so that there is a net gain to $n(c)$. In other cases the transition is permitted but the reversals are suppressed so that there are net losses to $n(c)$.

(1) When $x^2>x_0^2$ but both $c'^2<x_0^2$ and $x'^2<x_0^2$, k must be positive and

$$x_0^2-c^2>k>x^2-x_0^2.$$

Let $k=+l^2$. Then the loss to $n(c)\,dc$ is

$$-2\pi\Gamma^2m^2n(c')\,dc'\,dt\,\frac{2l\,dl}{l^6}\int_{(x_0^2-l^2)^{\frac{1}{2}}}^{x_0} n(x')\,.\,H(-l^2,x',c')\,dx', \tag{4.41}$$

the negative sign in $H(-l^2,x',c')$ occurring because the unbalanced transitions are losses to c'. Equation (4.41) holds from $l^2=0$ to $l^2=x_0^2-c^2$.

(2) When $x'^2>x_0^2$ but both $c'^2<x_0^2$ and $x^2<x_0^2$, k is negative, equal to $-l^2$, say. Then

$$x_0^2>x^2>x_0^2-l^2$$

and the loss to $n(c)\,dc$ is

$$2\pi\Gamma^2m^2n(c)\,dc\,dt\,\frac{2l\,dl}{l^6}\int_{(x_0^2-l^2)^{\frac{1}{2}}}^{x_0} n(x)H(-l^2,x,c)\,dx \tag{4.42}$$

valid from $l^2=0$ to $l^2=c^2$.

(3) When $c'^2>x_0^2$, k is positive and greater than $x_0^2-c^2$. Then $x^2>x_0^2-c^2$ as the x star cannot give up more energy than it has. The loss to $n(c)\,dc$ is

$$2\pi\Gamma^2m^2n(c)\,dc\,dt\,\frac{2l\,dl}{l^6}\int_{(x_0^2-c^2)^{\frac{1}{2}}}^{x_0} n(x)H(l^2,x,c)\,dx \tag{4.43}$$

valid from $l^2=x_0^2-c^2$ to $l^2=x_0^2$.

Case (3) is unimportant except when c^2 is nearly equal to x_0^2.

5. Accurate evaluation of the function $G(k, x, c)$ is a matter of great complexity. We shall assume that (when $x>c$)

$$G(-l^2, x, c)=\frac{8c^2}{3x}\frac{(1+\alpha^3)l^6}{l^6+\alpha^3 l_0{}^6}, \tag{5.1}$$

a form which makes $G=F$ when $l=l_0$ and which keeps Gl^{-6} finite when $l=0$. The value of α may be chosen to make the total number of collisions

$$2\pi\Gamma^2m^2n(x)\int_{-c^2}^{x^2}H(k, x, c)\frac{dk}{|k^3|} \tag{5.2}$$

equal to the number of collisions given (accurately) by (3.11) or,

$$n(x).\pi D_0{}^2(3x^2+c^2)/3x. \tag{5.3}$$

Substituting (5.1) in (5.2) and making approximations suitable to $x_0{}^2\gg l_0{}^2$ and $c^2\gg l_0{}^2$ the number of collisions given by (5.2) is

$$2\pi\Gamma^2m^2n(x)\frac{8c^2}{3x}\left\{\frac{1}{l_0{}^4}\left(1+\frac{1+\alpha^3}{\alpha^2}\left[\tfrac{1}{3}\ln\frac{(1+\alpha)^3}{1+\alpha^3}+\frac{2}{\sqrt{3}}\left(\tan^{-1}\frac{2-\alpha}{\alpha\sqrt{3}}+\frac{\pi}{6}\right)\right]\right)\right\}$$

and equating this to (5.3) with $2\Gamma mR^2=D_0$ and $l_0{}^2=2xc/R^2(x^2-c^2)$ we find

$$1+\frac{1+\alpha^3}{\alpha^2}\left[\tfrac{1}{3}\ln\frac{(1+\alpha)^3}{1+\alpha^3}+\frac{2}{\sqrt{3}}\left(\tan^{-1}\frac{2-\alpha}{\alpha\sqrt{3}}+\frac{\pi}{6}\right)\right]=\frac{3x^2+c^2}{8c^2}\cdot\frac{8x^2c^2}{(x^2-c^2)^2}.$$

This value of α makes the total number of collisions given by the approximate formula (5.1) correct.

The case in which we are most interested is $x\gg c$, and then

$$\alpha=(4x^2/7c^2)^{1/3}$$

approximately: α therefore takes large values. This has been established to show that the terms involving α in equation (6.3) can be neglected.

6. From equations (4.41), (4.42) and (4.43)

$$\begin{aligned}\frac{1}{2\pi\Gamma^2m^2}\frac{1}{n(c)}\frac{dn(c)}{dt}=\frac{cn(c')}{c'n(c)}&\int_0^{\sqrt{(x_0{}^2-c^2)}}\frac{2l\,dl}{l^6}\int_{\sqrt{(x_0{}^2-l^2)}}^{x_0}n(x')H(-l^2, x', c')\,dx'\\&-\int_0^{c}\frac{2l\,dl}{l^6}\int_{\sqrt{(x_0{}^2-l^2)}}^{x_0}n(x)H(-l^2, x, c)\,dx\\&-\int_{\sqrt{(x_0{}^2-c^2)}}^{x_0}\frac{2l\,dl}{l^6}\int_{\sqrt{(x_0{}^2-c^2)}}^{x_0}n(x)H(l^2, x, c)\,dx.\end{aligned} \tag{6.1}$$

It is now necessary to approximate. If $x_0{}^2-c^2$ is not small, the third integral may be neglected in comparison with the other two, since l^6 occurs in all denominators. We further take $x_0{}^2-c^2>c^2$ and neglect the range from $l=c$ to $l=\sqrt{(x_0{}^2-c^2)}$ in the first integral, again because small values of l contribute most to the integrals. We are left with

$$\frac{1}{2\pi\Gamma^2m^2}\cdot\frac{1}{n(c)}\frac{dn(c)}{dt}=\int_0^{c}\frac{2l\,dl}{l^6}\int_{\sqrt{(x_0{}^2-l^2)}}^{x_0}\left\{\frac{cn(c')}{c'n(c)}H(-l^2, x, c')-H(-l^2, x, c)\right\}n(x)\,dx. \tag{6.2}$$

Now $cn(c')/c'n(c)=c'/c\exp\{j^2(c^2-c'^2)\}=(1+l^2/c^2)^{1/2}e^{-j^2l^2}$, and we can approximate to $H(-l^2, x, c)$ by

$$H(-l^2, x, c)=\frac{8c^2}{3x}f(l),$$

where $f(l)=1$ when $l>l_0$,

$f(l)=\dfrac{(1+\alpha^3)l^6}{l^6+\alpha^3 l_0{}^6}$ if $l<l_0$, following Section 5.

Then

$$\frac{1}{n(c)}\frac{dn(c)}{dt} = \frac{16\pi}{3}\Gamma^2 m^2 N' c^2 \int_0^c \left\{\left(1+\frac{l^2}{c^2}\right)^{3/2} e^{-j^2l^2} - 1\right\}\frac{f(l)}{l^5}\left\{\int_{\sqrt{(x_0^2-l^2)}}^{x_0} 2xe^{-j^2x^2}\,dx\right\} dl$$

$$= 32\sqrt{\pi}\Gamma^2 m^2 j^3 N e^{-J^2}\left(1-\tfrac{2}{3}j^2c^2\right)\int_0^c f(l)\frac{dl}{l}$$

$$= 16\sqrt{\pi}\Gamma^2 m^2 j^3 N e^{-J^2}\left(1-\tfrac{2}{3}j^2c^2\right)\left[\ln\frac{c^2}{l_0^2} + \tfrac{1}{3}(1+\alpha^3)\ln\left(\frac{1+\alpha^3}{\alpha^3}\right)\right]. \quad (6.3)$$

The terms involving α are unimportant, with α large, since c^2/l_0^2 is large. This justifies the approximation in Section 5. In what follows, these terms will be neglected.

We now define the time of relaxation $T(c, x_0)$ by

$$-\frac{1}{n(c)}\frac{dn(c)}{dt} = \frac{1}{T(c, x_0)}.$$

Then, substituting $\frac{1}{2}R^2x_0c$ for c^2/l_0^2 (supposing $x_0 \gg c$) we have finally

$$[T(c, x_0)]^{-1} = 16\sqrt{\pi}\Gamma^2 m^2 j^3 N\left(\tfrac{2}{3}j^2c^2 - 1\right)\ln\left(\tfrac{1}{2}R^2x_0c\right)e^{-J^2}. \quad (6.4)$$

This may be compared with Chandrasekhar's time of relaxation* $\overline{T}_E$ which is given, in our notation, by

$$\overline{T}_E^{-1} = \frac{32\sqrt{(2\pi)}}{9}\Gamma^2 m^2 j^3 N \ln\left(3R^2/2j^2\right). \quad (6.5)$$

7. For small values of c, namely $j^2c^2 < \frac{2}{3}$, the time of relaxation due to the Maxwellian truncation is negative, i.e. the number of stars with small velocities *increases*. Now if $n(c) = 4\pi^{-1/2}j^3c^2e^{-j^2c^2}$,

$$-\frac{1}{n(c)}\frac{dn(c)}{dj} = \frac{3}{j}\left(\tfrac{2}{3}j^{-2}c^2 - 1\right)$$

so that equation (6.4) gives

$$\frac{dj}{dt} = \frac{16\sqrt{\pi}}{3}j^4\Gamma^2 m^2 N \ln\left(\tfrac{1}{2}R^2x_0c\right)e^{-J^2},$$

showing that the collisions in the truncated distribution bring about an increase in the quantity j, i.e. a decrease in the "temperature". But the main difference between equations (6.4) and (6.5) is the appearance of the term e^{-J^2} in the former. Accordingly if e^{-J^2} is a small number, that is to say if the cut occurs far out in the Maxwellian distribution, the inverse time of relaxation is much smaller, and therefore the time of relaxation much larger, than the quantities given by Chandrasekhar. If then his time of relaxation is of the order of magnitude of the time required to set up, substantially, a Maxwellian velocity distribution, this distribution will be stable over a much larger period of time if the escape of fast stars cuts off the high velocities. This is the point which the present paper attempts to establish, and the work is offered as a justification of the "model" velocity distribution taken in the writer's earlier paper.

8. *Acknowledgment.*—I am indebted to Mr J. Burr who has checked nearly all the algebra shown in this paper.

Commonwealth Observatory,
Canberra:
1954 *June* 17.

* S. Chandrasekhar, *Principles of Stellar Dynamics*, equation (2.379), p. 67, Chicago, 1942.

TEMPERATURE AND TURBULENCE IN THE CHROMOSPHERE

R. O. Redman and Z. Suemoto

(Received 1954 September 4)

Summary

Measures of chromospheric line profiles in high resolution spectrograms obtained at the total solar eclipse of 1952 February 25 have been used to investigate further the question of temperature and turbulence in the solar chromosphere. In trying to deduce a distribution of line-of-sight velocities, arising from either temperature motions or turbulence, two problems are encountered: (*a*) to estimate the chromospheric heights to which the spectra refer, and (*b*) to correct the measures for broadening by self-absorption and Stark effect. Heights have been estimated partly from a comparison of line intensity ratios with those measured by Dr J. Houtgast on slitless spectrograms obtained at the same eclipse, and partly from the time of exposures, using the motion of the Moon relative to the Sun. Broadening by self-absorption has been estimated in the case of metallic lines by an empirical method. The corrected line widths, together with others of He I, suggest an approximately linear increase of line-of-sight velocity with height, from $\xi_0 \simeq 2{\cdot}5$ km/sec at the base of the chromosphere, to $\xi_0 \simeq 16$ km/sec at height 2600 km. Taking into account the uncertainty in effective height, these results agree with those obtained in 1940.

The hydrogen Balmer lines have been examined in more detail. The earlier members of the series are broadened by self-absorption, while later members are broadened by Stark effect. Both kinds of broadening were first estimated by an empirical method, which led to the conclusion that the temperature of the lower chromosphere does not exceed 10 000 deg. K. The hydrogen line widths were then computed more elaborately by a theoretical method, which showed that the observations could be fitted almost as well by a temperature 6 000 deg. as by 10 000 deg. It seems unlikely that the present data will yield any closer estimate of temperature than this.

At the total solar eclipse of 1940 October 1 line widths in the chromospheric spectrum were measured which seemed to indicate two important results: (*a*) the turbulence in the low chromosphere is small, the average (horizontal) line-of-sight velocity being about 1·8 km/sec, (*b*) the kinetic temperature of the low chromosphere is about 30 000 deg. K.* While no objection has so far been raised to the first of these conclusions, the second has provoked a great deal of discussion and the general trend of opinion today is that such a high temperature is most unlikely. Thus there has been a call for more work, first to re-measure the line profiles to ensure that the 1940 measures contain no substantial error, and then, if they turn out to be correct, to seek some alternative explanation consistent with a temperature not far from that of the photosphere.

With this in mind, observations were made at the total eclipse of 1952 February 25, in Khartoum, with a large grating spectrograph. A preliminary

* R. O. Redman, *M.N.* **102**, 140, 1942 (Paper I).

description of this work has already been given elsewhere* and further details are now in the press.† The more essential points may be repeated here. The spectrograph used the second order of a 6-inch Rowland concave grating, having 15 000 lines per inch, in a Wadsworth mounting. The collimator mirror had a focal length 12 feet, the nominal grating radius was 21 feet. For thermal protection the instrument was installed in a pit in the ground. The slit was set tangential to the solar image near the point either of second or third contact. The solar image had a diameter 52 mm; the slit width was 0·03 mm; scintillation was estimated to give an image spread roughly 2 seconds of arc. Eight photographs were taken at second contact covering the region 5550–6040 A, with dispersion 2·2 A/mm, and seven at third contact covering 3430–4110 A, with dispersion 2·4 A/mm. The average exposure time was about 1·5 seconds, with an interval between the centres of successive exposures about 2·3 seconds. The plates were calibrated with a Hilger rhodium step wedge, and the instrumental profile was determined by means of a water-cooled ^{198}Hg isotope lamp. The spectrograph gives very satisfactory definition. The sum of the Rowland ghosts in the second order is about one per cent of the parent line. The general photometric procedure was in principle the same as in 1940, although almost all the instrumental details were different.

Results from narrow lines are given in Paper III and confirm quite closely the 1940 measures. The assumption that for these lines the observed width, after correction for instrumental broadening, is chiefly due to line-of-sight motion, is supported by the fact that the two spectrum regions yield nearly the same mean velocities. Following Unsöld's notation‡, the velocities ξ are taken to have a distribution given by $\exp -(\xi/\xi_0)^2$, so that the results may be expressed in terms of the parameter ξ_0. The 1940 measures (Paper I) were given in terms of the arithmetical mean velocity $\bar{v}$. The two parameters are connected by $\xi_0 = \bar{v}\sqrt{\pi}$.

In this paper we shall merely quote the results for narrow lines and then concern ourselves mainly with the problem of wider lines, very many of which are known to be broadened by self-absorption. Two results will emerge: (*a*) evidence is found which suggests a considerable increase of velocity with chromospheric height, (*b*) the kinetic temperature in the low chromosphere does not exceed 10 000 deg. K, while 6 000 deg. K may almost equally well be reconciled with the line widths. At present it appears doubtful whether a more accurate kinetic temperature can be deduced from the available line profiles.

Heights.—The practical problem of deducing a velocity distribution from chromospheric line profiles leads to two other questions: (1) the determination of effective heights, (2) the correction of the measured line widths for various distortions, by the instrument, by self-absorption, and in the case of hydrogen by Stark effect.

The assignment of a chromospheric height to observations made with a slit spectrograph is a difficult question to which no entirely satisfactory answer has been found. As explained in Paper III, the only tolerably satisfactory way of estimating the heights at which our ultra-violet (third contact) observations were made is to compare line intensity ratios with those from slitless spectra.

* R. O. Redman, *Accademia Nazionale dei Lincei, Convegno Volta*, **11**, 72, 1953 (Paper II).
† R. O. Redman, *Vistas in Astronomy*, in press, 1955 (Paper III).
‡ A. Unsöld, *Z. f. Naturforschung*, **7a**, 121, 1952.

What we aim at getting is only an apparent height, measured from the solar limb, and we try to express the physical properties of the chromosphere in terms of what would be seen, integrated along the line of sight, in ideal conditions. What ultimately we require are the physical properties in terms of true heights within the chromosphere, but the derivation of these can be regarded as a separate problem, which is not tackled here.

The apparent heights deduced from line intensity ratios are not very precise for at least two reasons: (*a*) What the *slit* spectrograph records is an indeterminate blend of spectra from an appreciable range in chromospheric height, the degree of mixing depending chiefly on scintillation, guiding and length of exposure (the coelostat having been rated to follow the Moon), (*b*) the structure of many of the spectrum lines changes greatly with height, and what *slitless* spectrographs record is the sum of all the chromosphere not covered by the Moon at the time of exposure. If the seeing is very good and the instrumental resolution high enough, these various line structures tend to be recorded side by side; if the scintillation is great they are all blurred together.

However, despite various difficulties, this method of height determination, i.e. by comparison of line intensity ratios between slit and slitless spectrograms, appears to be the least unsatisfactory for the present case. Using data kindly supplied in advance of publication by Dr J. Houtgast, apparent heights have been estimated as follows:

3rd contact	exposure	1	1200: km
		2	1100
		3 level 1	< 50
		2	<100
		3	600

The chief cause of the small differences of effective height between exposures 1 and 2 is probably poor guiding. This arose from a slight mishap with the coelostat drive, which slipped out of gear about 30 seconds before the end of totality. The solar image was recovered only just in time for third contact. The three heights on exposure 3 refer to measures made from different points of the spectrograph slit.

For the yellow observations at second contact, heights have been estimated from the motion of the Moon across the Sun. The last traces of Fraunhofer spectrum are seen on exposure 3 and the narrow lines measured in Paper III are from exposure 4, at a height <500 km. Subsequent exposures show nothing but Na I, D_1 and D_2, and He I D_3. For these the estimated heights were based on the assumption that second contact took place between exposures 3 and 4, and that the guiding was good. In some respects this method is more satisfactory than the use of relative line intensities, but when a rather slow succession of exposures is made, as here, it can be applied only to strong lines which extend to comparatively great heights. The adopted heights are as follows:

2nd contact	exposure	4	200 km
		5	800
		6	1400
		7	2000
		8	2600

Metallic lines.—In the violet and ultra-violet spectrum from low chromospheric levels, say less than 600 km, there is an adequate selection of lines, notably

of the singly ionized rare earths, which appear to be little broadened by self-reversal, and these give the line-of-sight velocities already reported and reproduced here in Table I.

TABLE I

Line-of-sight velocities from narrow lines

	Height	$\bar{v}$	ξ_0	Number of lines
ultra-violet	< 50 km	1·5 km/sec	2·7 km/sec	38
	<100	1·8	3·2	54
	≃600	2·2	3·9	27
yellow	<500	1·2	2·1	18
1940 violet	<500	1·8	3·1	30

At these same comparatively low levels the strong metallic lines, especially those which are also strong in the Fraunhofer spectrum, are generally considerably broader than the narrowest lines, and often their profiles show clear indication of of self-reversal.* At greater heights, unfortunately, practically the only lines which persist in sufficient strength to be measurable are these same lines which at low levels are known to be affected strongly by self-reversal. True, the optical depth in the line of sight decreases with increasing height, so that the self-absorption decreases and somewhere becomes negligible, but we cannot be sure without further examination that this happens before the line becomes too weak to measure.

A fairly certain answer may be obtained if there are enough lines to construct a curve of growth, for on the first linear part of the curve there should be negligible self-absorption. Construction of an empirical curve of growth from Fe I multiplets showed that most of the easily measurable iron lines on our u.v. spectrograms fall near or on the second section of the curve, so that their profiles are unlikely to give satisfactory line-of-sight velocity distributions without correction. It is possible to compute the necessary corrections on the basis of some model chromosphere, but here we have preferred to use an empirical method, from extrapolation of the observed data.

As many lines as possible of a given element are measured at some given height, and their half-widths (ordinates) plotted against line intensities (abscissae). As expected, the widths increase with growing intensity, as the broadening by self-absorption increases. Extrapolation of the observed curve back to zero intensity should, however, give a " true " line width, free of the effect of self-absorption. The extrapolated curve is assumed to start from the ordinate axis with zero slope. This procedure was first tried for u.v. exposure 3, at the 600 km level, where there are also sufficient rare-earth and other narrow lines to give a "true" half-width without correction. The extrapolated half-widths (corrected for instrumental broadening) for Fe I and Ti II give reasonably accordant results:

600 km	rare earths, etc.	$\bar{v} = 2{\cdot}2$ km/sec	$\xi_0 = 3{\cdot}9$ km/sec
	extrapolated Fe I	2·2	3·9
	extrapolated Ti II	2·7	4·8

At higher levels there were rather few lines measurable, even of Fe I and Ti II, and since exposures 1 and 2 refer to approximately the same height they were combined, with the following result:

1200 km	extrapolated Fe I	$\bar{v} = 5$ km/sec	$\xi_0 = 9$ km/sec
	extrapolated Ti II	5	9

* Not merely self-absorption, but an actual self-reversal at the centre of the line profile.

The exact coincidence of the Fe and Ti velocities here should be regarded as fortuitous, and not a sign of great accuracy in the result.

In the yellow the only metallic lines visible above 500 km were the *D* lines of sodium. These are very heavily self-reversed in the low chromosphere, in the manner typical of all low-excitation lines which are also strong in the Fraunhofer spectrum. However, at the highest level at which they are measurable, 1400 km, both *D* lines have the same width and we have supposed them to be free of serious self-absorption broadening at this height. (We note, however, that their intensities here are in the ratio 1 : 1·4):

1400 km *D* lines $\bar{v} = 5{\cdot}3$ km/sec $\xi_0 = 9{\cdot}4$ km/sec

As far as these spectrograms are concerned there are no further data to be obtained from metallic lines at greater heights; for such levels a faster spectrograph or longer exposures would be required.

Helium.—The only He I lines measurable on our spectrograms are 5876 A (D_3), 4026 A, and on one exposure 3819 A. A few other helium lines could be expected in the 3500–4000 A region, but at the fairly low levels where they might otherwise be measurable they are concealed by blends with other lines. Throughout the violet and ultra-violet spectrum, blending is generally severe at low levels, especially below 100 km, and owing to the intrinsic width of the lines an increase of instrumental resolving power can bring only partial amelioration.

All three of the measured He I lines are multiple. D_3 consists of a close unresolved doublet with a partially resolved fainter companion, the others contain a single line with a partially resolved fainter companion. In each case the fainter companion has, as far as possible, been removed from the measures. After this correction, and after correction for instrumental broadening, we get:

Height	Line		
600 km	4026 A	$\bar{v} = 6{\cdot}2$ km/sec	$\xi_0 = 11{\cdot}0$ km/sec
1100	4026	6·6	11·7
1100	3819	6·6	11·7
1400	5876	6·0	10·7
2000	5876	7·5	13·3
2600	5876	8·9	15·7

On the 1940 spectrograms only the 4471 A He I line was measured, without correction for the faint companion, giving $\bar{v} = 8$, $\xi_0 = 14$ km/sec at some uncertain height probably less than 1500 km. It was remarked at the time that this line width was probably a little too great.

Variation of ξ_0 with height.—If now we plot all our results for ξ_0 against height, including those of Paper III, we find an almost linear increase from about $\xi_0 = 2{\cdot}2$ km/sec, at the base of the chromosphere, to 16 km/sec at 2500 km (Fig. 1). No definite explanation can be offered for the two seriously discordant points, from He I 4026 and 3819 A, but the figures for all the He I lines have to be accepted with some reserve. In the first place no examination has been made of possible widening by self-absorption, but if comparable with self-absorption in hydrogen lines of the same intensity, the effect is quite weak for 4026 and 3819 A at 1100 km. In the case of D_3 nothing can be said except that the line is weakening from exposure 6 to 8, but at the same time the measured line width actually increases; that is, if there is really an appreciable amount of self-absorption broadening (which must diminish with height), the velocity increase with height is still greater than that just deduced.

There is another complication in the case of helium. As already explained, the heights we have tried to assign to the measures are those at which the spectrograph slit would have to be placed to give the observed line widths in perfect observing conditions (no scintillation, etc). These apparent heights are not the same as heights in the chromosphere itself. For instance, were there an exponential intensity distribution with height, with no self-absorption, half the scale height would need to be added to the apparent height to give the true mean height in the chromosphere. With helium the relation between intensity and height is certainly more complicated than this. Many observers have noted that at low levels He I

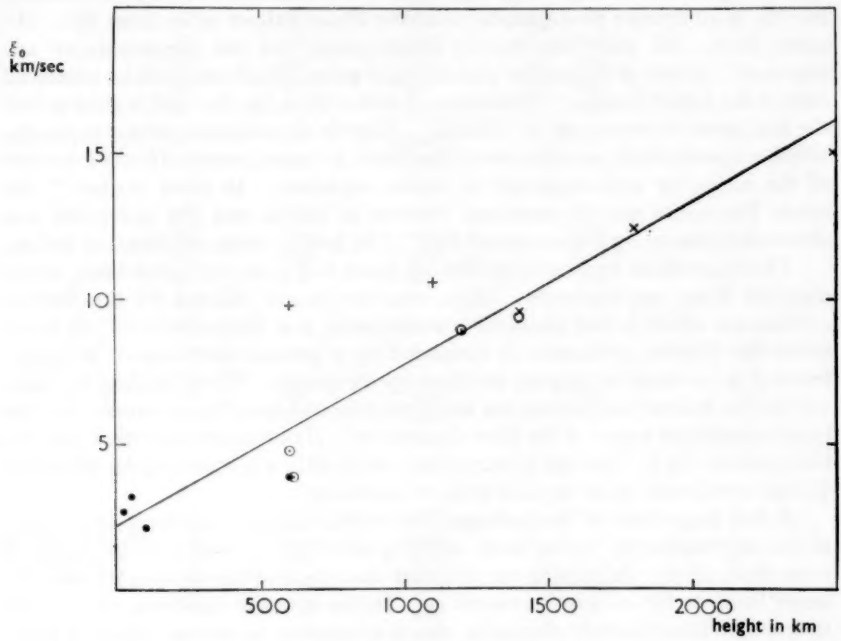

FIG. 1.—● *"narrow lines" in u.v., rare earths, etc. in yellow, mainly Fe* I.
⊙ *extrapolated Fe* I, *Ti* II.
○ *Na* I *D lines.*
\+ *He* I 4026, 3819.
× *He* I D_3.

Helium line widths have been corrected for an assumed $T=6000$ deg.

lines tend to behave differently from most others, in that their intensities at first *increase* with apparent height, a behaviour which is presumably closely associated with the general increase of spectrum excitation with height. A simple exponential law does not represent the facts adequately. The conversion of behaviour with regard to apparent height to behaviour in terms of true height can be made sufficiently well only with slitless spectra and we do not attempt it here. Fig. 1 ignores the correction from apparent height to true height, and we have to remember that the relation between these heights is probably less simple for He I than for any other element.

Thus although the evidence for an increase of ξ_0 with height is fairly convincing, the linear relation of Fig. 1 should not be taken too readily at face value. The points have been taken from a variety of lines, and the height question in particular cannot yet be regarded as properly settled. The evidence, taken together with what follows on the hydrogen lines, suggests that the velocity increase is chiefly one of turbulence, rather than of temperature, although more observations are certainly needed before there can be a really satisfactory separation of turbulent from thermal motions. The idea of a turbulence increasing with height has been favoured by some theorists, especially Unsöld.*

Hydrogen.—There are no hydrogen lines on the plate exposed at second contact, but the third contact photographs cover the whole Balmer series from Hδ to the series limit. Hδ itself was heavily overexposed, and not measurable on any exposure; others of the earlier and stronger series members could be measured only at the higher levels. The measured half-widths, i.e. the total widths at half the maximum intensity, are in Table II. Gaps in the measures are due to blends, which are particularly troublesome at low levels, to overexposure of lower members of the series, or underexposure of higher members. In cases marked * the whole line could not be measured because of blends and the half-width was obtained by assuming a symmetrical line. The heights were estimated as before.

Three specimen hydrogen profiles are given in Fig. 2, the points being single readings from one exposure. Lines near $n=30$ are affected by the Balmer continuum, which is just measurable on exposure 3, at height 600 km. At lower levels the Balmer continuum is concealed by a general continuum; at higher levels it is too weak to appear on these spectrograms. When finding the half-widths the Balmer continuum has not been removed from the measures, but has been regarded as a part of the lines themselves. (It becomes important only for lines with $n>25$.) The behaviour of line width with n is more regular when the Balmer continuum is left in than when it is removed.

A first inspection of the hydrogen line widths shows a tendency to increase as one approaches the series limit, which qualitatively is what is to be expected from Stark effect. In passing we may note that the lines do not overlap near the series limit, as far as these measures go. In the opposite direction, as one goes to stronger lines there is ultimately also a systematic widening, which is fairly certainly due to self-absorption. All lines now measured are substantially narrower than the widths for Hβ, Hγ and Hδ ($n=4$, 5, 6) on the 1940 spectrograms, which tends to support the suggestion that all the earlier and stronger members of the Balmer series are considerably broadened by self-absorption when observed at fairly low chromospheric levels.

We suppose now that the measured hydrogen line widths are due to (*a*) instrumental broadening, (*b*) Stark effect, (*c*) self-absorption, (*d*) Doppler effect. Of these (*a*) has already been removed and we wish chiefly to find (*d*). There is a weakness in the raw material, inevitable in the present case, and not easily avoided altogether in eclipse spectroscopy of this kind, that because of over-exposure the accuracy of measurement falls off with the strongest lines, on which we mostly rely for estimating the effect of self-absorption, and because of underexposure it falls off also with the weakest lines, from which we deduce the Stark effect. Ideally, the measures should cover a considerably greater range than is possible on a single photographic exposure.

* A. Unsöld, *loc. cit.*

TABLE II

Half-widths of chromospheric hydrogen lines

Blended lines marked* have been assumed symmetrical; other blended lines have been omitted. Uncertain measures are marked with a colon. The half-width is the total line width at half the maximum intensity.

	n	Total intensity	Measured half-width	h.w. corrected for instrumental distortion
Height 100 *km*	13*	1360	0·374 A	0·349 A
	14*	1085	·345	·321
	15	865	·328	·304
	16	765	·333	·308
	17*	548	·333	·308
	18	458	·347	·323
	19*	402	·313	·287
	20*	316	·308	·282
	21	265 :	·318 :	·294 :
Height 600 *km*	15	1375	0·342	0·318
	16	1190	·335	·311
	17	955	·318	·294
	18	815	·328	·304
	19	725	·340	·316
	20	615	·364	·340
	21	508	·342	·318
	22	452 :	...	...
	23	345	·364	·340
	24	...	...	...
	25	...	...	...
	26	263	·422	·398
	27	207	·422	·398
	28	...	...	...
	29	...	·443	·419
	30	...	...	...
	31	...	·472	·451
Height 1100 *km*	13	1144	0·345	0·321
	14	960	·357	·333
	15	736	·328	·304
	16	599	·335	·311
	17	488	·340	·316
	18	354	·316	·289
	19	331	·352	·328
	20	257	·330	·306
	21	227	·366	·342
	22	192	·410	·386
	23	162	·398	·374
	24	...	·378	·354
	25	...	·427	·402
	26	...	·424	·400
Height 1200 *km*	7	1905	0·506	0·484
	8*	1635	·458	·436
	9	1190	·393	·369
	10	900	·345	·321
	11	655	·333	·308
	12	519	·308	·282
	13	380	·292	·265
	14	318	·323	·299
	15	275	·308	·282
	16	187	·296	·270
	17	156	·337	·313
	18	140	·342	·318
	19	91	·337	·313
	20	106	·419	·395

Empirical reduction of hydrogen line widths.—The measures cover $n=7$ to 31, but not all on one exposure or at one level. There are not enough observations to determine the variation of Stark effect with height, so that we have taken all the measures together, assuming they refer to some average height between 600 and 1200 km. The Stark effect has been taken to give a line width proportional to $n(n-1)$. This is a good approximation for large n, and is amply accurate for our present needs. We shall find that for $n<15$ the Stark effect makes a very small contribution to the total line width; for $n>25$ it dominates the line profile. The self-absorption broadening has been taken to vary only with the measured total line intensity, irrespective of height. What is left after Stark effect and self-absorption broadening have been removed is taken to be the Doppler profile, which is of course proportional to wave-length, although the range of variation with the lines measured here is less than ten per cent.

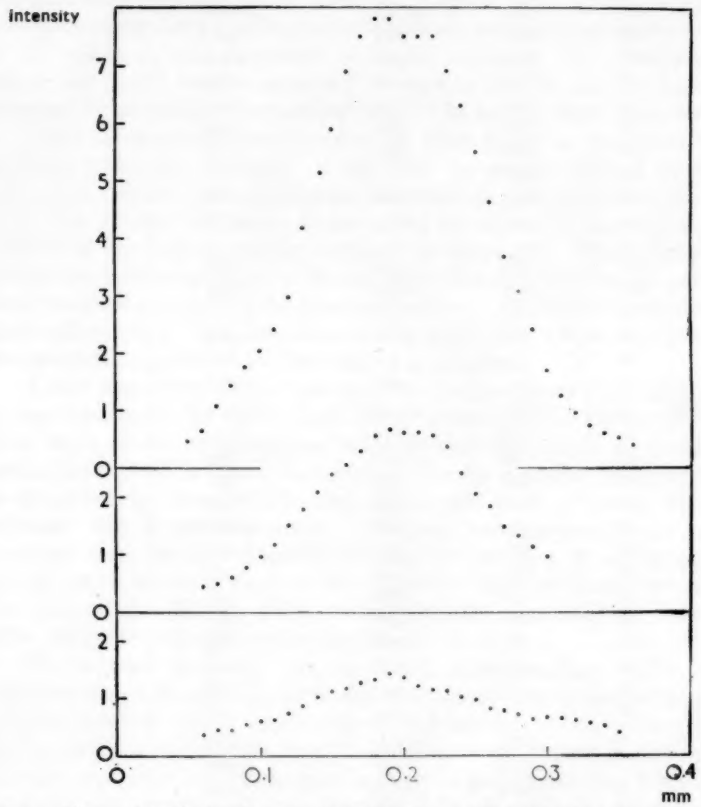

FIG. 2.—*Measured profiles (single readings) of H16, H21 and H26 at height* $\simeq$ 600 *km.* 1 *mm*=2·4 *A.*

With these considerations in mind, empirical values for the Stark broadening and self-absorption broadening were estimated by graphical means and the results are in Table III. It was assumed that for this preliminary examination

TABLE III A

Doppler half-widths of hydrogen lines, empirical reduction

n	100 km	600 km	1100 km	1200 km
7				0·253 A
8				·282
9				·308
10				·289
11				·289
12				·270
13	0·258 A		0·260 A	·253
14	·265		·289	·287
15	·265	0·214 A	·275	·268
16	·275	·236	·284	·253
17	·277	·241	·289	·294
18	·292	·255	·258	·294
19	·246	·268	·292	·282
20	·234	·292	·263	(·364)
21	·236 :	·260	·294	
22		...	·337	
23		·265	·313	
24		...	·275	
25		...	·321	
26		·296	·301	
27		·275		
28		...		
29		·260		
30		...		
31		·248 :		

TABLE III B

Stark half-widths from empirical reduction

n	h.w.
7	0·017 A
10	·036
15	·085
20	·154
25	·243
30	·352

TABLE III C

Corrections for self-absorption from empirical reduction

(to be subtracted from the observed half-width)

I	Correction
250	0·002 A
500	·007
750	·018
1000	·036
1250	·068
1500	·121
1750	·187
1905	·233

Stark and Doppler widths could be combined as Gaussian errors. The self-absorption was estimated as a correction to be subtracted from the measured half-width.

After removing Stark and self-absorption broadening the mean Doppler half-width is 0·276 A at a mean wave-length 3699 A. In obtaining this value a few of the strongest and weakest lines were rejected. This width gives a kinetic temperature 11 000 deg., if no allowance is made for turbulence. The correction for turbulence, following the earlier part of the paper, will depend on the assumed height. If we take this to be 850 km, with a ξ_0(turbulence)$=7$, the corrected kinetic temperature is about 10 000 deg. K.

Theoretical calculation of hydrogen line widths.—This treatment assumes that for present purposes we can regard the chromosphere as a layer of gas with a given constant temperature and pressure at all points along any particular line of sight. The Stark profile of a hydrogen Balmer line has been taken from Verweij, as quoted by Miss van Dien.* The profile is $U(\beta)$, where β is the ratio of the field strength to a standard field $F_0 = 2{\cdot}61 N^{2/3} e$. N is the number of charged particles per cm^3 and e the charge on the electron. β has a certain probability distribution, a property of the inter-particle fields in the gas.

For convenience $U(\beta)$ is represented by a Voigt profile, $V(a_s, \Delta\lambda_s)$, where the parameters a_s, $\Delta\lambda_s$ can be regarded as a fictitious damping width and Doppler width respectively. a_s is expressed in units of $\Delta\lambda_s$. By trial and error a satisfactory fit for $U(\beta)$ was found with $a_s = 0{\cdot}4$, the quality of the representation being shown in Table IV. Here v is the distance from the centre of the line, expressed as a fraction of the (fictitious) Doppler width; $V(v)$ is the Voigt profile, taken from Hjerting's computations (his Table 4).† The ratio of β to v has been chosen so that $V(v)$ fits $U(\beta)$ at $v = 1$. The fifth column in Table IV gives the Voigt profile, and the sixth gives the Stark profile, each in units of its central value.

The $\Delta\lambda_m = s_n \beta F_0$ of Miss van Dien is identified with $\Delta\lambda_s$ when $v = 1$, $\beta = 1{\cdot}35$. Hence $\Delta\lambda_s = 1{\cdot}35 s_n F_0$, where $F_0 = 2{\cdot}61 N^{2/3} e = 1{\cdot}253 \times 10^{-9} \times N^{2/3}$ e.s.u. and, with $\Delta\lambda_s$ measured in angstroms,

$$s_n = 0{\cdot}00256 \left(\frac{n^2}{n^2-4}\right)^2 \{n(n-1)+2\}.$$

Some typical values of $\Delta\lambda_s$ are given in Table V.

We must now combine a real Doppler broadening with the Stark profile, the latter being now expressed as a Voigt profile with a pseudo-damping width a_s and a pseudo-Doppler width $\Delta\lambda_s$. The real Doppler width, following Hjerting's convention and in the customary notation is

$$\Delta\lambda_t = \sqrt{\left(\frac{2kT}{m_H}\right)} \frac{\lambda}{c}.$$

The resulting profile is another Voigt profile, $V(a, \Delta\lambda_a)$, where $\Delta\lambda_a = \sqrt{(\Delta\lambda_t^2 + \Delta\lambda_s^2)}$. If we continue to express the (pseudo-) damping parameter in terms of the (pseudo + real) Doppler width, now $\Delta\lambda_a$, it becomes $a = 0{\cdot}4 \dfrac{\Delta\lambda_s}{\Delta\lambda_a}$. Some figures for the particular case $T = 6000$ deg., $\log N = 11{\cdot}5$, are given in Table VI.

* Elsa van Dien, *Ap. J.*, **109**, 452, Table I, 1948.
† F. Hjerting, *Ap. J.*, **88**, 514, 1938.

TABLE IV

v	$V(v)$	β	$U(\beta)$	$V(v)/V(0)$	$U(\beta)/U(0)$
0·0	0·67	0·00	0·287	1·00	1·00
0·5	·57	0·68	·243	0·85	0·85
1·0	·36	1·35	·154	·54	·54
1·5	·19	2·02	·082	·28	·29
2·0	·090	2·70	·041	·134	·143
2·5	·049	3·38	·022	·073	·077
3·0	·030	4·05	·014	·045	·049
3·5	0·021	4·72	0·008	0·031	0·028

TABLE V

Values of $\Delta\lambda_s$

	log N=12·0	11·5	11·0
n= 5	0·0135 A	0·00627 A	0·00290 A
10	·0432	·0201	·00931
15	·0951	·0442	·0205
20	·169	·0783	·0363
25	·264	·123	·0569
30	0·381	0·177	0·0820

TABLE VI

T=6000 deg. log N=11·5

n	$\Delta\lambda_s$	$\Delta\lambda_t$	$\Delta\lambda_a$	$\Delta\lambda_s/\Delta\lambda_a$	a
5	0·00627 A	0·1446 A	0·145 A	0·0432	0·017
10	·0201	·1266	·128	·157	·063
15	·0442	·1237	·131	·338	·135
20	·0783	·1227	·146	·537	·215
25	·123	·1223	·173	·711	·284
30	0·177	0·1220	0·215	0·823	0·329

Having obtained the Stark plus Doppler profile for various n, the next step is to compute the effect of self-absorption. For this it is necessary to know the absorption coefficient κ_ν at each point within the hydrogen line. The first stage is to determine κ_0, the value of κ_ν at the line centre, and this we have obtained by way of $B_{12}h\nu$, the total strength of the Balmer line. B_{12} is the Einstein probability of absorption, and may be computed from Menzel and Pekeris' values of A_{21} by the relation

$$B_{12}=\frac{g_2}{g_1}\frac{c^2}{2h\nu^3}A_{21}.$$

Table VII gives an outline of the results.

TABLE VII

n	λ	log A	log B	log $h\nu$	log $Bh\nu$
5	4340 A	6·401	9·512	$\bar{1}2$·660	$\bar{2}$·172
10	3798	4·850	8·389	$\bar{1}2$·718	$\bar{3}$·107
15	3712	3·962	7·823	$\bar{1}2$·728	$\bar{4}$·551
20	3683	3·334	7·425	$\bar{1}2$·732	$\bar{4}$·157
25	3669	2·849	7·139	$\bar{1}2$·733	$\bar{5}$·872
30	3662	2·452	6·897	$\bar{1}2$·734	$\bar{5}$·631

In order to find κ_0 the values of $B_{12}h\nu$ must be divided by a factor depending on the line width. First we remark that Hjerting, whose computations we use,

tabulated κ_ν/κ_0^* † as a function of v, the distance from the line centre in units of the Doppler width, and normalized his profiles so that

$$\int_0^\infty \frac{\kappa_\nu}{\kappa_0^*} dv = \frac{\sqrt{\pi}}{2}.$$

We now define an effective line width v_{eff}, so that

$$\left(\frac{\kappa_\nu}{\kappa_0^*}\right)_{v=0} . v_{\text{eff}} = \int_0^\infty \left(\frac{\kappa_\nu}{\kappa_0^*}\right) dv = \frac{\sqrt{\pi}}{2}.$$

$(\kappa_\nu/\kappa_0^*)_{v=0}$ is the actual absorption coefficient at the line centre, as tabulated by Hjerting. Then the relative values of the absorption coefficients at the Balmer line centres are $B_{12}h\nu/2\Delta\nu_{\text{eff}}$, where

$$2\Delta\nu_{\text{eff}} = \frac{c}{\lambda^2} 2\Delta\lambda_{\text{eff}} = \frac{c}{\lambda^2} . 2v_{\text{eff}} . \Delta\lambda_a.$$

A summary of the results of this section of the work is in Table VIII.

TABLE VIII

$T=6000$ deg. $\log N=11{\cdot}5$

n	$\Delta\lambda_a$	a	$(\kappa_\nu/\kappa_0^*)_{v=0}$	v_{eff}	$\log 2\Delta\nu_{\text{eff}}$	$\log \frac{B_{12}h\nu}{2\Delta\nu_{\text{eff}}}$
5	0·145 A	0·017	0·981	0·903	10·619	$\bar{1}3{\cdot}553$
10	·128	·063	·934	0·948	10·701	$\bar{1}4{\cdot}406$
15	·131	·135	·866	1·024	10·765	$\bar{1}5{\cdot}786$
20	·146	·215	·797	1·112	10·856	$\bar{1}5{\cdot}301$
25	·173	·284	·748	1·184	10·960	$\bar{1}6{\cdot}912$
30	·215	·329	·714	1·241	11·076	$\bar{1}6{\cdot}555$

Suppose now that the optical depth of the chromosphere in the line of sight at the centre of a certain line is τ_0, and is $\tau_{0\cdot5}$ at the point where the observed intensity is one-half the central intensity. The intensity distribution within the line, including the effect of self-absorption, is taken to be

$$I \propto (1-\exp[-\tau]),$$

so that

$$\tfrac{1}{2} = \frac{1-\exp(-\tau_{0\cdot5})}{1-\exp(-\tau_0)}.$$

The relation between $\log\tau_0$ and $\log\tau_{0\cdot5}/\tau_0$ is given in Table IX. τ_0 is proportional to $B_{12}h\nu/2\Delta\nu_{\text{eff}}$ for the particular Balmer line which is in question. We

TABLE IX

$\log\tau_0$	$\log\tau_{0\cdot5}/\tau_0$
$-\infty$	$\bar{1}{\cdot}699$
$\bar{2}{\cdot}000$	$\bar{1}{\cdot}699$
$\bar{1}{\cdot}000$	$\bar{1}{\cdot}681$
$\bar{1}{\cdot}699$	$\bar{1}{\cdot}642$
0·000	$\bar{1}{\cdot}580$
0·301	$\bar{1}{\cdot}453$
0·477	$\bar{1}{\cdot}332$
0·602	$\bar{1}{\cdot}228$
0·699	$\bar{1}{\cdot}137$
1·000	$\bar{2}{\cdot}839$
2·000	$\bar{3}{\cdot}839$
3·000	$\bar{4}{\cdot}839$
4·000	$\bar{5}{\cdot}839$

† κ_0^* is Hjerting's κ_0, the fictitious absorption coefficient at the centre of the line when the damping is vanishingly small.

proceed by assuming τ_0 for one convenient line of the series, and choose $n=30$. Table IX then gives $\tau_{0\cdot5}/\tau_0$, and from Hjerting's Table 4, with $a=0\cdot4$. $(\Delta\lambda_s)/(\Delta\lambda_a)$, values of v are chosen so that

$$\left(\frac{\kappa_v}{\kappa_0^*}\right)_v \Big/ \left(\frac{\kappa_v}{\kappa_0^*}\right)_{v=0} = \frac{\tau_{0\cdot5}}{\tau_0}.$$

v is the distance from the line centre in units of the Doppler width, so that $2v \times \Delta\lambda_a = 2\Delta\lambda_{\text{cal}}$ should be the half-width of the line as observed.

TABLE X

Values of $2\Delta\lambda_{\text{cal}}$

T	6000 deg.	6000 deg.	6000 deg.	6000 deg.	6000 deg.	8000 deg.
log N	12·0	12·0	11·5	11·5	11·0	11·5
$\tau_0(n=30)$	0·1	0·05	0·1	0·05	0·1	0·05
$n=$ 5	0·844 A	0·722 A	0·682 A	0·624 A	0·626 A	0·702 A
10	·528	·446	·412	·346	·358	·388
15	·436	·372	·310	·272	·262	·304
20	·478	·446	·304	·290	·246	·314
25	·628	·624	·364	·352	·256	·378
30	0·872	0·860	0·452	0·448	0·292	0·466

T	8000 deg.	10000 deg.	10000 deg.	10000 deg.	10000 deg.	12000 deg.
log N	11·5	11·5	11·5	11·0	11·0	11·0
$\tau_0(n=30)$	0·03	0·05	0·02	0·05	0·02	0·02
$n=$ 5	0·654 A	0·776 A	0·674 A	0·734 A	0·628 A	0·682 A
10	·346	·422	·344	·374	·318	·344
15	·290	·336	·306	·304	·284	·308
20	·314	·342	·340	·294	·294	·318
25	·374	·400	·396	·312	·308	·332
30	0·460	0·484	0·478	0·342	0·334	0·356

Table X contains half-widths calculated in this manner for various combinations of parameters within the ranges

$$\begin{aligned} 6\,000 \text{ deg.} \leqslant T &\leqslant 12\,000 \text{ deg.}, \\ 11\cdot0 \leqslant \log N &\leqslant 12\cdot0, \\ 0\cdot02 \leqslant \tau_0(n=30) &\leqslant 0\cdot1. \end{aligned}$$

For a number of reasons, some of which will be briefly discussed in a moment, a perfect fit with the observations cannot be expected. Fig. 3 shows the observations with two computed curves:

(*a*) $T=$ 6000 deg. $\log N = 11\cdot5$ $\tau_0(n=30)=0\cdot1$

(*b*) 10000 deg. 11·5 0·02

Both curves lie fairly near the observations. Of the two, (*b*) appears to be somewhat the better, but it is doubtful whether much significance can be attached to this. The results suggest that an accurate determination of the kinetic temperature by this method is difficult, and could be made only from more comprehensive observations covering most of the Balmer series to $n=30$ at a number of different heights.

The difficulties may be summarized as follows:

(1) Owing to the large range of light intensity to be covered the present observational accuracy falls off at each end of the measured range of n.

(2) Measures at different heights 600–1200 km have been combined, although it is to be expected that both self-absorption broadening and Stark broadening will decrease with increasing height. The computed half-widths for the earlier members of the series are rather sensitive to the assumed "Balmer optical depth" (expressed as τ_0 at $n=30$), so that they are strongly dependent on height. There are two places at which this fact needs particularly to be borne in mind. In the measures quoted in Table II there is a strong suggestion that those from effective height 1200 km correspond to a substantially smaller τ_0 ($n=30$) than the others, so that to combine them all together is not entirely satisfactory. We should also refer to the 1940 measures, in which the half-width for $n=5$ was 0·53 A. This is smaller than one would expect either from extrapolation of the 1952 measures, or from the computed cases (*a*) or (*b*) above. Satisfactory data are not available for the height at which the 1940 measures were made, although 1500 km was tentatively suggested at the time. No great reliance can be placed on this figure, but it suggests a τ_0 lower than for the 1952 measures, and qualitatively this agrees with the line widths.

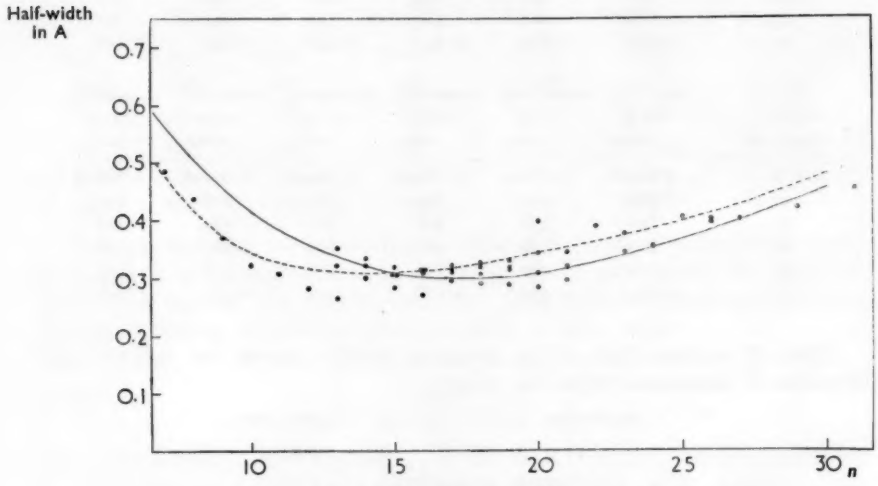

FIG. 3.—*Half-width of hydrogen Balmer lines plotted against n.*
—— *Curve* (*a*), *for* $T=6\,000$ deg. - - - - - - *Curve* (*b*), *for* $T=10\,000$ deg.

(3) We have made no allowance for turbulence in our computations. If the increase with height suggested by Fig. 1 is substantially correct, turbulence is becoming important, even for hydrogen, at a height about 2500 km. The turbulence makes a kinetic temperature determination from metallic lines virtually impossible by present techniques, and not very practicable from helium.

(4) The computations have neglected all variations in the properties of the chromosphere along the line of sight. Even in a static atmosphere, what is observed is an integration over a wide range of physical parameters. If the chromosphere has to be treated as a field of filaments or jets the question becomes forbiddingly complicated.

Since this paper was completed, work by Kawaguchi has appeared* in which he fits theoretically computed hydrogen profiles to the 1940 measures made by one of us. His conclusion with regard to these lines is the same as ours, viz. that it is possible to interpret the observed profiles with a kinetic temperature of 10 000 deg. K or less, if self-absorption is taken into account.

Acknowledgments.—The observations on which this work is based were made by the Cambridge 1952 Eclipse Expedition to Khartoum, which was financed wholly by the Joint Permanent Eclipse Committee. Special thanks are due to Dr D. E. Blackwell and Mr I. Kendall, who gave essential help with the spectrograph. The construction of the spectrograph was due to Mr R. Overhill of the Cambridge Observatories staff.

One of us (Z. S.) is indebted to the I.A.U., through the President of Commission 38, Professor F. J. M. Stratton, for a grant permitting him to spend a year of study in Europe, chiefly at the Cambridge Observatories.

The Observatories,
Madingley Road,
Cambridge:
1954 *September* 3.

Tokyo Astronomical Observatory,
Mitaka,
Tokyo.

* I. Kawaguchi, *Publ. Astro. Soc. Japan*, **5**, 137, 1954.

THE APPARATUS FUNCTION OF THE OXFORD SOLAR SPECTROSCOPE

R. J. Bray

(Communicated by the Director, University Observatory, Oxford)

(Received 1954 September 29)

Summary

The apparatus function of the Oxford solar spectroscope has been determined in the wave-length region λ 5461–λ 5945. Comparison with Plaskett's determination of the core of the profile at λ 4320 shows that Redman's suggestion that the linear dimensions of the profile are independent of wave-length requires modification. Differences between the curves at the two regions can be accounted for by the existence of large-scale inhomogeneities of the order of 3×10^{-5} in the refractive index of the prisms. The wings of the apparatus function show a number of sharp subsidiary maxima, whose spacing is six to seven times the spacing of the subsidiary maxima of the theoretical diffraction pattern. They are attributed to diffraction by striae, known to be present in the prisms.

Introduction.—In his well-known investigation of the central intensities of certain Fraunhofer lines (**8, 9**) Redman made a very accurate and extensive determination of the apparatus function of the $f/77{\cdot}6$ McClean prismatic spectroscope. He found two noteworthy departures from the predictions of diffraction theory. Firstly the core was much wider and the wings stronger than the diffraction-theory curve. Secondly the linear dimensions of the core of the apparatus function over the spectral range λ 4200–λ 6400 did not vary linearly with the wave-length but were approximately constant—a slightly greater observed linear width at λ 4200 being attributed by Redman to errors caused by temperature changes in the spectroscope.

As a step towards finding the profiles of certain Na lines, the apparatus function of the Oxford prismatic spectroscope (**7**) has recently been determined in the region λ 5461–λ 5945. The technique of this determination, essentially the same as that used by Redman and based on his experience, is briefly described in the final section of this paper. This apparatus-function determination, supplemented by the apparatus-function core determined at λ 4320 by Plaskett (**7**), shows that some of Redman's results cannot be applied to the Oxford spectroscope without slight modification. The wings, moreover, show a number of subsidiary maxima which appear to be a newly observed phenomenon with prism instruments. The new results and conclusions, together with possible theoretical explanations, are set forth in the first two sections.

1. *The core.*—The continuous curve of Fig. 1 shows the core of the apparatus function as determined from the profiles of the emission lines λ 5461, λ 5770 and λ 5791 given by a mercury-isotope lamp and from λ 5945 given by a neon discharge

tube. Ordinates are intensities and abscissae are millimetres in the focal plane of the spectroscope. The filled circles are the mean observed points and the vertical lines through them show the r.m.s. errors of these means found from the residuals. The dashed curve is that found by Plaskett from the Kr line λ 4320, the abscissae again being millimetres in the focal plane. Both the full line and dashed curves were obtained with field-lens illumination of the spectroscope slit. For comparison the dash-dot curve gives the profile of the mercury-isotope line λ 5461 for a mode of slit illumination mimicking that given by the solar telescope.

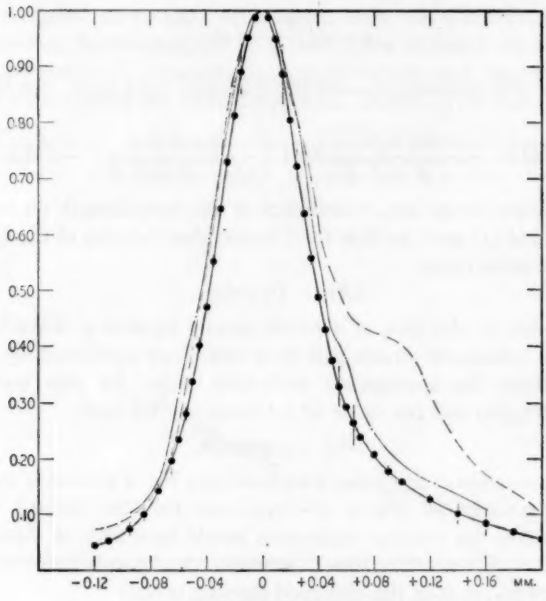

FIG. 1.—*Apparatus-function core.*
Abscissae: millimetres in the focal plane.
Ordinates: intensity.

The continuous curve refers to a mean wave-length of λ 5730, the dots being observed points and the vertical lines r.m.s. errors; the dashed curve refers to λ 4320. The dash-dot curve was obtained at λ 5461 with a mode of slit illumination mimicking that produced by the solar telescope.

Comparison of the full-line curve for a mean wave-length of λ 5730 and the dashed curve for a wave-length of λ 4320 shows fairly close agreement on the violet side. On the red side, however, there is a marked difference between the two profiles, that for λ 4320 showing a strong satellite which is almost completely absent at λ 5730. This difference is also well shown in Plate 1 *b* where on the right appears a fifteen-minute exposure of λ 5461 and on the left a three-hour exposure of λ 4320—the latter showing the satellite.

A possible explanation of the appearance of the satellite at λ 4320 can readily be offered. In accordance with Hilger's standard practice the prisms of the spectroscope have been locally figured to compensate for inhomogeneity of refractive index in the glass. This compensation, however, can only be effective

at the wave-length for which the prisms have been tested in Hilger's Twyman-Green interferometer. At any other wave-length, the re-figured portion of the prisms will divert light from the central part of the line image. A simple numerical example shows that a very small variation in refractive index is sufficient to account for the satellite observed at λ 4320. Assume that we can replace the actual prism by two prisms placed one on top of the other. Let the upper one have refracting angle A and refractive index n and the lower an angle $A+\delta A$ and index $n+\delta n$, where for simplicity we shall assume δn to be independent of wave-length. Then since at minimum deviation

$$n = \sin\frac{A+\theta}{2} \Big/ \sin\frac{A}{2},$$

the two prisms will produce at some wave-length, say λ 5730, two lines separated by

$$\delta\theta = \frac{2\sin A/2}{\sqrt{1-n^2\sin^2 A/2}}\delta n + \left\{\frac{n\cos A/2}{\sqrt{1-n^2\sin^2 A/2}} - 1\right\}\delta A. \qquad (1)$$

To bring these two lines into coincidence at this wave-length we must make the right-hand side of (1) zero, so that for Chance glass 613369 of the Oxford prisms and $A = 60°$ we must make

$$\delta A = -1{\cdot}2376\,\delta n. \qquad (2)$$

This corresponds to the case of a prism locally figured at wave-length λ 5730. At λ 4320 this composite prism will give two lines separated by $\delta\theta$ according to (1). Inserting the appropriate refractive index for this wave-length for Chance glass 613369 and the value of δA from (2), we find

$$\delta\theta = -0{\cdot}0700\,\delta n. \qquad (3)$$

Now for the equivalent of five prisms we find from Fig. 1 a satellite with an angular separation of 0·1 mm/F, where $F = 8958$ mm for the Oxford spectroscope. For a single prism the angular separation would be a fifth of this; hence from (3) the difference in refractive index between the top and bottom halves of the prism necessary to produce the observed satellite is only

$$\delta n = -\frac{\delta\theta}{0{\cdot}0700} = -\frac{1}{0{\cdot}0700}\left(\frac{1}{5}\times\frac{0{\cdot}1}{8958}\right) = -3{\cdot}2\times10^{-5},$$

a very small amount.

The strength of the satellite at λ 4320 suggests that the Oxford prisms are composed of a localized mixture in roughly comparable amounts of two glasses with refractive indices differing by $3{\cdot}2\times10^{-5}$. Equally the greater width of the violet wing at this wave-length suggests the presence of other irregularly distributed inhomogeneities with differences of refractive index still smaller by a factor of the order of ten. It seems unlikely that large blocks of optical glass can at present be made without large-scale refractive index variations of the order of 10^{-5} or 10^{-6}*, so we can conclude that in most cases local figuring will be necessary even to yield moderate performance in one wave-length region. For such locally figured prisms the width of the core of the apparatus function will be a minimum for that wave-length at which the re-figuring has been carried out,

* F. Twyman (11) quotes W. M. Hampton as follows: "If a piece of glass is uniform in temperature while being held prior to the annealing operation, the only index changes introduced into it will be the plus or minus variations due to the temperature gradient during cooling, and these will probably be small, probably not more than a few units in the fifth decimal place . . . ."

and for any other wave-length will depend on the difference between the refractive index at this wave-length and that at the wave-length of re-figuring, and also on the extent of the re-figuring. It therefore seems that Redman's tentative suggestion that the width of the core is independent of wave-length should be modified in the light of the above facts.

A word should be added about the dash-dot curve of Fig. 1. As already mentioned, this curve was found for a slit illumination mimicking that given by the solar telescope. In so far as this type of illumination is non-coherent and the field-lens illumination used for the other two curves is coherent, the greater width of the dash-dot curve is in accordance with van Cittert's prediction (**2**). It should, however, be emphasized that this curve is based on long exposures during which atmospheric pressure changes occurred, and though a first-order correction has been applied for these changes (cf. Section 3) the resulting apparatus

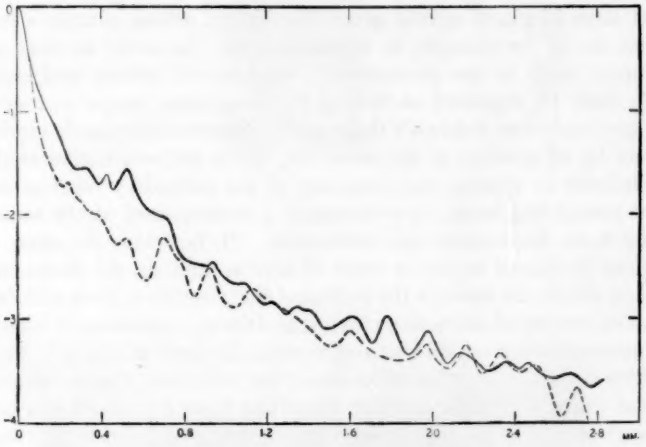

FIG. 2.—*Apparatus-function wings.*
Abscissae: millimetres in the focal plane.
Ordinates: logarithm of intensity.
Continuous and dashed curves are red and violet wings respectively.

function is subject to some uncertainty. The difference between the results obtained with the two modes of illumination may therefore be more apparent than real.

2. *The wings.*—The red and violet wings of the apparatus function are shown in Fig. 2 as continuous and dashed curves respectively. Ordinates are proportional to the logarithm of the intensity, abscissae are millimetres in the focal plane, and the curves may be taken to refer to the same mean wave-length, λ 5730, as the core. Because of the importance of the far wings of the apparatus function in fixing the observed central intensities of Fraunhofer lines, a fact originally pointed out by Allen and Redman (**8, 10**), the present determination has been carried down to 9×10^{-5} of the central intensity.

In agreement with Redman's results, the wings are considerably stronger than the maxima of the side bands of the theoretical diffraction pattern. They differ, however, from those of the McClean solar spectroscope in showing a number

of irregularly spaced subsidiary maxima. These maxima are well shown in Plate 1*a*—an over-exposed spectrum of the Na *D* lines given by a Philips' discharge lamp taken through a step wedge. Such maxima, however, tend to be washed out by atmospheric pressure changes, and their absence from the wings of the apparatus function of the McClean spectroscope may possibly be due to the occurrence of such pressure changes during the long exposures which Redman required to reach out into the wings (twenty-five hours as opposed to only four hours in the present work).

The secondary maxima in Plate 1*a* bear some resemblance to diffraction maxima, and this resemblance is heightened by their rough symmetry about the core. Nevertheless, they cannot be due to diffraction over the whole aperture of the spectroscope, since this would lead to some eighty maxima on either side of the central peak instead of the twelve to fifteen observed. The maxima may, however, arise from diffraction by striae in the glass of the prisms. In common with most large blocks of optical glass, the Oxford prisms contain a number of striae, well shown for example in Foucault tests. In so far as these striae are opaque, occur more or less at random throughout the prisms and, much more dubiously, may be regarded as having the same size, shape and orientation, they will give rise from Babinet's theorem to diffraction side bands identical with those given by an *aperture* of the same size, shape and orientation as the striae. The irregularity in spacing and intensity of the secondary maxima in Fig. 2, somewhat resembling beats, is presumably a consequence of the striae not all having the same dimensions and orientation. If, however, the striae are such that they can be placed in one or other of several families, the members of each family being closely the same in the pertinent characteristics, then each family will give rise to its own set of diffraction maxima and the superposition of these maxima will produce oscillations which wax and wane as do those in Fig. 2. Superposed on these hypothetical diffraction effects are of course effects due to inhomogeneity of the glass (for example, the satellite extending from 0·3 to 0·8 mm on the red wing), together with a general background of scattered light, some considerable part of which is probably produced by the striae. In so far as this interpretation is correct and in so far as striae are common to all large blocks of optical glass, secondary maxima similar to those shown in Plate 1*a* may be expected to occur in the wings of the apparatus function of any large prismatic spectroscope.

3. *Experimental procedure.*—In general the experimental procedure followed that of Redman, differing to some extent, however, in the method of slit illumination, sources of light, and photometric procedure. A field-lens was used to produce coherent illumination. The lens was illuminated by a diaphragmed light source and produced an extra-focal patch covering the full length of the slit, where a step wedge was situated, the image being in focus on the collimator and filling it with light. The second arrangement was designed to mimic the non-coherent illumination produced by the solar telescope. This was done by means of a good-quality lens stopped down to the appropriate focal ratio and provided with a central stop to represent the obscuration caused by the Cassegrain mirror. In this case the image of the diaphragmed light source was formed on the slit. This second arrangement is uneconomical of light, and for reasons described later produced results of very low weight. For both arrangements the slit width was set at 0·036 mm, the value used for solar work in the region λ 5500–λ 6000.

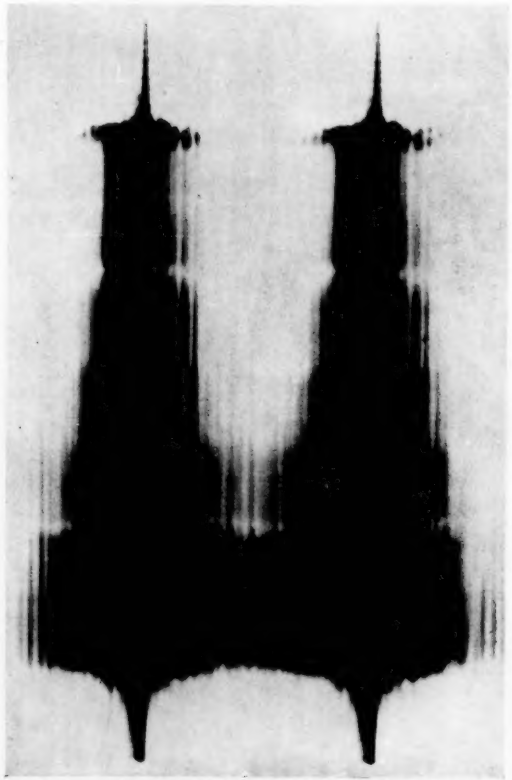

(a)

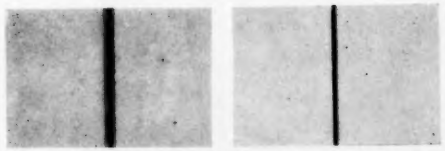

(b)

SCALE: 1 MM.

RED TO LEFT

(a) Over-exposed spectrum of D lines taken through step wedge.

(b) The apparatus-function core : right- and left-hand lines are Hg λ 5461 and Kr λ 4320 respectively. The latter shows the satellite.

The three light sources used were a water-cooled ^{198}Hg isotope lamp made by G.E.C., a B.T.-H. neon discharge lamp, and a Philips' sodium lamp. The isotope lamp has been described by Barrell (**1**), who states that at 17 deg. C the half-width is 0·008 A, being chiefly due to Doppler effect and collisional broadening, a value less than one-tenth of the apparatus-function half-width at the wave-lengths concerned. The lines λ 5461, λ 5770 and λ 5791 were used. The neon discharge lamp contains neon at a pressure of a few millimetres in a tube 9 mm in diameter; the operating current is 0·5 amp. Jackson (**4**) finds that the conditions of excitation necessary to obtain the lines free from self-reversal are not particularly stringent. From Jackson's published interferograms the half-width of the particular line used, λ 5945, is $<$0·02 A, which is only one-sixth the apparatus-function half-width at this wave-length. The weak satellite 0·02 A to the violet of the main line, due to ^{22}Ne, present in atmospheric neon to the extent of one part in ten, can be neglected. Redman has also used neon lines (**8**). Finally, a Philips' sodium lamp was used for the far wings. The use of such a bright source enabled an intensity of 9×10^{-5} of the central intensity to be recorded in exposure times extending only up to four hours. Owing to the danger of self-reversal, this lamp was not used for the core of the profile. Table I gives a summary of the observational material obtained with the three light sources.

TABLE I

Observational material

Wave-length	Mode of illumination	No. of plates	Exposure times	Minimum intensity recorded
λ 5461	coherent	6	15^m–6^h	0·02
λ 5770, λ 5791	,,	3	2^h–$4\frac{1}{2}^h$	·4
λ 5890, λ 5896	,,	10	30^s–4^h	·00009
λ 5945	,,	6	10^m–14^h	·02
λ 5461	non-coherent	5	2^h–9^h	·1

Plate calibration was performed by means of a step wedge consisting of six steps of rhodium evaporated on to glass together with a "clear glass" step. The wedge, which was made by A. Hilger, Ltd according to Plaskett's specifications, is designed for use on the slit of the solar spectroscope, a method of use which automatically corrects for scattered light. In order to avoid the formation of Edser-Butler fringes, which would occur if the glass base upon which the rhodium is deposited were plane parallel, the base is made in the form of a double prism, the two glasses being chosen so that the deviation of the light passing through the wedge is nearly zero for all wave-lengths in the range for which the step wedge is required. (Owing to the large focal length of the spectroscope, a *single* prism cannot be used, since the corresponding deflection of the beam would throw the light off the collimator.) The wedge is so constructed that by shifting it parallel to itself across the slit the light can be made to pass through the glass base without passing through the rhodium steps. This makes it possible to correct the characteristic curves for any residual deviation produced by the glass base, and more important, for any non-uniformity of the slit illumination.

The photometric procedure differed from that of Redman (**9**), who used either a separate calibrating spectroscope or a tube sensitometer. The method

adopted here was the method of self-calibration. In this method a single exposure, taken through the step wedge, exhibits both the profile under measurement and the calibration marks necessary for constructing the characteristic curve, the profile being obtained through the "clear glass" step. An additional exposure, with the wedge displaced to one side, allows one to correct the characteristic curve for any non-uniformity of slit illumination in the manner described above. The great advantage of the method is that both profile and calibration marks are obtained under identical photometric conditions. Provided the centre of the wedge exposure is not "burned out", the characteristic curve can be constructed in terms of the central intensity. The reduction then gives directly the intensity at any given point in the profile in units of the central intensity. In determining the outer parts of the profile, however, it is necessary to over-expose the centre of the line (cf. Plate 1*a*), and the characteristic curve must then be constructed from some reference point other than the centre. If the intensity at this point is known from the reduction of previous plates in the series, however, relative values may readily be converted to central intensity units. The subsidiary maxima described in Section 2 were chosen as reference points; they served very conveniently for the measurement of distance from the centre of the profile as well as intensity.

Backed Ilford Rapid Process Panchromatic plates were used throughout. The plates were "brush" developed, using a felt pad, in order to reduce Eberhard effect, and were developed in Parkhurst two-solution developer, which produces extremely little background fog. Microphotometry was performed with the Observatory microphotometer (**6**), a Moll-type instrument, using a plate-tracing magnification of fifty. Since the width of the microphotometer-slit image on the plate is only about one-seventh the half-width of the profile being measured, the microphotometer reproduces very closely the true profile.

The Oxford solar spectroscope is immune to temperature changes in its surroundings owing to thermostatic control (**7**). When the source is so faint that the core of the profile requires a long exposure time, however, there is a chance that a sufficiently large atmospheric pressure change (accompanied by a change of the refractive index of the air in the spectroscope) may occur to distort the profile seriously. This condition is not met with in solar use, of course, nor was any difficulty experienced in any of the twenty-five plates taken with field-lens illumination, since the exposure times for the core of the profile were short in the case of λ 5461 and λ 5945, while in the case of λ 5770 and λ 5791, although the exposure times were relatively large (see Table I), the pressure changes happened to be moderate, never exceeding 0·2 mm. However, three of the five plates taken with non-coherent illumination, none of which recorded more than the core of the profile, were affected by pressure changes of 0·9, 0·9 and 1·8 mm of mercury respectively. Calculation shows that the latter value causes a line shift on the plate comparable with the half-width of the profile. Rather than discard the three plates, which gave profiles whose half-widths were well correlated with the pressure changes, it was decided to correct the profiles for the known changes which had occurred. This was done as follows: if we assume a linear variation of pressure with time which causes a total line shift $\delta\lambda$, then the observed profile is the true profile obliterated by a rectangular obliterating function of width $\delta\lambda$, and the true profile may be found from the observed profile by solving the equation of obliteration. In view of the magnitude

of the shifts, it is clear that low weight should be attached to the curve obtained with non-coherent illumination.

Finally a few remarks are necessary concerning the step-wedge calibration. Calibration was originally performed using the solar spectroscope and four "neutral" filters which had been calibrated at six wave-lengths by the National Physical Laboratory. This calibration, however, gave a suspicious wave-length variation for the transmission of rhodium. A check calibration using a Zeiss platinum step wedge (**3**) showed that the Hilger step wedge was in fact neutral, so it was decided to carry out a full-scale re-calibration using a Hilger E.316 spectrograph. The photometric standards for this calibration were seven perforated diaphragms (**5**). A continuous source of light was used, microphotometry of the plates being performed at the three wave-lengths at which the original calibration had been made. The results of this final calibration (see Table II) show that over the wave-length range involved, and within the experimental error, the transmission of rhodium is independent of wave-length.

TABLE II

Transmission of Hilger rhodium-on-glass step wedge

Step	λ 5461	λ 5780	λ 6143	Mean
clear	1·000	1·000	1·000	1·000
vi	·652 ± ·003	·649 ± ·006	·668 ± ·005	·656 ± ·003
v	·431 ± ·007	·433 ± ·003	·427 ± ·003	·430 ± ·003
iv	·266 ± ·004	·265 ± ·003	·259 ± ·003	·263 ± ·002
iii	·158 ± ·001	·155 ± ·002	·155 ± ·002	·156 ± ·001
ii	·108 ± ·001	·103 ± ·001	·102 ± ·001	·104 ± ·001
i	...	·0737 ± ·0004	·0731 ± ·0005	·0735 ± ·0003

It was suspected that the error in the original wedge calibration was due to unexpectedly sharp variations in the transmissions of the four filters, making it unsafe to interpolate values from a smooth curve through the six points at which the filters had been calibrated. One of the filters was accordingly returned to the National Physical Laboratory for re-calibration at intermediate points. The resulting transmission curve confirmed this suspicion. Moreover, when the step-wedge values given in Table II were applied to the calculation of the transmission of the filter, using the original wedge calibration plates, the filter transmissions found by the National Physical Laboratory were correctly reproduced. Confidence can therefore be placed in the values given in Table II.

The writer wishes to express his deep sense of gratitude to Professor H. H. Plaskett for his unfailing encouragement and generous assistance, particularly in the theoretical interpretation of the results, and to thank the Master and Fellows of Balliol College and the Department of Scientific and Industrial Research for awards during the tenure of which the work was carried out.

University Observatory,
Oxford:
1954 *September* 29.

References

(1) H. Barrell, *Proc. Roy. Soc.* A, **209,** 132, 1951.
(2) P. H. van Cittert, *Zeits. f. Phys.*, **65,** 547, 1930.
(3) D. S. Evans, *M.N.*, **100,** 156, 1940; *Comm. Univ. Obs., Oxford,* No. 17, 1940.
(4) C. V. Jackson, *Proc. Roy. Soc.* A, **143,** 124, 1933.
(5) H. H. Plaskett, *M.N.*, **91,** 870, 1931.
(6) H. H. Plaskett, *M.N.*, **95,** 160, 1934; *Comm. Univ. Obs., Oxford,* No. 4, 1934.
(7) H. H. Plaskett, *M.N.*, **112,** 177, 1952; *Comm. Univ. Obs., Oxford,* No. 33, 1952.
(8) R. O. Redman, *M.N.*, **95,** 742, 1935.
(9) R. O. Redman, *M.N.*, **97,** 552, 1937.
(10) R. O. Redman, *M.N.*, **98,** 311, 1938.
(11) F. Twyman, *Prism and Lens Making,* p. 134, London, 1942.

FIELD REVERSAL IN MAGNETIC VARIABLE STARS

P. A. Sweet

(Communicated by the Director of the University of London Observatory)

(Received 1954 August 24)

Summary

In connection with oscillation theories of magnetic variable stars the limitation in the variation of the observed magnetic field strength H_e imposed by Cowling's boundary condition is examined.

Discussion is restricted to fields that remain symmetrical about a fixed axis during their variation. In spherical stars with a coefficient of limb darkening 0·45 it is found that, provided suitable gas motions can arise, reversal is possible only in the following cases :—

(i) dipole-type fields with distortions that are not symmetrical about the equatorial plane, when the inclination i of the magnetic axis to the line of sight exceeds 79°;

(ii) symmetrical quadrupole-type fields with symmetrical distortions, when $50° < i < 69°$;

(iii) quadrupole-type fields with unsymmetrical distortions, for all values of i;

(iv) certain fields of higher complexity even when symmetrical, for all values of i.

Statistical considerations indicate that it is improbable that dipole or symmetrical quadrupole-type fields can account for observations.

The paper is not concerned with the dynamics of the gas motions.

---

1. *Introduction.*—Cowling has shown (1) that in the so-called oscillation theories of magnetic variable stars, where the magnetic field variation is ascribed to distortion in the lines of force by moving material in the star, the field in the reversing layer would be equal to the surface value of the field outside the star. As this latter is a potential field a condition is imposed on the reversing layer field. This condition limits the possible variation in the resultant field strength H_e derived from the longitudinal Zeeman effect in the star's spectrum. In particular the question arises as to whether this resultant field could change sign as is observed in a considerable proportion of magnetic variables. By showing that no reversal occurred in a particular case of extreme distortion, Cowling illustrated the difficulty of finding a distortion which could produce a reversal. It is the purpose of the present paper to examine this question more fully.

2. *The invariance of field type.*—As mentioned in the Summary the discussion will be restricted to axially symmetric fields. By this it is meant that the fields remain axially symmetric throughout the oscillation cycle. It is shown in Section 7 that it is the type of field, whether dipole or quadrupole, etc., that determines the possibility of reversal when the star is viewed from any particular direction in relation to the magnetic axis.

Since the field outside the star is axially symmetric and potential it has no ϕ-component (component perpendicular to meridian planes). Furthermore, because the movement of gas inside the star is supposed to be axially symmetric,

the meridian-plane component of the field inside the star is independent of the ϕ-component.* Hence the meridian-plane component is all that needs to be considered in the present work. It will therefore be regarded, in what follows, as the whole field.

The field is determined by the system of lines of force in a meridian half-plane bounded by the axis. Any field produced by finite electric currents in the star possesses neutral points in this plane; these are of two types. A point encircled by closed lines of force in its neighbourhood will be called a circular neutral point†, while a point at which two lines of force intersect will be called an x-type neutral point.

A dipole-type field is defined as any field, vanishing at infinity, possessing one circular neutral point. There can be no x-type neutral points in such a field.

A quadrupole-type field is defined as any field vanishing at infinity, possessing two circular neutral points of opposite polarities, while the x-type neutral points involved lie on the axis. In an unsymmetrical quadrupole-type field there are two of these points, the positions of which depend on the positions of the circular neutral points and the strengths of the electric current systems associated with them. If the field is symmetrical about the equatorial plane one of the points is at the centre of the star and the other is at infinity.

In the neighbourhood of circular neutral points an electric current density is present, consequently all these points lie inside the star. The typical times of variation in magnetic variable stars are sufficiently small, and the electrical conductivity sufficiently high, to use the familiar picture of lines of force frozen into the gas. Since the field referred to is an independent meridian-plane field all its lines of force, except a finite number of limiting ones that extend to infinity, are closed curves. Because gas cannot cross the lines of force any given closed tube of force contains a constant total mass of gas. The requirement of mass conservation therefore shows that no tube of force can be created or destroyed. Consequently the number and polarity of the circular neutral points are unaltered by any gas motion in the star. The field type is therefore invariant.

3. *The reversing layer field.*—The external field is potential, solenoidal and axially symmetric. It can therefore be expressed in the form

$$\mathbf{H} = -\operatorname{grad} V, \tag{3.1}$$

where

$$V = R \sum_{n=1}^{\infty} a_n \left(\frac{R}{r}\right)^{n+1} P_n(\mu). \tag{3.2}$$

The a_n are constants, the P_n are Legendre polynomials, R is the radius of the star, r is the distance from the centre of the star and $\mu = \cos\theta$, θ being the angular distance from the axis. Cowling's boundary condition is that the field $\mathbf{H}_s$ in the reversing layer is the surface value of the above field, hence $\mathbf{H}_s$ is given by

$$H_{sr} = \sum_{n=1}^{\infty} (n+1)\, a_n P_n(\mu), \tag{3.3}$$

$$H_{s\theta} = \sin\theta \sum_{n=1}^{\infty} a_n P_n'(\mu). \tag{3.4}$$

* This would not necessarily be true if the Hall effect had to be allowed for; this effect, however, is negligible in stars.

† This term also includes neutral areas encircled by lines of force.

The surface of the star has been assumed spherical; according to Cowling (**2**) the effect of ellipticity is not large, consequently the assumption is not considered to be unduly restrictive.

4. *The observed field strength H_e.*—Denoting the line-of-sight component of $\mathbf{H}_s$ by H_L and the surface brightness by I at any point on the star's disk, H_e is given by

$$H_e = \iint_{\text{disk}} H_L I \, dS \Big/ \iint_{\text{disk}} I \, dS, \tag{4.1}$$

where dS is an element of area of the disk. Referring to Fig. 1 it is seen that at a point Q on the surface of the star

$$H_L = H_{sr} \cos\theta_1 - H_{s\theta} \cos\eta \sin\theta_1. \tag{4.2}$$

From the theory of limb-darkening I is usually expressed in the form

$$I = I_0 (1 - u + u \cos\theta_1) \tag{4.3}$$

when u is the coefficient of limb-darkening. An element of area of the surface of the star is $\sin\theta_1 \, d\theta_1 \, d\phi_1$, thus an element dS of the disk is given by

$$dS = \cos\theta_1 \sin\theta_1 \, d\theta_1 \, d\phi_1. \tag{4.4}$$

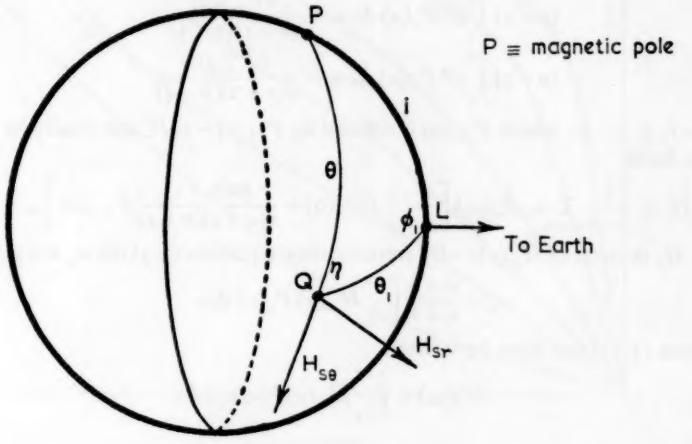

FIG. 1.—*Geometry of star with magnetic axis inclined to line of sight.*

Using the last three expressions, together with equations (3.3) and (3.4), equation (4.1) can be written

$$H_e = \frac{6}{\pi(3-u)} \sum_{n=1}^{\infty} a_n \int_{\phi_1=0}^{\pi} \int_{\mu_1=0}^{1} [(n+1) P_n(\mu)\mu_1 - P_n'(\mu) \sin\theta \cos\eta \sin\theta_1] \times [1 - u + u\mu_1]\mu_1 \, d\mu_1 \, d\phi_1, \tag{4.5}$$

where $\mu_1 = \cos\theta_1$. From the spherical triangle LPQ

$$\sin\theta \cos\eta \sin\theta_1 = \mu_0 - \mu\mu_1, \tag{4.6}$$

$$\mu = \mu_0\mu_1 + \sin i \sin\theta_1 \cos\phi_1, \tag{4.7}$$

where $\mu_0 = \cos i$. Differentiating equation (4.7) partially with respect to μ_1, keeping ϕ_1 constant,

$$\frac{\partial\mu}{\partial\mu_1} = \mu_0 - \mu_1 \frac{\sin i \cos\phi_1}{\sin\theta_1} = \frac{\mu_0 - \mu\mu_1}{\sin^2\theta_1}. \tag{4.8}$$

Thus

$$P_n'(\mu)\sin\theta\cos\eta\sin\theta_1 = P_n'(\mu)(\mu_0-\mu\mu_1) = \sin^2\theta_1\frac{\partial}{\partial\mu_1}[P_n(\mu)]. \tag{4.9}$$

Using this relation the second term in the integral in equation (4.5) can be integrated by parts, and (4.5) further reduces to

$$H_e = \frac{6}{\pi(3-u)}\sum_{n=1}^{\infty} a_n \int_{\mu_1=0}^{1}\left[\int_{\phi_1=0}^{\pi} P_n(\mu)\,d\phi_1\right][(1-u)(\{n-2\}\mu_1^2+1) + u(\{n-3\}\mu_1^3+2\mu_1)]d\mu_1. \tag{4.10}$$

By integrating the addition formula (3) for Legendre polynomials with respect to ϕ_1 it is seen that

$$\int_{\phi_1=0}^{\pi} P_n(\mu)\,d\phi_1 = \pi P_n(\mu_1)\,P_n(\mu_0). \tag{4.11}$$

Using this formula in conjunction with the following relations

$$\left.\begin{aligned} &\int_0^1 P_n(\mu)\,d\mu = \frac{P_{n-1}(0)}{n+1}\,; \qquad \int_0^1 \mu P_n(\mu)\,d\mu = \frac{P_{n-2}(0)}{n(n+2)}\,; \\ &(n-2)\int_0^1 \mu^2 P_n(\mu)\,d\mu = -\frac{2P_{n-1}(0)}{(n+1)(n+3)}\,; \\ &(n-3)\int_0^1 \mu^3 P_n(\mu)\,d\mu = -\frac{6P_{n-2}(0)}{n(n+2)(n+4)} \end{aligned}\right\} \tag{4.12}$$

for $n = 1, 2, \ldots \infty$, where $P_{-1}(0)$ is defined by $P_{-1}(0) = 1$, H_e can finally be written in the form

$$H_e = \frac{6}{3-u}\sum_{n=1}^{\infty} a_n P_n(\mu_0)\left[\frac{1-u}{n+3}P_{n-1}(0) + \frac{2u(n+1)}{n(n+2)(n+4)}P_{n-2}(0)\right]. \tag{4.13}$$

5. *H_e in terms of $H_{sr}(\mu)$.*—By transforming equation (3.3) the a_n are given by

$$a_n = \frac{n+\frac{1}{2}}{n+1}\int_{-1}^{+1} H_{sr}(\mu)\,P_n(\mu)\,d\mu. \tag{5.1}$$

Equation (4.13) can then be written

$$H_e(\mu_0) = \int_{-1}^{+1} H_{sr}(\mu) f(\mu,\mu_0)\,d\mu, \tag{5.2}$$

where

$$f(\mu,\mu_0) = \frac{6}{3-u}\sum_{n=1}^{\infty}(n+\tfrac{1}{2}) \times\left[\frac{1-u}{(n+1)(n+3)}P_{n-1}(0) + \frac{2u}{n(n+2)(n+4)}P_{n-2}(0)\right]P_n(\mu)\,P_n(\mu_0). \tag{5.3}$$

For large n, $P_n(0) \simeq \cos\frac{n\pi}{2}\sqrt{\frac{2}{n\pi}}$; also, $|P_n(\mu)\,P_n(\mu_0)| \leqslant 1$ for μ and μ_0 in the ranges $|\mu| \leqslant 1$, $|\mu_0| \leqslant 1$. Thus the terms in the above series tend to zero at least as fast as $n^{-3/2}$. The series is therefore convergent, although rather slowly. $f(\mu,\mu_0)$ was computed numerically, with $u = 0{\cdot}45$, for a series of values of μ and μ_0. The function is shown graphically in Fig. 2*a*. For the purpose of calculation the first 32 terms of the series in equation (5.3) sufficed, in general, for the order of accuracy required. Tallquist's tables (4) were used for the P_n. In the region $\mu = 1$, $0 < \mu_0 < 0{\cdot}2$ it was found necessary to make a correction for the remainder of the series. This was carried out by taking the asymptotic forms of $P_n(0)$ and $P_n(\mu)$ for

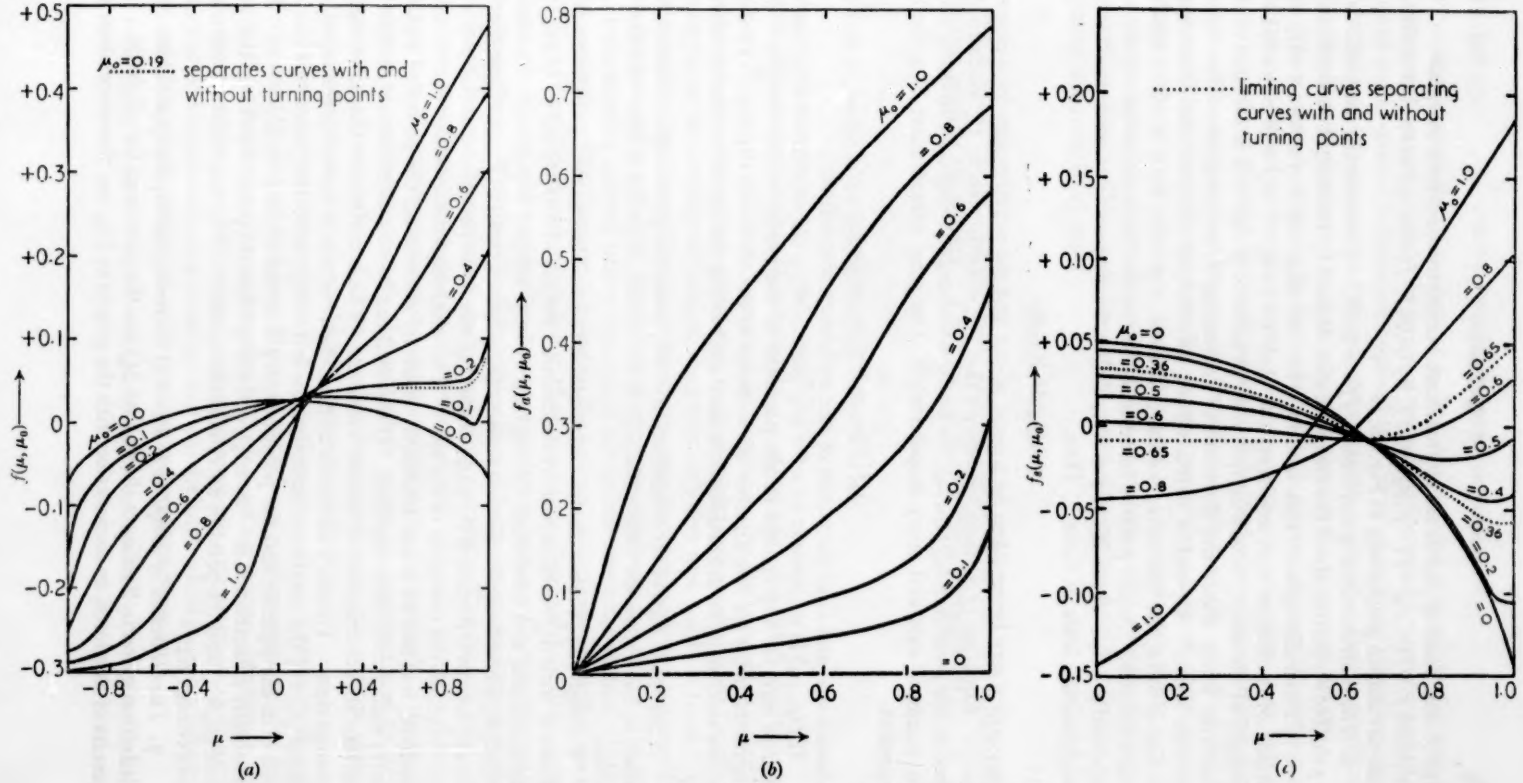

FIG. 2.—*Functions giving H_e in terms of magnetic flux at star surface.*

large n and making the usual approximate transformation into integrals. The functions $f_s = f(\mu, \mu_0) + f(-\mu, \mu_0)$ and $f_a = f(\mu, \mu_0) - f(-\mu, \mu_0)$ were also derived; these are shown graphically in Fig. 2*b*, *c*.

6. *The contribution of a single shell of force to H_e.*—Consider the magnetic field in a shell of revolution about the magnetic axis, defined by two neighbouring lines of force in a meridian-plane cross-section. Let the magnetic flux across a strip of a surface of revolution that intersects the shell be $2\pi\Delta Q$. ΔQ will be called the strength of the shell; it will be reckoned as positive if the field is directed in the clockwise sense about the direction of increasing ϕ, and negative when in the opposite sense. A point of exit is where, travelling in the clockwise sense along the line of force, the line leaves the star; likewise, a point of entry is where the line enters the star. At any point of intersection of the shell with the surface of the star let μ and $\mu + \Delta\mu$, where $\Delta\mu$ is positive, define the intersections made by the two neighbouring lines of force. Then

$$\pm \Delta Q = H_{sr}(\mu)\, \Delta\mu, \tag{6.1}$$

the positive sign being taken for a point of exit and the negative sign for a point of entry. Equation (5.2) therefore shows that the contribution to H_e made by the shell at this point is $\pm \Delta Q f(\mu, \mu_0)$, the positive and negative signs again being taken for points of exit and entry respectively. The total contribution of a shell is therefore

$$\Delta Q\,[f(\mu_1, \mu_0) - f(\mu_2, \mu_0)], \tag{6.2}$$

where $\mu = \mu_1$ and μ_2 at the points of exit and entry, respectively.

If $f(\mu, \mu_0)$ is monotonic in μ for any particular μ_0 the expression (6.2) cannot change sign for any change in the positions of the points of intersection. The argument holds for any number of re-entries of the shell into the star. Thus for such a value of μ_0 no distortion of the shell can reverse the sign of its contribution to H_e.

A change in sign of the contribution is only possible, given suitable distortions, when μ_0 has values for which $f(\mu, \mu_0)$, as a function of μ, has at least one turning point.

For a given μ_0 the maximum and minimum contributions that could be made by the shell, with ΔQ taken as positive for definiteness, are when $f(\mu_1, \mu_0) - f(\mu_2, \mu_0)$ has its maximum and minimum values, respectively, subject to $\mu_1 > \mu_2$. To take an example, when the star is viewed pole-on ($\mu_0 = 1$) the graphs in Fig. 2*a* show that the maximum contribution is $0{\cdot}77\Delta Q$, occurring when the points of exit and entry are convected to the two poles of the star. The minimum contribution in this case is positive, but can be made arbitrarily small by convecting the points of exit and entry sufficiently close together. If the shell can be convected entirely below the surface its contribution of course vanishes. The contribution therefore cannot change sign. To take a second example, when the star is viewed in the equatorial plane ($\mu_0 = 0$) the maximum contribution is $0{\cdot}10\Delta Q$, occurring when the point of exit is at the equator and the point of entry is at the south pole ($\mu_0 = -1$). The minimum contribution is $-0{\cdot}10\Delta Q$, occurring when the point of exit is at the north pole ($\mu_0 = 1$) and the point of entry is at the equator. The contribution can therefore change sign.

7. *The behaviour of complete fields.*—(*a*) Unrestricted dipole-type fields. The definition given in Section 2 shows that ΔQ has the same sign for all shells. The results of Section 6, in conjunction with the graphs in Fig. 2*a*, therefore show that

H_e cannot change sign if $0{\cdot}19 \leqslant \mu_0 \leqslant 1$, but that reversal is possible, for suitable distortions, if $0 \leqslant \mu_0 < 0{\cdot}19$. In terms of the inclination i of the magnetic axis to the line of sight, reversal is therefore impossible if $i \leqslant 79°$. It could take place, however, for inclinations greater than 79° if movements of gas of sufficient amplitude, alternately northwards and southwards, took place at the surface of the star.

The maximum range in H_e for cases in which reversal is possible arises when the star is viewed in the equatorial plane ($\mu_0 = 0$). H_e can then vary between $\pm 0{\cdot}10Q$, where Q is the total shell strength of the field when these extreme values occur. The maximum value $+0{\cdot}10Q$ is effected when all the points of exit are convected into a small area near the equator while the points of entry are compressed into a small area near the south pole. The minimum value $-0{\cdot}10Q$ arises when the points of exit are all near the north pole and the points of entry are near the equator. The shell strength Q_0 for a dipole-type field is given by integrating equation (6.1) thus:

$$Q_0 = \int_{\mu'}^{1} H_{sr}(\mu)\, d\mu, \tag{7.1}$$

where $\mu = \mu'$ is the point at which the limiting shell of force that just fails to leave the star touches the surface. For a simple dipole field, for example,

$$H_{sr} = \mu H_p,$$
$$\mu' = 0, \tag{7.2}$$

where H_p is the polar field strength; thus

$$Q_0 = \tfrac{1}{2} H_p \tag{7.3}$$

The extreme values of H_e attainable by distorting this field are therefore $\pm 0{\cdot}05\, H_p Q/Q_0$. If the movement of gas producing the distortion is confined to a thin layer near the surface of the star, such as might be expected from Cowling's work (**1**) on horizontal oscillations, then relatively few new shells of force would be convected to the surface from inside the star, and few existing ones would be carried below the surface. According to a theorem of Bondi and Gold (**5**) no lines of force running entirely below the surface can appear above the surface whatever the motions. This theorem is based on the fact that in hydrodynamic flow no two adjacent particles can be separated. However, hydrodynamic flow often breaks down at surfaces, as for example when a greased body in water floats to the top and breaks surface. Fluid motion is free along lines of force, hence the surface of shells of force behave like greased surfaces in this respect. The Bondi and Gold theorem therefore breaks down; the effective shell strength Q might therefore vary if suitable motions arose in the interior of the star. For example, if the neutral point were convected towards the surface it might be expected that Q would increase, and vice versa. But, as has just been mentioned, for surface motions $Q \simeq Q_0$ in any case, thus H_e would vary between $\pm 0{\cdot}05\, H_p$.

Hence in general the variation in H_e is within $\pm 0{\cdot}05\, H_p$. To take an example, for the star HD 125248 Babcock (**6**) gives a variation of approximately $\pm$ 2000 gauss in H_e.* Therefore in the undistorted field $H_p > 4 \times 10^4$ gauss. Moreover, since the case on which this limit is based probably represents a far more severe distortion than could be realized in any actual gas motion, the limit would probably have to be exceeded by a large margin in order to show the required range in H_e.

* The figures -6000 to $+7000$ actually quoted refer to an equivalent polar field strength equal to $H_e/0{\cdot}303$.

(*b*) Symmetrical dipole-type fields. It should be noted in the previous example that the gas motions required to reverse H_e are not symmetrical about the equatorial plane. If the actual motions are symmetrical and the undistorted field is symmetrical, as seems more likely for mechanical reasons, the field remains symmetrical during the oscillation cycle. In this case $H_{sr}(-\mu) = -H_{sr}(\mu)$, and equation (5.2) can be written

$$H_e(\mu_0) = \int_0^1 H_{sr}(\mu) f_a(\mu, \mu_0)\, d\mu. \tag{7.4}$$

The contribution of a single shell of force intersecting the surface at $\pm\mu$ is therefore $\Delta Q f_a(\mu, \mu_0)$. The graphs in Fig. 2*b* show that $f_a(\mu, \mu_0) \geqslant 0$ for all relevant μ and μ_0. Reversal of H_e is therefore impossible in all cases.

(*c*) Symmetrical quadrupole-type fields. Here $H_{sr}(-\mu) = H_{sr}(\mu)$, thus equation (5.2) can be written

$$H_e(\mu_0) = \int_0^1 H_{sr}(\mu) f_s(\mu, \mu_0)\, d\mu. \tag{7.5}$$

Again only the field in the northern hemisphere ($0 < \mu \leqslant 1$) need be considered. This part of the field contains only one circular neutral point, and it can therefore be treated as an unrestricted dipole-type field. The same argument as in part (*a*) of this section can therefore be applied in conjunction with the graphs of $f_s(\mu, \mu_0)$ in Fig. 2*c*. These graphs show that reversal is allowed if $0{\cdot}36 < \mu_0 < 0{\cdot}65$, corresponding to $49^\circ{\cdot}5 < i < 68^\circ{\cdot}9$.

Using arguments similar to those employed in the second part of (*a*) it can be shown that for HD 125248 $H_p > 8 \times 10^5$ gauss, where H_p is the polar strength of an undistorted quadrupole field.

(*d*) Unrestricted quadrupole-type fields. If $0{\cdot}19 \leqslant \mu_0 \leqslant 1$, $f(\mu, \mu_0)$ is monotonic in μ, thus the two systems of shells associated with the two circular neutral points make contributions to H_e of opposite signs. By convecting all the lines of force of one of the systems, say the one with positive shell strength, assumed to be in the northern hemisphere for definiteness, into the same region, or by convecting them below the surface, the contribution of this system can be made arbitrarily small. The negative system would then predominate and H_e would be negative. By similarly suppressing the negative system instead H_e could be made positive. H_e can therefore be made to reverse.

If $\mu_0 < 0{\cdot}19$, then by sufficiently suppressing one of the systems the field can be made to behave like a dipole-type, and the results of part (*a*) of this section show that reversal is again possible.

(*e*) Other fields. An example will be given of a symmetrical field that can change sign for all inclinations.

Consider a symmetrical field with four circular neutral points, the two neutral points in each hemisphere having opposite polarities. The contributions of the two systems in one hemisphere have opposite signs, hence by suppressing each system in turn H_e can be made to change sign. Surface motions would be sufficient for producing this reversal.

8. *Statistical considerations.*—There are two statistical reasons why it is unlikely that any axially symmetric dipole-type or quadrupole-type field with the additional restriction of symmetry about the equatorial plane can account for the fields actually observed.

In the first place, the ranges of i within which reversal is possible are rather narrow. If it is assumed that the axes of the stars are randomly orientated then, for unsymmetrical dipole-type fields the condition $i<79^\circ$ means that less than 19 per cent of the stars could have reversing fields. For symmetrical quadrupole-type fields the range $49^\circ{\cdot}5<i<68^\circ{\cdot}9$ means that less than 29 per cent of the stars could show reversal. Further, for the reasons mentioned in (*a*) of Section 7, the above limiting percentages are probably far in excess of what would actually occur.

A recent table of magnetic variables given by Babcock (**2**), however, lists 35 stars of which 37 per cent are definitely reversing, while it seems likely that some of the others will eventually turn out to be reversing.

Secondly, it was shown in Section 7 that, for the unsymmetrical dipole types, the median strength of the field at the poles of a star in which reversal is observable is at least 20 times the extreme values observed in H_e. The same star if viewed pole-on would therefore show an H_e of at least 6 times the extreme reversing value. A similar argument holds for the symmetrical quadrupole types. It would be expected from this that, on the whole, those stars that do not show reversal would have a much higher H_e than the reversing ones. Babcock's table, on the other hand, lists a total of 13 reversing stars for which the mean range in H_e ($=0{\cdot}303\times$ tabulated H_p) is about ± 840 gauss, while 10 non-reversing stars in which the variation is given have a mean H_e of about 810 gauss, a comparable value.

9. *Conclusions.*—It has been shown in the present paper that, in oscillation theories, the simplest magnetic fields, i.e. axially symmetrical dipole and quadrupole types are capable of showing a reversing H_e when suitable gas motions can be maintained in the stars, provided the magnetic axes are suitably inclined to the line of sight. The gas motions referred to need only be confined to the surface layers. It is unlikely, however, for statistical reasons, that, with the exception of the non-symmetrical quadrupole types, such fields could account for the observations. More complex or non-axially symmetric fields are required in oscillation theories.

University of London Observatory,
Mill Hill Park,
London, N.W.7:
1954 *August* 16.

References

(1) T. G. Cowling, *M.N.*, **112**, 527, 1952.
(2) H. W. Babcock and T. G. Cowling, *M.N.*, **113**, 357, 1953.
(3) See E. T. Whittaker and G. N. Watson, *Modern Analysis* (4th edition), p. 328, Cambridge, 1952.
(4) H. Tallquist, *Acta. Soc. Sci. Fenn.* A, **2**, No. 11, 1938.
(5) H. Bondi and T. Gold, *M.N.*, **110**, 607, 1950.
(6) H. W. Babcock, *Ap. J.*, **114**, 1, 1951.

ON THE DEVELOPMENT OF THE Fe I CHROMOSPHERIC LINES DURING THE 1951 ECLIPSE OF 31 CYGNI*

Anne B. Underhill

(Received 1954 May 3)

Summary

The development of the Fe I lines λλ 3920, 3922, 3927 and 3930 in the chromospheric spectrum of 31 Cygni during ingress is studied from high-dispersion spectrograms. Intensity tracings of the B-type spectrum and chromospheric features are presented and a light curve of the B star during ingress is derived. It is found that the light of the B star at λλ 3915–3950 is reduced relative to that from the K star for several days prior to first contact. Evidence is presented that this dimming, which is probably caused by continuous absorption, and a sudden increase in the equivalent widths of the Fe I lines occur when the line of sight begins to pass through a dense region in the atmosphere of the K star. It is found that the Fe I lines are somewhat broadened by turbulence.

Although chromospheric absorption lines of Ca II appear in the spectrum of 31 Cygni some two to three months before the total eclipse of the B star by the K star, chromospheric lines due to Fe I are not observed until just a few days before eclipse. The present paper traces the development of some of these lines during the 1951 eclipse of 31 Cygni. A good series of high-dispersion plates was obtained at the Dominion Astrophysical Observatory during the last days of ingress, but because of unfavourable weather few plates were obtained during the first days of egress. Consequently it is possible to study in detail the development of the Fe I chromospheric lines during ingress only. All of the plates were obtained under the direction of A. McKellar and all are calibrated for intensity work.

The observations.—The chromospheric Fe I lines are barely perceptible on a plate taken 12 days before totality and are definitely absent 15 days after totality. The present study will be based on the series of third-order grating plates, dispersion 4·6 A mm at λ 3925, obtained during ingress, together with plates of the K-type spectrum obtained during totality and plates of the composite spectrum obtained in June and July of 1952. All of the plates used give spectra of excellent definition and good density in the region $3900 < \lambda < 4000$ A.

In order to separate the chromospheric features from those due to the B-type star, it is convenient to study chromospheric lines which fall in regions free from B-type absorption lines. For this reason and because the lines appearing early in the chromospheric spectrum are intrinsically strong lines arising from the ground level of the carrier atom, the lines λλ 3920·260, 3922·914, 3927·922 and 3930·299 of multiplet number 4 (1) of Fe I were chosen for study. The other lines in this multiplet were found to be unsuitable for detailed study either because they lay in the wing of a B-type hydrogen line, or because they were disturbed by strong features which could not be unambiguously defined in the K-type spectrum.

* *Contributions from the Dominion Astrophysical Observatory*, No. 37. Published by permission of the Deputy Minister, Department of Mines and Technical Surveys, Ottawa, Canada.

Microphotometer tracings magnified 100× in the direction of the dispersion were made of all the plates for the wave-length region $3700 < \lambda < 4100$ A, and these density records were transformed to intensity tracings magnified 200× in the direction of the dispersion and rectified so that the apparent continuum lay at a height of 10 inches above the level of zero light for all wave-lengths. A correction of 5 per cent of the continuous spectrum was made to allow for the grating ghosts. In all the spectra peak intensities were found to occur at certain well-defined wave-lengths. The apparent continuum was determined by putting a smooth line through these points of peak intensity. Particularly in the region $3900 < \lambda < 4000$ A it was found that this apparent continuum could be consistently and uniquely defined. All the measures of intensity on any one plate are made with reference to this apparent continuum, which hereafter will be referred to as "the continuum". In the region $3915 < \lambda < 3950$ A, which is to be studied here, the continuum represents the mean peak intensity of short spectral regions near $\lambda 3915$ and $\lambda 3950$. At all phases in the light variation of 31 Cygni, the monochromatic flux at these wave-lengths is greater than that at any neighbouring wave-lengths. It is not assumed that this mean peak intensity, called here the continuum, represents the true intensity of the light which would be emergent from both stars if there were no absorption lines present. That level of light intensity represents strictly the sum of the continua of the two stars. However, the true continuum is an unobservable quantity for a K star in the wave-length region being studied and is of limited practical interest.

In the study of narrow spectral lines, the distortion of the true shape of the absorption line by the instrumental profile of the spectrograph may be important, especially in the case of astronomical spectra, which are usually obtained with a relatively wide slit. The instrumental profile of the spectrograph (designated Litt GIII, BL84) was estimated by deriving the mean profile of the four lines $\lambda\lambda 3920$, 3922, 3927 and 3930 in the iron arc comparison spectrum. The central part of the profile was obtained from lightly exposed spectra, while the wings were derived from heavily exposed spectra. The mean instrumental profile is given in Table I. The linear dispersion on the tracings is about 0·586 A/inch in this wave-length region. For each individual line no measurements were made over wave-length regions where a blending line might be suspected to occur. The asymmetry of the wings of the instrumental profile reflects the asymmetrical distribution of the intensities of the grating ghosts, one of which lies very close to the main line. With this instrumental profile estimates were made of the instrumental distortion that might be present in the observed profiles of the stellar features. It was found that the central parts of the observed profiles of narrow lines had been distorted by the spectrograph and that the true line profiles are deeper, by approximately 15 per cent of the continuum, than the observations indicate. In view of the large observational uncertainties in the final line profiles (see below), it hardly seems significant to attempt to correct the observations for instrumental broadening. However, instrumental broadening is an important source of error in the numerical value of any result dependent on the measured apparent residual intensities of the narrow spectral lines.

The tracings described above give the variation with wave-length of the intensity of radiation of the K star alone (from spectra obtained during totality), of the K star plus the B star (from spectra obtained when the stars were far from eclipse), and of the K star plus B star plus chromospheric features (from spectra

obtained during atmospheric eclipse). In each case these intensities for the wave-length range $3915<\lambda<3950$ A are expressed relative to the peak intensities at $\lambda 3915$ and $\lambda 3950$. It is evident that if the mean brightnesses at these wave-lengths of the B star and of the K star are b and k, respectively, and that if $b+k=1$, then if the intensity tracing for the K star be reduced in vertical scale by a factor k and subtracted from the tracing for the K star plus B star, the result will be an intensity tracing giving the B-type spectrum. Since the spectrum of the B star

TABLE I

Instrumental profile for Litt GIII BL84 spectrograph

x*	Intensity	x	Intensity
−13	0·0	+ 2	25·8
12	0·2	3	13·9
11	0·4	4	7·1
10	0·8	5	4·6
9	0·9	6	3·8
8	1·3	7	3·5
7	1·8	8	2·7
6	1·5	9	1·9
5	1·0	10	0·9
4	2·8	11	1·6
3	10·2	12	1·0
2	29·3	13	1·0
− 1	75·6	14	1·0
0	100·0	15	0·8
+ 1	71·1	+16	0·2

* Units of x are 0·1 inch on a tracing magnified 200× from the plate in the direction of the dispersion. Negative displacements are to the violet; positive to the red. Tracings were made from a plate having a projected monochromatic slit-width of 0·0020 inches.

is known to have constant intensity (no absorption lines except perhaps a narrow, weak K-line) over the wave-length interval $3915<\lambda<3950$ A, the result of the subtraction should be a straight line at intensity $1-k$. Similarly if the K-type spectrum reduced in vertical scale by the factor k be subtracted from a tracing of the K star plus B star plus chromospheric features, the result will be a tracing giving the B-type spectrum as a straight line at intensity $1-k$ with absorption lines at the wave-lengths of the chromospheric features. The relative brightness of the B star to the K star will be

$$\alpha=(1-k)/k. \qquad (1)$$

Intensity tracings of the B-type spectrum and of the B-type spectrum plus chromospheric features have been obtained by this method from the intensity tracings of the composite spectrum of 31 Cygni at various phases. The subtraction of the tracings is done semi-automatically using the intensitometer of this Observatory in the manner described by K. O. Wright (**2**). The ratio k by which to reduce the K-type spectrum is found by trial. A series of tracings of the K-type spectrum reduced by a series of factors k is prepared; by superposing these tracings in turn on a tracing of the composite spectrum one may quickly determine which value of k yields a result such that the B-type spectrum in regions outside the chromospheric lines falls along a line of constant intensity $1-k$. The tracing of the B-type spectrum will vary in a random manner about the constant value

$1-k$ which represents the continuum of the B star, for the irregularities due to grain will be somewhat increased over those for a single tracing. The mean tracing from two grating plates obtained during totality was used as the standard intensity tracing of the K-type spectrum. The resultant intensity tracings of the B star alone, the B star plus chromospheric features and the K star alone are shown in Figs. 1 and 2. The result for the B star alone (phase +258 days) is the mean of two plates, while those for the B star plus chromospheric features are each from one plate. In spite of the irregularities due to grain and to small differences in placing the continuum on each original tracing, it is clear that the main features of the growth in complexity of the chromospheric spectrum are portrayed.

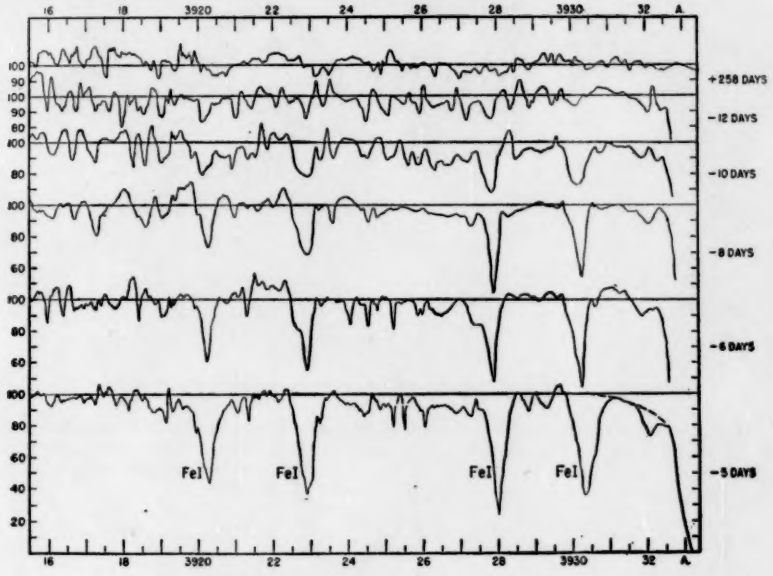

FIG. 1.—*The chromospheric spectrum of 31 Cygni at various phases during ingress in the atmospheric eclipse. The intensity is expressed in terms of the continuum of the B star. The phase is recorded in days from second contact, 1951 August 12. The spectrum of the K star has been subtracted, leaving only the spectrum of the B star as it is modified by passage through the outer layers of the atmosphere of the K star.*

If during the atmospheric eclipse because of obscuration or occultation the B star appears fainter with respect to the K star than when the stars are far apart, the empirically determined factor k will increase to k'. The apparent relative brightness of the B star to the K star will then be

$$\alpha' = \beta\alpha = (1-k')/k'. \qquad (2)$$

Hence one will be able to determine the loss of light of the B star relative to the mean intensity of the K star in the wave-length range $3915 < \lambda < 3950$ A. The results are given in Table II. The phase during ingress is counted in days from second contact, which is assumed to have occurred (3) on 1951 August 12 (U.T.). During egress the phase is measured in days from third contact, 1951 October 13 (U.T.). The second column of Table II gives the phase, the third gives the

empirically determined ratio k or k', the fourth gives α or α', while the fifth gives β, the factor by which the light of the B star has been reduced. The uncertainty in the determination of the factor k is about $\pm 0{\cdot}03$. This results in an uncertainty of

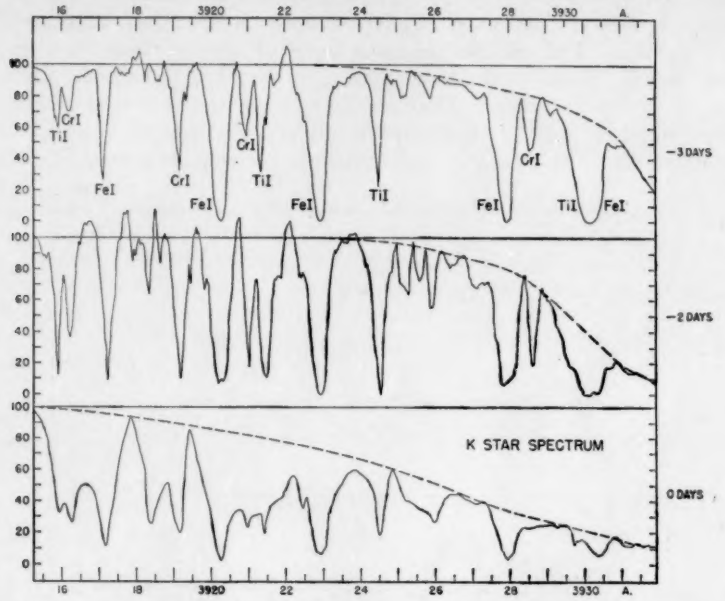

FIG. 2.—*The chromospheric spectrum of 31 Cygni just before totality and the spectrum of the K star during totality. The intensity of the chromospheric spectrum is expressed in terms of the continuum of the B star. The intensity of the K-type spectrum is expressed in terms of the apparent continuum of the K star in the spectral range* λλ 3915–3950.

TABLE II

Light curve of the B star at λλ 3915–3950

Date U.T.	Phase	k	α	β
1951 July 31·3	−12 days	0·30	2·3	1·00
Aug. 2·3	−10	0·30	2·3	1·00
Aug. 4·3	− 8	0·30	2·3	1·00
Aug. 6·3	− 6	0·33	2·0	0·87
Aug. 7·3	− 5	0·36	1·8	0·76
Aug. 9·3	− 3	0·40	1·5	0·64
Aug. 10·3	− 2	0·60	0·7	0·29
Aug. 12·8*	0	1·00	0·0	0·00
Oct. 15·2	+ 3	0·40	0·7	0·29
1952 June 25·9*	+258	0·30	2·3	1·00

* The mean date of two exposures.

some 20 to 25 per cent in α. However, even such a large uncertainty does not mask the result that the light received from the B star begins to decrease some time near phase −6 days, and that the loss of light increases rapidly with the approach of second contact.

The equivalent widths of the chromospheric Fe I lines λλ 3920, 3922, 3927 and 3930 were measured at each phase, and are presented in Table III. The mean equivalent width of the four lines is given in the last column. At phases −3, −2 and +3 days this mean is for λλ 3920, 3922 and 3927 only, since at these phases a moderately strong chromospheric line of Ti I blends with Fe I λ3930. These mean equivalent widths are plotted against time in Fig. 3, which shows a general similarity to comparable curves for ζ Aurigae (4).

TABLE III

Equivalent widths of chromospheric Fe I lines

Date U.T.	Phase Days	λ3920 A	λ3922 A	λ3927 A	λ3930 A	Mean A
1951 July 31·3	−12	0·04	0·03	0·05	0·02	0·04
Aug. 2·3	−10	·08	·11	·13	·15	·12
Aug. 4·3	− 8	·08	·13	·16	·15	·13
Aug. 6·3	− 6	·10	·15	·22	·18	·16
Aug. 7·3	− 5	·29	·29	·30	·35	·31
Aug. 9·3	− 3	·51	·57	·56		·55
Aug. 10·3	− 2	·51	·56	·58		·55
Oct. 15·2	+ 3	·44	·49	·70		·54

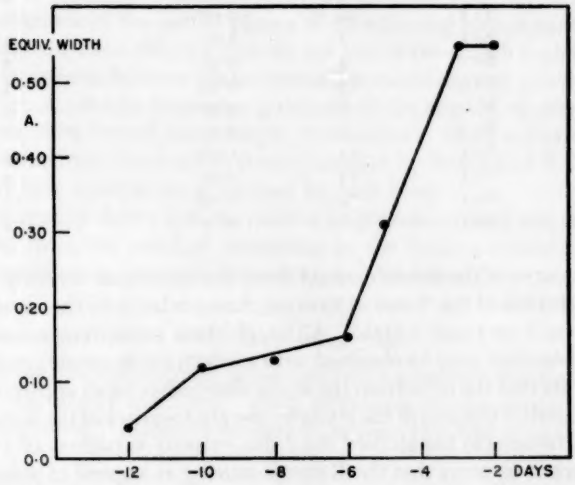

FIG. 3.—*The growth of the chromospheric Fe I lines of 31 Cygni. The mean equivalent width of the lines λλ 3920, 3922, 3927 and 3920 is plotted against the phase expressed as days before second contact.*

Discussion.—The growth of the chromospheric spectrum as the B star approaches the photosphere of the K star is illustrated in Figs. 1 and 2. At phase −12 days the Fe I lines λλ 3920, 3922, 3927 and 3930 are barely visible although the *K* line of Ca II is quite strong. However, two days later the Fe I lines are quite distinct. These lines increase in strength as the light from the B star traverses deeper and deeper layers of the atmosphere of the K star. By phase −3 days many other chromospheric lines have appeared. The strongest of these

lines, identified from Miss Davis' list of lines in the spectrum of β Pegasi (**5**) and from the *Revised Multiplet Table* (**1**), are listed in Table IV. They arise from energy levels with excitation potentials from 0 to 3 volts, and they strengthen greatly as the line of sight approaches the photosphere of the K star. Their relative intensities are roughly as in the K-type star except for Fe I λ3918, which is weak relative to Cr I λ3919. Also the relative intensities of Ti I λ3915 and Cr I λ3916 appear to be reversed in the chromosphere to what they are in the K star. However, in view of the observational uncertainties of the intensity tracings shown in Figs. 1 and 2, it is not certain that this apparent reversal is significant.

TABLE IV

Chromospheric lines in the region $3915 < \lambda < 3933$ *A*

Laboratory λ	Element	Multiplet number	Low E.P.	Phase from second contact at which first seen
			eV	days
3915·88	Ti I	15	0·02	− 3
3916·24	Cr I	23	0·96	− 3
3917·18	Fe I	20	0·99	− 3
3919·16	Cr I	23	1·03	− 3
3920·26	Fe I	4	0·12	−12
3921·02	Cr I	23	0·98	− 3
3921·42	Ti I	14	0·00	− 3
3921·80	Zr I	8	0·07	− 3
3922·91	Fe I	4	0·05	−12
3924·53	Ti I	13	0·02	− 3
3925·24	V I	8	0·07	− 5
3927·92	Fe I	4	0·11	−12
3928·64	Cr I	23	1·00	− 5
3929·88	Ti I	13	0·00	− 3
3930·29	Fe I	4	0·09	−12
3933·66	Ca II	1	0·00	−72

The light curve of the B star derived from the spectra as set forth in Table II gives the brightness of the B star at various phases relative to the mean brightness of the K star at λ3915 and λ3950. Although these measurements are inferior in accuracy to those that may be obtained with modern photometric equipment, they serve to indicate that the light from the B star diminishes by an appreciable amount before occultation of the disk of the B star by the photosphere of the K star can occur. Miss Vinter Hansen (**6**) has studied the radial-velocity variations of 31 Cygni and from her work it appears that the B star is moving at a speed of about 35 km/sec with respect to the K star. General considerations suggest that the spectral type of the B star is about B3 V or B5 V and that its diameter probably does not exceed 10 solar radii. Since a star moving at a speed of 35 km/sec takes 2·3 days to traverse a distance of 10 solar radii, it follows that the occultation of the disk of the B star will probably not commence prior to phase −3 days. However, our observations indicate that by this time approximately one-third of the light of the B star had been extinguished. It is suggested that at about phase −6 days the line of sight begins to pass through a more dense region of the atmosphere of the K star, and that this region causes an extinction of the light of the B star. This extinction is not due to the occurrence of chromospheric absorption lines, for the present results are based on a comparison of the flux from the B star with that from the K star in spectral

regions free from chromospheric line absorptions. It must be caused by some process varying little with wave-length in the region $3915 < \lambda < 3950$ A. It is assumed that no significant intrinsic fluctuations in the light of the K star (or of the B star) occurred during the period of observation. Unpublished observations by C. M. Huffer* and observations by F. Bradshaw Wood (**7**) indicate that the light of the K star was constant during totality. Also unpublished observations by E. F. Carpenter* indicate that during egress there was extinction in the ultra-violet similar to that found here for ingress. Wood (**7**) also presents photometric data for egress, suggesting that atmospheric extinction plays an important part in the eclipse.

The conclusion that before first contact the B star may be partially obscured by continuous absorption in the atmosphere of the K star is supported by observations of ζ Aurigae. Fracastoro (**8**), from a spectrophotometric study of low-dispersion plates of ζ Aurigae obtained during the 1947–48 eclipse, finds for ζ Aurigae that the light of the B star has been dimmed by some 25 per cent at λ 3933 when first contact occurs. Roach and Wood (**9**), from a detailed study of photometric data on the eclipse of ζ Aurigae, also conclude that the B star is dimmed, particularly at shorter wave-lengths, by chromospheric absorption in the atmosphere of the K star. They conclude that the dimming is chiefly due to the growth of chromospheric absorption lines, although they cannot rule out the possibility that it is due to continuous absorption in the atmosphere of the K star. Photometric observations of the partial phases of an eclipsing system such as 31 Cygni, made with narrow-band filters which do not pass wave-length regions containing strong chromospheric features whose intensities would change greatly with phase, would be of great value in determining accurately the amount of extinction at each wave-length and its overall wave-length dependence. Only a limited interpretation can be made from data such as those discussed by Roach and Wood because of the relatively long spectral range covered by each filter.

It may be readily shown that the relative brightness of the B and the K star may be estimated from the residual intensities in the totality spectrum and in the composite spectrum at phases far from eclipse. We have

$$\alpha = \frac{R_{BK} - R_K}{1 - R_{BK}}, \tag{3}$$

where R_{BK} is the residual intensity in the composite spectrum and R_K is the residual intensity in the totality spectrum. Both intensities are measured relative to the apparent continuum. Equation (3) may be written in terms of equivalent widths (W):

$$\alpha = \frac{W_K}{W_{BK}} - 1. \tag{4}$$

It is assumed that the intensity in the B-type spectrum is independent of wave-length and that the absorption lines appearing are due solely to the K star.

From the apparent residual intensities at the centres of the lines $\lambda\lambda$ 3920, 3922, 3927, 3930 and 3944, the mean value of α is 1·7. From the equivalent widths of regions centred on these lines and about 1 A wide $\alpha = 1{\cdot}9$. The result found above from the subtraction of the intensity tracings is $\alpha = 2{\cdot}3$. The value 2·3 is felt to be more correct than the other values, for it is found by a method in which the distortions due to instrumental broadening are not important. The effects of

* Private communication to A. McKellar.

instrumental broadening on the present spectra are sufficient to cause the differences in α noted here. The use of equations (3) and (4) to estimate α is not to be recommended except for spectra insignificantly distorted by the spectrograph. Theoretically equation (4) should not be affected by instrumental broadening, but practically it is difficult to be sure of integrating the whole broadened profile when W is measured in a many-lined spectrum such as the present one.

The variation of the mean equivalent widths of the Fe I lines $\lambda\lambda$ 3920, 3922, 3927 and 3930 with time during ingress is shown in Fig. 3. It is significant that a rapid increase in strength occurred after phase -6 days when the light of the B star first became dimmed. The lines do not change appreciably in equivalent width after phase -3 days. This is probably because the lines have become saturated and the curve of growth has become more or less flat. Reference to studies of K-type spectra by K. O. Wright (**10**) shows that the curve of growth begins to flatten out when the equivalent width is about 0·1 A. This growth in strength of the Fe I chromospheric lines is similar in many respects to that of the Ca II K line (**11**).

If it be assumed that the Fe I lines fall on the linear part of the curve of growth, as seems likely when the equivalent widths of these lines are small, then the equivalent width will be proportional to the number of atoms in the line of sight. If the density of neutral Fe atoms is $\rho(r)$ at a distance r from the centre of the K star, then the number of atoms in an element of length ds along a column 1 cm^2 in cross-section which passes within a minimum distance p from the centre of the star is

$$dN = \rho(r)\,ds = \rho(r)\,p\,\mathrm{cosec}^2\phi\,d\phi, \tag{5}$$

where ϕ is the angle between the radius r passing through the element of volume and the line of sight. The total number of atoms in the line of sight is

$$N(p) = p\int_{\varphi_1}^{\varphi_2}\rho(r)\,\mathrm{cosec}^2\phi\,d\phi, \tag{6}$$

where ϕ_1 and ϕ_2 are the limiting values of ϕ. If R be the outer radius of the zone containing neutral Fe I atoms, that is, the outer radius of the stellar atmosphere, then

$$N(p) = 2p\int_{\sin^{-1}p/R}^{\pi/2}\rho(r)\,\mathrm{cosec}^2\phi\,d\phi. \tag{7}$$

For purposes of illustration let us assume that

$$\rho(r) = C/r^2 = C/p^2\,\mathrm{cosec}^2\phi. \tag{8}$$

Then

$$N(p) = \frac{2C}{p}\int_{\sin^{-1}p/R}^{\pi/2}d\phi = \frac{2C}{p}\left[\frac{\pi}{2} - \sin^{-1}\frac{p}{R}\right]. \tag{9}$$

The equivalent widths of the chromospheric absorption lines formed along lines of sight with minimum distances p_1 and p_2 will then be in the ratio

$$\frac{W(p_1)}{W(p_2)} = \frac{p_2\left[\frac{\pi}{2} - \sin^{-1}\frac{p_1}{R}\right]}{p_1\left[\frac{\pi}{2} - \sin^{-1}\frac{p_2}{R}\right]}. \tag{10}$$

Let the unit of distance be the daily motion of the B star. Then at any date the quantity p is the number of days from mid-eclipse. It will be assumed that the K-type atmosphere extends to twice the radius of the photosphere, as seems likely from observations of the Ca II chromospheric lines. Then $R=62$. The ratios of equivalent widths, $W(p)/W(39)$, where $W(39)$ is the equivalent width at phase -8 days, computed from equation (10), and the observed ratios are given in Table V. The computed ratios agree reasonably with the observed ratios in the first part of the table but between phases -6 days and -2 days the observed ratios are much greater than the computed ratios. Since allowance for a possible departure of the curve of growth from linearity would further reduce the computed ratios, it is clear that after phase -6 days the line of sight must pass through a region in the atmosphere of the K star where the density increases much more rapidly than the assumed law $\rho \sim 1/r^2$. We conclude that the break in the curve relating strength of the chromospheric lines to phase represents a real discontinuity in the density of the outer atmosphere of the K star. The density in the region traversed by the line of sight between phases -6 and 0 days is significantly greater than that of the outer region of the atmosphere.

TABLE V

The mean relative strengths of the Fe I lines at various phases

Phase	p	Computed $W(p)/W(39)$	Observed $W(p)/W(39)$
Days			
−12	43	0·82	0·31
−10	41	0·91	0·92
− 8	39	1·00	1·00
− 6	37	1·10	1·23
− 5	36	1·16	2·39
− 3	34	1·28	4·23
− 2	33	1·34	4·23

It has been pointed out that the line profiles shown in Figs. 1 and 2 are distorted to some extent by the spectrograph. The true profiles of the Fe I chromospheric lines are somewhat deeper and a little narrower than these profiles. However, a measure of the mean half-width of these profiles will give an upper limit to the half-width of the line absorption coefficient. The mean half-width at all phases corresponds to a Doppler width of 20 km/sec. Since the thermal motion of Fe atoms at $T=3500$ deg will give a Doppler width of 1 km/sec to the line absorption coefficient, it is clear that there is some turbulent broadening of the profiles of the chromospheric Fe I lines. This conclusion is interesting in view of the results for Ca II at higher atmospheric levels during egress in late October, November and December 1951. McKellar, Odgers, Aller and McLaughlin (**12**) have shown in a preliminary study of the K line of Ca II that part of the material in the outermost regions of the atmosphere of the K star was in rapid motion a good deal of the time during egress, although the effect was scarcely, if at all, detectable for the Ca II lines during ingress. The amount of turbulent broadening of the Fe I chromospheric lines of 31 Cygni is a little larger than the results for ζ Aurigae. For this star O. C. Wilson and H. Abt (**13**) have found by curve-of-growth methods that the turbulent velocity is about 8 km/sec for neutral atoms and about 12 km/sec for ionized atoms. The general experience in the analysis of stellar spectra has been

to find that the turbulent velocity derived from curves of growth is equal to or less than that derived from the shapes of the line profiles (**14**).

Acknowledgments.—I am indebted to P. E. Argyle for making all the microphotometer tracings and some of the intensity tracings used in this study, and to S. H. Draper for assistance with "subtracting" the intensity tracings to isolate the chromospheric spectrum and for making the illustrations. My thanks are specially due to A. McKellar for permission to study the series of spectra of 31 Cygni obtained under his direction, and to K. O. Wright and R. M. Petrie as well for valuable discussions of the problem.

Dominion Astrophysical Observatory,
Victoria, B.C.:
1954 *March* 26.

References

(1) C. E. Moore, *Contr. Princeton O.* No. 20, 1945.
(2) K. O. Wright, *P. Dom. Ap. O.*, **10**, 1, 1954.
(3) D. B. McLaughlin, *A.J.*, **57**, 18, 1952.
(4) W. H. Christie and O. C. Wilson, *Ap. J.*, **81**, 213, 1935.
(5) D. N. Davis, *Ap. J.*, **106**, 28, 1947.
(6) J. M. Vinter Hansen, *Ap. J.*, **100**, 8, 1944.
(7) F. B. Wood, *A.J.*, **58**, 51, 1953.
(8) M. G. Fracastoro, *Harv. Circ.* No. 456, 1950.
(9) F. E. Roach and F. B. Wood, *Ann. d'Ap.*, **15**, 21, 1952.
(10) K. O. Wright, *P. Dom. Ap. O.*, **8**, 281, 1950.
(11) A. McKellar, *J.R.A.S. Can.*, **48**, 81, 1954.
(12) A. McKellar, G. J. Odgers, L. H. Aller and D. B. McLaughlin, *Nature, Lond.*, **169**, 990, 1952; *Contr. Dom. Ap. O.* No. 24.
(13) O. C. Wilson and H. Abt, *Ap. J. Supplement. Series*, **1**, 1, 1954.
(14) O Struve, *Ap. J.*, **104**, 138, 1946.

TWO-COLOUR PHOTOELECTRIC PHOTOMETRY OF GO CYGNI

M. W. Ovenden

(Communicated by the Director of the Cambridge Observatories)

(Received 1954 August 23)

Summary

Photoelectric light-curves in the blue and yellow have been obtained for GO Cygni from observations with the Cambridge pulse-counting photometer during the period 1950 August to 1951 October. The paper reports, analyses and discusses these observations. Both light-curves show strong asymmetrical terms in the variation of light between eclipses; the observations show that the processes giving rise to these terms suffer intrinsic variations. The observed differences of magnitude at maxima are compared with O'Connell's statistical conclusions. Elements for the binary are derived by Russell's method, Pearce's spectrographic observations being utilized. The comparison of the light-curves in the two colours gives evidence that the observed secondary spectrum (type A0) is due to reflection, the spectral type of the secondary if unaffected by reflection being later than F8. The assumption that the radiation of the secondary arises from a point close to the primary star serves to reconcile the deduced masses with the general mass–spectral type relationship.

---

1. *Introduction.*—GO Cygni (BD + 34°4095) was chosen for observation with a view to testing, under observing conditions at Cambridge, the suitability of the pulse-counting photoelectric photometer for the photometry of eclipsing variables. The sensitivity of the photometer set an upper limit about 11^m to the magnitude of the variable at primary minimum, and the behaviour of the Cambridge sky suggested that the star's period should be less than 3 days, but not close to a multiple of a day. To examine the value of photometry with the given equipment in the problem of eclipsing binaries, it was decided to take a star for which satisfactory visual and photographic observations were available, in addition to spectrographic observations. GO Cygni was chosen because Pierce's visual observations (**1**) showed that the star was a critical case in which more extensive and accurate observations might have been expected to provide a much more accurate knowledge of the elements of the system. In the event, this promise has not been fulfilled, owing to an intrinsic variability of the light-curve, but the photoelectric observations have enabled an analysis of these variations to be made.

The variability of GO Cygni was discovered photographically by Schneller (**2**) in 1928. Kukarkin (**3**) showed that the star was a short-period eclipsing binary, and Szczyrbak (**4**) gave the first elements of the light-curve, considering the system to be of the Algol type. Kukarkin's visual observations from 1929 to 1931 (**5**) (which were analysed by Kopal (**6**)) showed variation of the β-Lyrae type, with equal maxima and no displacement of the secondary minimum. Kordylewski's

visual observations (**7**) also show equal maxima, but give the phase of the secondary minimum as $0^{P}.509$. A series of visual observations by Beyer (**8**) gave a strong eccentricity, but the observations are few. A set of photographic observations by Iwanowska and Dziewulski (**9**) gave no eccentricity and symmetrical minima, but the maximum following the primary eclipse about $0^{m}.1$ brighter than the maximum following the secondary minimum. Observations by Payne-Gaposchkin (**10**) a few years later gave a similar excess of the first maximum in the photoblue, but an excess of about the same amount of the second maximum in the photored, both colours showing strong asymmetry of both minima.

The most complete series of observations, with discussions, are those of Liau (photographic) and Pierce (visual, polarizing photometer). Liau (**11**) finds the primary minimum asymmetric, in the sense that ascent is more rapid than decline, and the first maximum $0^{m}.075$ brighter than the second maximum. Pierce (**1, 12**) finds no asymmetry of minima, and equal maxima. Neither Pierce nor Liau found any evidence of eccentricity.

The only published spectrographic observations are those of Pearce (**13**), from which radial velocities were obtained for both components. The spectral types of the components were given as B9n and A0n, but, as will be seen later, the radiation of the secondary is due almost entirely to reflection.

2. *Experimental details.*—The present paper reports and discusses some 700 individual photoelectric measures of GO Cygni made between 1950 August and 1951 October with the pulse-counting photoelectric photometer designed by Yates (**14**) and mounted on the Huggins 15-inch visual refractor of the Cambridge Observatories. A graphical investigation of the resultant spectral transmissions of the two filters used (Wratten 5 yellow and Wratten 39 blue), the photomultiplier (from a sensitivity curve for a typical photocell) and the objective (from data for a typical 15-inch visual object glass (**15**)) gave maximum sensitivity at 5250 A (yellow) and 4200 A (blue). The blue transmission curve is sensibly symmetrical, with 50 per cent transmission at 3840 A and 4540 A, but the yellow curve is markedly asymmetric, with 50 per cent transmission at 4920 A and 5770 A. These figures are only approximate, for in any case variations in sensitivity from one cell to another may occur.

At the beginning of the programme, two comparison stars were chosen, viz.

Star	BD No.	HD mag.	HD spectral type
A	35° 4197	8·2 (7)	A2
E	34° 4098	7·9 (2)	K2

but star A appeared to show some variability, and only the comparisons of the variable with star E have been used. The correlation of the deviations of the observations of the variable from a mean curve with the phase of the variable, and the lack of any systematic effects of differential extinction give assurance that the use of only one comparison star has not caused any loss of accuracy in the measures.

Observations were made in two colours on the comparison star, then in two colours on the variable, and then in two colours on the comparison star again. Sky readings were taken between every other pair of comparisons, except on nights of bright moonlight, when they were made between every pair of comparisons. A single cycle giving two comparisons in each colour took about 10 minutes, each exposure being of half a minute. The one minute exposures more usual with this photometer proved too slow for the variable at certain phases.

For each determination of the variable, the count on the sky and on the comparison star was found by linear interpolation of adjacent readings. After subtraction of the sky reading, the ratio of counts on the variable and the comparison star was converted to a magnitude difference. Although the Cambridge programme of standard photometry provides a curve in each colour for the correction of the observed magnitudes to the NPS system, according to colour index, no attempt has been made to reduce the original observations of the variable to the NPS system, since the correction curves are obtained from observations of supposedly single stars. Not only does the spectral distribution of the binary not correspond to that of a single star of the same mean colour index, but furthermore the relative contributions of the two components vary throughout the eclipses. This is a fundamental difficulty of eclipsing variable work, if the photometry is not monochromatic, and for this reason caution must be exercised in any attempts to combine in a single light-curve observations made with more than one photometer. These considerations do not affect the validity of the analysis of a light-curve made entirely in one photometric system. The whole analysis of GO Cygni has therefore been made in the photometric systems of the photometer, and the standard colour correction curves have been used only in the discussion of the colour of the binary when the contribution of each component can be estimated.

For reference and comparison with other observations, a series of observations of the comparison star E were made on two nights with a view to placing it upon the NPS scale. Four stars of Kapteyn Selected Area No. 81, stars BD 16°2466, 13°2643, 15°2561 and 16°2514, were compared with E. This selected area was chosen because it could be observed at equal zenith distances with the field of the variable, and for the four chosen stars satisfactory magnitudes on the NPS scale are available from the standard photoelectric programme. Comparisons of E with BD 13°2643 were made over a range of time including the instant of equal altitude, and the magnitude differences were plotted against the difference of the secants of the zenith distances of the two stars; this provides a correction curve against relative altitude which can be used for the comparisons of E against the other three stars of the selected area. The magnitude of the Selected Area stars on the NPS scale from the Cambridge standard photometry were taken as:

Star	Ipg	Ipv
BD 13°2643	9·17	8·32
BD 16°2466	8·62	7·77
BD 15°2561	10·19	9·00
BD 16°2514	9·23	8·23

The reduced magnitudes for each night, with the mean deviations for each night, and the adopted mean magnitudes for the comparison star E are:

Date	Ipg	Mean δ	Ipv	Mean δ
	m	m	m	m
1952 May 15–16	8·78	0·03	7·84	0·03
1952 May 22–23	8·74	0·05	7·78	0·04
Adopted	8·76		7·81	

3. *Elements of the light-curve.*—Light-time corrections were found from Prager's tables (**16**), graphically interpolated to the nearest minute.

Pierce gave the elements of the light-curve as

$$\text{JD } 2\,426\,509{\cdot}461 + 0^{d}{\cdot}717\,763\,2\,E.$$

The best-determined minimum of the present series of observations, at corrected time JD 2 433 861·499, gave a period of $0^{d}{\cdot}717\,762\,6 \pm 0^{d}{\cdot}000\,000\,5$. An attempt was made to improve this value of the period by utilizing the whole of the light-curve. The observations were assembled on a period of $0^{d}{\cdot}717\,762\,6$, and for each night the sum of the individual deviations along the time axis from a mean curve drawn freehand through the observations was divided by the total number of observations for that night, and plotted against the number of periods from an arbitrary zero. Each point was then weighted according to the number of observations and the quality of the night, and mean points found for three ranges of E, the number of periods from the arbitrary zero. The points so found lay close to a straight line, giving a correction of $+0^{d}{\cdot}000\,003\,5$ to the period, but the scatter of the individual points, due mainly to phases outside the primary minimum, gave no confidence in this correction, and the period of $0^{d}{\cdot}717\,762\,6$ was adopted. A comparison of this figure with previous values of the period by earlier observers does not give any definite evidence of a change in the period of the binary.

4. *Formation of normal points.*—For forming normal points an objective criterion of the photometric quality of a given night is desirable. The stability of the response of the pulse-counting photometer provides such a criterion in the internal agreement of the counts of the comparison star alone. Each observation of the comparison star was compared with the reading obtained by linear interpolation of the adjacent counts of the comparison star, and the mean deviation in magnitudes, η, of these comparisons found for each night. For a large number of such comparisons, with Gaussian errors, the empirical weight to be attached to observations on a given night would be proportional to η^{-2}, but this gives too strong a weighting in view of the uncertainty of η on a given night due to the limited number of comparisons available. An empirical weight in the range 1 to 5 was therefore adopted for each observation, the weight factor being approximately proportional to η^{-1} for the night of observation.

Normal points were made for ranges of about 15 minutes throughout the cycle, the normal values being taken as the arithmetic means of the weighted individual magnitude determinations. The empirical weight, w_e, of a normal point was taken to be the sum of the empirical weights of the observations contributing to the normal point. According to Kopal (**17**), the intrinsic weight, w_i, of a normal point is given by $\sqrt{w_i} \propto dl/d(\sin^2\theta)$ for errors constant on an intensity scale, and by $\sqrt{w_i} \propto l^{-1}.\,dl/d(\sin^2\theta)$ for errors constant on a magnitude scale, l being the intensity of the binary in terms of the intensity at maximum. Observations by Yates on a standard laboratory source with the same photometer showed that the instrumental mean deviation is of the order of $0^{m}{\cdot}005$, whereas the mean deviations found in practice in these observations and the standard photometric programme are of the order of $0^{m}{\cdot}02$. Thus the errors are due to variation of sky transparency, and would be approximately constant on a magnitude scale. An intrinsic weight $w_i \propto l^{-2}.\,(dl)^2/(d(\sin^2\theta))^2$ was therefore adopted, the final weight for each normal point being taken as $w = w_e.\,w_i$.

The normal points and their weights are given in Tables I and II. Light-curves on a magnitude scale are given in Figs. 1 and 2.

TABLE I

Normal points (yellow curve)

Phase	Var-Comp.	No. of obs.	$\sqrt{w_e}$	$\sqrt{w}$	Phase	Var-Comp.	No. of obs.	$\sqrt{w_e}$	$\sqrt{w}$
P	m				P	m			
0·0067	+1·056	5	3·3	6·0	0·5000	+0·734	9	4·5	0·1
·0208	+1·046	5	3·3	5·8	·5157	+0·723	12	5·2	0·3
·0344	+0·985	2	2·8	4·2	·5290	+0·747	12	4·8	0·5
·0489	+0·935	2	2·8	3·4	·5447	+0·705	8	4·2	0·7
·0658	+0·825	3	3·5	3·1	·5585	+0·698	6	3·5	0·8
·0831	+0·764	3	3·0	2·0	·5738	+0·696	5	3·0	0·7
·0963	+0·716	5	3·3	1·7	·5894	+0·702	3	2·0	0·5
·1108	+0·673	4	3·1	1·3	·6045	+0·616	6	3·1	0·7
·1229	+0·618	3	2·5	0·9	·6167	+0·628	6	3·7	0·9
·1407	+0·603	2	2·2	0·6	·6312	+0·610	10	4·2	0·9
·1529	+0·564	1	2·0	0·4	·6460	+0·575	5	2·6	0·6
·1671	+0·541	3	3·5	0·6	·6585	+0·562	4	2·5	0·5
·1805	+0·545	2	2·8	0·4	·6747	+0·588	4	2·5	0·4
·1945	+0·508	3	3·5	0·4	·6885	+0·533	4	2·2	0·3
·2093	+0·505	5	4·7	0·4	·7047	+0·526	2	1·4	0·1
·2253	+0·507	3	3·6	0·2	·7192	+0·525	6	3·1	0·1
·2361	+0·500	3	3·6	0·2	·7331	+0·525	7	3·5	0·2
·2531	+0·495	6	4·1	0·2	·7463	+0·518	7	3·5	0·2
·2700	+0·489	5	3·0	0·1	·7615	+0·503	9	4·0	0·2
·2818	+0·500	4	2·8	0·1	·7764	+0·486	4	2·8	0·2
·2966	+0·512	5	3·5	0·3	·7847	+0·537	3	2·5	0·2
·3072	+0·515	3	2·0	0·2	·8165	+0·532	3	2·5	0·3
·3227	+0·547	2	2·0	0·3	·8339	+0·573	5	3·0	0·5
·3389	+0·527	6	3·5	0·7	·8491	+0·571	4	2·5	0·6
·3585	+0·544	2	2·0	0·4	·8620	+0·590	4	2·6	0·7
·3698	+0·595	5	3·1	0·7	·8776	+0·648	3	2·0	0·7
·3863	+0·605	5	3·1	0·7	·8906	+0·656	6	3·0	1·3
·3977	+0·576	6	3·5	0·8	·9066	+0·715	3	2·6	1·4
·4136	+0·621	8	4·2	0·9	·9195	+0·751	5	3·9	2·7
·4271	+0·664	5	3·6	0·9	·9358	+0·821	7	4·1	3·7
·4417	+0·652	9	4·5	1·0	·9497	+0·904	12	5·1	5·9
·4576	+0·690	9	4·6	0·8	·9632	+0·958	8	4·0	5·8
·4714	+0·693	7	4·0	0·4	·9782	+1·052	7	3·7	6·7
0·4840	+0·750	6	3·7	0·2	0·9978	+1·087	10	4·2	8·5

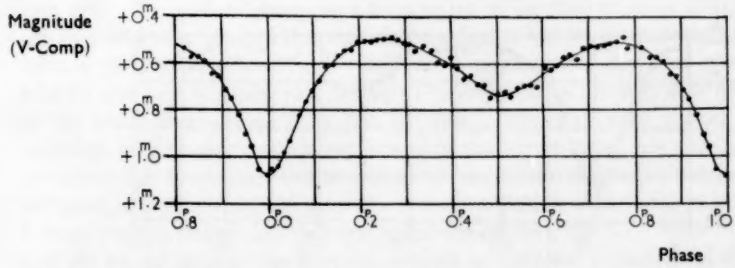

FIG. 1.—*The light-curve from the normal points in the yellow system. Ordinates give the magnitude of GO Cygni minus the magnitude of the comparison star, on the system of the photometer. An approximation to international photovisual magnitudes, based on a colour correction corresponding to the mean colour index of the variable, may be obtained by taking the zero of the magnitude scale as* $+7^{m}\cdot93$.

Table II

Normal points (blue curve)

Phase	Var-Comp.	No. of obs.	$\sqrt{w_e}$	$\sqrt{w}$	Phase	Var-Comp.	No. of obs.	$\sqrt{w_e}$	$\sqrt{w}$
P	m				P	m			
0·0068	+0·025	5	2·6	5·1	0·5150	−0·371	11	4·5	0·3
·0215	−0·001	4	2·4	4·6	·5284	−0·371	10	4·1	0·5
·0334	−0·032	2	2·0	3·5	·5422	−0·355	9	4·1	0·7
·0475	−0·107	2	2·0	3·0	·5565	−0·393	6	3·1	0·6
·0642	−0·255	3	2·4	2·8	·5734	−0·394	7	3·0	0·6
·0819	−0·325	3	2·2	1·9	·5879	−0·405	6	2·6	0·5
·0954	−0·414	5	2·6	1·5	·6020	−0·436	4	2·2	0·4
·1089	−0·405	4	2·4	1·0	·6147	−0·434	7	3·5	0·7
·1273	−0·478	6	2·8	0·9	·6317	−0·476	10	3·7	0·7
·1634	−0·485	4	2·8	0·6	·6466	−0·514	6	2·6	0·5
·1805	−0·527	2	2·0	0·5	·6591	−0·501	4	2·0	0·4
·1952	−0·526	3	2·4	0·4	·6744	−0·500	4	2·0	0·4
·2093	−0·548	5	2·8	0·3	·6889	−0·491	4	2·0	0·3
·2245	−0·576	3	2·2	0·2	·7041	−0·524	3	1·7	0·2
·2375	−0·582	3	2·2	0·1	·7172	−0·534	5	2·2	0·1
·2531	−0·558	6	2·8	0·1	·7315	−0·547	7	2·6	0·1
·2684	−0·544	5	2·8	0·1	·7448	−0·533	8	2·8	0·1
·2821	−0·536	4	2·4	0·2	·7605	−0·558	9	3·0	0·2
·2963	−0·561	5	2·8	0·3	·7760	−0·595	3	1·7	0·1
·3223	−0·535	7	3·3	0·6	·7856	−0·573	3	1·7	0·2
·3398	−0·542	4	2·8	0·5	·8188	−0·556	4	2·2	0·4
·3590	−0·502	2	2·0	0·4	·8414	−0·541	6	2·4	0·5
·3706	−0·448	5	3·1	0·6	·8641	−0·511	4	2·0	0·5
·3838	−0·457	4	2·6	0·5	·8772	−0·468	4	2·2	0·7
·3978	−0·487	8	3·7	0·7	·8918	−0·399	5	2·6	1·1
·4135	−0·478	7	3·5	0·7	·9080	−0·368	5	2·8	1·8
·4295	−0·484	5	2·8	0·5	·9216	−0·283	4	2·6	2·5
·4427	−0·425	8	3·7	0·7	·9347	−0·219	7	3·1	3·6
·4571	−0·429	9	4·2	0·7	·9485	−0·168	12	4·0	5·6
·4701	−0·391	8	4·0	0·5	·9631	−0·076	6	2·8	4·7
·4856	−0·366	8	4·2	0·3	·9779	+0·020	9	3·3	6·3
0·5001	−0·379	9	4·2	0·3	0·9925	+0·058	9	3·3	6·7

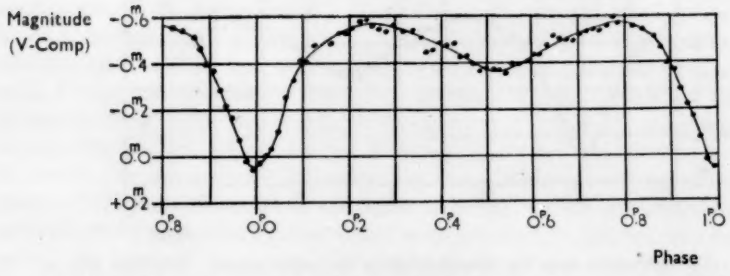

Fig. 2.—*The light-curve from the normal points in the blue system. Ordinates give the magnitude of GO Cygni minus the magnitude of the comparison star, on the system of the photometer. An approximation to international photographic magnitudes, based on a colour correction corresponding to the mean colour index of the variable, may be obtained by taking the zero of the magnitude scale as* $+8^{m}\cdot90$.

5. *Deviations of the individual observations from the mean curve, in magnitudes.*— In addition to the supposedly random variation of sky transparency, four sources of deviation from the mean curve suggest themselves, viz. (i) lack of constancy of the comparison star, (ii) differential colour extinction due to the difference in colour of the variable and the comparison star, (iii) errors in timing of the observations, and (iv) intrinsic variations of the light-curve of the variable.

The possible effects of differential colour extinction may be investigated by making use of the stability of the response of the photometer from night to night over long periods. The absorption of the atmosphere is reflected both in the observed colour index of the comparison star (defined by the ratio of the counts in the two colours) and in the actual count in any one colour, e.g. the blue, which is the more sensitive to changes in atmospheric absorption. The absorption being a logarithmic effect, a linear relationship should exist between the logarithm of the count of the comparison star in the blue, and the colour index of the comparison star. Such a linear relationship was found to exist, with a mean deviation of about 2 per cent, for a given colour index. However, no correlation of the deviation of the variable from the mean light curve (δ) with the logarithm of the adjacent count of the comparison star was apparent; differential colour extinction does not, therefore, contribute appreciably to the observed deviations.

A cursory glance at the plots of the individual observations shows that the deviations from the mean curve show some systematic variations with phase of the binary motion in both colours. To examine the variation of deviation with phase it is necessary to allow for the quality of the night on which a given observation was made. Although the magnitude of the mean deviation of the observations of the variable due to atmospheric effects will depend upon the photometric quality of the night, the ratio δ/η may be expected not to vary from this cause, δ being measured in magnitudes from the mean curve drawn freehand through the normal points.

For the blue curve the mean value of δ/η for equal ranges of $|\sin 2\theta|$ was plotted against $|\sin 2\theta|$, and a strong correlation was found (**29**). The variation of light between eclipses in the blue shows a sin 2θ term with a large negative coefficient. Liau also found a variation of error with phase, although he made no detailed analysis.

Treated in the same way, the yellow observations showed no correlation with $|\sin 2\theta|$. The yellow curve has a term in sin 2θ for the variation of light between eclipses which is of doubtful significance, but it has an important term in sin θ with a positive coefficient. Treated in a similar way for the variation with $|\sin \theta|$, the yellow deviations showed a correlation in the opposite sense to that of the blue observations with $|\sin 2\theta|$ (**29**). Since in each colour the major variation of intensity outside eclipses is of the cos 2θ type, any changes in mean deviation due to changes in the measured magnitude difference between variable and comparison star would show the same correlation with phase in both colours. It may thus be concluded that the processes causing the sin θ term in the yellow and the sin 2θ term in the blue are subject to intrinsic variations of the order of a few hundredths of a magnitude.

If the effects of these intrinsic variations were removed, δ would be of the order of η, but somewhat smaller than η since the interval of interpolation of the original observations for obtaining the magnitudes of the variable was less than the interval of interpolation between adjacent observations of the comparison star

used to obtain η. The intercept in the blue correlation line is $\delta/\eta \simeq 0{\cdot}6$, and in the yellow correlation line is $\delta/\eta \simeq 0{\cdot}8$; this agrees with expectation if variations of the comparison star were making no significant contribution to the deviations.

To investigate possible errors of timing, a correlation of δ/η with the slope of the blue-light curve (in magnitudes) was sought. None was found; errors of timing are thus negligible.

6. *The variation of the colour of the variable with phase.*—Taking the colour index of the comparison star E as zero, the relative colour index of the variable was found from each pair of normal points (blue and yellow). The phase of the combined colour normal was taken to be the arithmetic mean of the phases in the two colours without any relative weighting, and the weight of each colour normal was taken to be the sum of the empirical weights of the individual observations in the two colours. The weighted colour normals were then combined into new colour normals for ranges of $0^{P}{\cdot}05$, these final colour normals being plotted in Fig. 3, which shows the variation of the colour of the variable with phase.

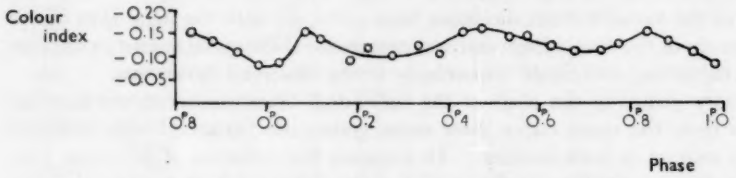

FIG. 3.—*The variation with phase of the colour of GO Cygni. Ordinates give the variation of colour index on the systems of the photometer, but the zero of the ordinate scale has been adjusted to give an approximation to international colour indices.*

7. *The variation of light between eclipses.*—The magnitudes of the normal points were converted into intensity ratios. A provisional analysis of the variation between eclipses by Merrill's graphical method (**18**) indicated that terms up to $\sin 2\theta$ should be included in the analysis in both colours. The variation of light between eclipses was therefore represented in both colours by the series

$$l = A_0 + A_1 \cos\theta + A_2 \cos 2\theta + A_3 \sin\theta + A_4 \sin 2\theta.$$

A difficulty frequently encountered with light-curves of the β Lyrae and W Ursae Majoris binaries is the finding directly from the light-curve of the duration of the eclipses. The slope $dl/d(\sin^2\theta)$ is more sensitive to the moments of first and last contacts, and some suggestion of a discontinuity of slope in the plot of this quantity with phase in the blue appeared at $\pm 0^{P}{\cdot}12$; no discontinuity was detected in the similar yellow plot. Least-squares solutions for the A-coefficients from the weighted normal points of the blue light-curve were made for various assumed eclipse durations, the results being shown in Table III. Solutions 2, 3 and 4 are similar, and give last contact at a phase close to $0^{P}{\cdot}125$, but as there is a danger of including some points actually in the primary eclipse in solution 4, solution 3 was accepted as being the best possible representation of the variation of light between eclipses. The weighted yellow normals were then subjected to a least-squares analysis for the A-coefficients on the single assumption of an eclipse duration of $\pm 0^{P}{\cdot}150$, and these coefficients are also shown in Table III.

The major cause of variation between eclipses in both colours is ellipticity of components, shown by the cos 2θ term. The yellow curve shows some

TABLE III

Variation of intensity between eclipses
Least-squares solutions for the A-coefficients

Eclipse	1	2	3	4	5
Duration	$\pm 0^{P}\cdot200$	$\pm 0^{P}\cdot175$	$\pm 0^{P}\cdot150$	$\pm 0^{P}\cdot125$	$\pm 0^{P}\cdot100$
Blue					
A_0	$+0\cdot965\pm0\cdot043$	$+0\cdot901\pm0\cdot009$	$+0\cdot916\pm0\cdot006$	$+0\cdot915\pm0\cdot003$	$+0\cdot899\pm0\cdot003$
A_1	$+0\cdot045\pm0\cdot013$	$+0\cdot003\pm0\cdot005$	$+0\cdot008\pm0\cdot004$	$+0\cdot010\pm0\cdot004$	$+0\cdot014\pm0\cdot004$
A_2	$-0\cdot018\pm0\cdot048$	$-0\cdot085\pm0\cdot012$	$-0\cdot069\pm0\cdot009$	$-0\cdot072\pm0\cdot007$	$-0\cdot098\pm0\cdot007$
A_3	$+0\cdot002\pm0\cdot003$	$+0\cdot004\pm0\cdot005$	$-0\cdot001\pm0\cdot002$	$-0\cdot006\pm0\cdot003$	$+0\cdot001\pm0\cdot003$
A_4	$-0\cdot023\pm0\cdot006$	$-0\cdot025\pm0\cdot003$	$-0\cdot023\pm0\cdot002$	$-0\cdot010\pm0\cdot002$	$-0\cdot006\pm0\cdot014$
Yellow					
A_0			$+0\cdot912\pm0\cdot005$		
A_1			$-0\cdot005\pm0\cdot003$		
A_2			$-0\cdot076\pm0\cdot008$		
A_3			$+0\cdot012\pm0\cdot002$		
A_4			$-0\cdot006\pm0\cdot002$		

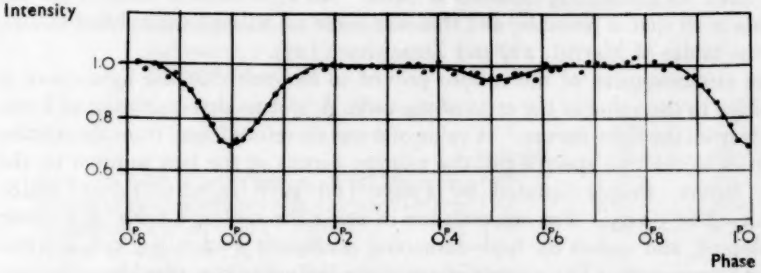

FIG. 4.—*The rectified light-curve in the yellow system, in intensity units.*

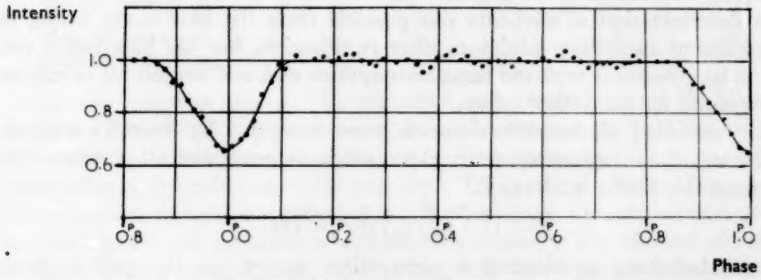

FIG. 5.—*The rectified light-curve in the blue system, in intensity units.*

reflection, but an amount much less than would be expected from the properties of the binary system. The reflection in the yellow may be partially disguised by a variation with $\cos\theta$ in the opposite sense corresponding to the significant "negative reflection" present in the blue curve. Strong asymmetric terms are present in both colours.

8. *Rectification.*—In the absence of any satisfactory theory for the causes of the asymmetric terms, and the "negative reflection", no precise rectification of the light-curves is possible. As far as possible, the rectification followed the method laid down by Russell (**19**). The reflection term in the yellow was treated as normal reflection, and the "negative reflection" term in the blue removed by subtraction. The $\sin\theta$ term in the yellow was removed by subtraction, following Dugan's hypothesis of a difference in brightness of the

advancing and receding hemispheres (**20**). The terms in sin 2θ and the ellipticity terms were removed by division.

The rectified curves are given in Figs. 4 and 5. The secondary minimum in the blue is due almost entirely to ellipticity, and disappears on rectification. A small residual secondary minimum remains in the yellow curve.

9. *Computation of the elements of the system.*—The absence of a significant secondary minimum to the rectified blue curve renders this curve virtually useless for the determination of the elements of the system, and the analysis was made with the yellow curve only.

An analytical computation of the elements, following Kopal's procedure (**17**), was attempted, but the iterations were found to diverge both for the assumption of primary transit and the assumption of primary occultation. The rectified curves do not, therefore, correspond exactly to the mutual eclipses of two spherical stars, and their failure to do so may be attributed to the presence of large terms which have no satisfactory theoretical basis. An approximate solution for the elements is all that is possible, and this was made on Russell's simplified model, using the tables of Merrill (**21**) and Zessewitsch (**22**).

The circumstances of the eclipse proved to be such that the light-curve is insensitive to the value of the ratio of the radii, k, and no determination of k was possible from the light-curves. A value of k was therefore found from the relative intensities of the two spectra and the relative depths of the two minima in the yellow curve. Pearce (quoted by Pierce (**1**)) gave $L_2 = 0{\cdot}07 \pm 0{\cdot}01$, which yields $k = 0{\cdot}67 \pm 0{\cdot}05$. For convenience in using the tables, a value of $k = 0{\cdot}65$ was adopted, and curves for limb-darkening coefficient $x = 0{\cdot}2$, $0{\cdot}4$, $0{\cdot}6$, $0{\cdot}8$ and $1{\cdot}0$ were computed. The curve for complete darkening was considered to give the best representation of the observations.

No determination of elements was possible from the blue curve owing to the absence of secondary minimum after rectification, but the blue curve was found to be consistent with the same assumptions of k and magnitude of eclipse as were found for the yellow curve.

The remaining photometric elements were computed by Russell's method. The factors N for conversion from photometric to geometric ellipticities were taken from the Roche model (**23**),

$$N = (15 + x)(1 + y)/(15 - 5x).$$

The limb-darkening coefficients x were taken as $1{\cdot}0$ for the yellow (from observation) and $0{\cdot}8$ for the blue (from Münch and Chandrasekhar's table (**24**) for an A1 star, the earliest type for which figures are given). These limb-darkening coefficients are not entirely satisfactory. For a B9 star, electron scattering may make a significant contribution to the opacity. Also, according to the theory of radiative transfer for a grey atmosphere, the limb-darkening coefficient should increase with decreasing wave-length. The calculations of Münch and Chandrasekhar for opacity due to neutral hydrogen atoms and negative hydrogen ions (**24**) show that the linear law of limb-darkening is a poor approximation, and particularly so in the photovisual region, for which they give no limb-darkening coefficients. The geometric ellipticities were calculated with $y = 1$ for want of a better approximation (**18**).

The remaining elements may be computed from Pearce's spectrographic observations. However, the radial velocity observations may be influenced by the fact that the secondary spectrum is due to reflection (see later) and will arise

from the hemisphere of the secondary which faces the primary. The observed radial velocities will thus correspond, not to the centre of the secondary star, but to a point on the line of centres which is displaced towards the primary star. If this displacement is ga, where $a=(a_1+a_2)$ is the separation of the two stars, then $0 \leqslant g \leqslant r_2$. With $r_2=0{\cdot}333$ as determined, elements have been derived on three assumptions as to the value of g, viz. 0·00, 0·25 and 0·33. The derived elements are given in Table IV.

TABLE IV

List of elements

Photometric

Ratio of radii, k	$=0{\cdot}67$
Radius of larger star, r_1	$=0{\cdot}513$
Radius of smaller star, r_2	$=0{\cdot}333$
Ellipticity, ϵ	$=0{\cdot}129$ (yellow obsns.)
	$=0{\cdot}134$ (blue obsns.)
	$=0{\cdot}131$ (adopted mean)
Max. eclipsed area of smaller star, α_0	$=0{\cdot}761$
Inclination, i	$=73^\circ$
Eccentricity, e	$=0{\cdot}00$

Spectrographic

	I	II	III
	$g=0{\cdot}00$	$g=0{\cdot}25$	$g=0{\cdot}33$
Radius of orbit of larger star, a_1 ($\times 10^6$ km) =	1·38	1·38	1·38
Radius of orbit of smaller star, a_2 ($\times 10^6$ km) =	1·62	2·62	3·12
Separation, a $(=a_1+a_2)$ ($\times 10^6$ km) =	3·00	4·00	4·50
Radius of larger star, r_1 ($\times 10^6$ km) =	1·54	2·05	2·30
Radius of smaller star, r_2 ($\times 10^6$ km) =	0·997	1·33	1·50
Ratio of masses, $\frac{M_2}{M_1}$ =	0·85	0·53	0·44
Mass of larger star, M_1 =	1·12 ⊙	3·2 ⊙	4·8 ⊙
Mass of smaller star, M_2 =	0·95 ⊙	1·7 ⊙	2·1 ⊙

10. *The reflection effect.*—The reflection will be confined to the secondary component, since this component contributes less than a tenth of the total light of the system. The observed spectral type of the secondary, A0, may well be due to reflection of the radiation of the primary. Eddington (**25**) has given a formula for the amount of radiation reflected at full phase from a point-primary, and this formula should give an order-of-magnitude estimate of the amount of reflected radiation in the present case. When applied, Eddington's formula gives a luminosity due to reflection of $0{\cdot}09L_1$, where L_1 is the luminosity of the primary. This is of the same order of magnitude as the observed luminosity of the secondary spectrum, which may therefore be attributed primarily to reflection. It is not possible to deduce the amount of reflected radiation from the photometric reflection effect in the yellow curve, for it may be masked by "negative reflection" corresponding to the observed "negative reflection" in the blue curve.

On the assumption that the quality of the radiation from any surface is that of a black body at some effective temperature, an estimate of the average spectral type of the area of the secondary which undergoes eclipse may be obtained, provided that the relative response of the photometer in the two colours to radiation from stars of various spectral types is known. The relative response may be found from the international colour indices and bolometric corrections on the assumption that the photometric systems of the photometer do not depart from the international systems. It is probable that this approximation would be

adequate for the present purpose, but a slightly better approximation can be obtained from the colour correction curves which convert the systems of the Cambridge standard photometry to the NPS systems, since the Cambridge standard photometry involved photoelectric observations with the same photometer as was used for the present investigation, in addition to photographic observations.

With the relative response of the photometer to surfaces of various spectral types known, the nature of the reflection effect may be examined. The relative brightnesses of the inside surfaces of the two stars may be computed for various assumptions of mean spectral type for the eclipsed area of the secondary and compared with the observed ratio of minima in the light-curves (uncorrected for reflection). In the yellow curve the observed ratio of depths of minima correspond to a mean spectral type of F8 for the eclipsed area of the secondary, taking the primary star to be of type B9.

In the blue curve it is possible to set only an upper limit of 0·10 for the ratio of the depths of minima. However, this upper limit is precise enough to enable some conclusions to be drawn concerning the nature of the reflection effect. If the radiation of the primary is reflected without change of quality, then the colour of the eclipsed area of the secondary should correspond to spectral type B9, this assumption giving a ratio of depths of minima in the blue of 0·17. If, on the other hand, the radiation of the primary is absorbed, and re-emitted at a lower effective temperature, then the colour of the eclipsed area of the secondary should correspond to spectral type F8, this assumption giving a ratio of 0·09. It may be concluded that the primary radiation is absorbed and re-emitted at a lower effective temperature. This is in agreement with the conclusion of Pismis (**26**) from a statistical consideration of many eclipsing systems.

Although the mean spectral type of the eclipsed area of the secondary is F8, Pearce's spectrographic observations show that some of the eclipsed area has an effective temperature corresponding to spectral type A0. This suggests that (i) the effective temperature must change rapidly over the inward hemisphere of the secondary, (ii) the observed radiation from the secondary must arise from a region close to the primary star, and not from the centre of the secondary star, and (iii) the spectral type of the secondary if unaffected by reflection would be later than F8.

11. *The masses of the components.*—These conclusions are confirmed by a comparison of the deduced masses of the components with the general mass–spectral type relationship. For this comparison the data given by Russell and Moore (**27**, Fig. 2) have been used.

The mean mass for spectral type B9 is about $3{\cdot}3\odot \pm 1{\cdot}4\odot$. Solution II of Table IV, corresponding to $g = 0{\cdot}25$, gives a mass of the primary close to the mean mass for this spectral type. Solution III is on the edge of the observed spread, but Solution I is outside the observed spread. (It should be noted that trigonometrical as well as spectroscopic binary data are available.) The mass-ratio deduced from the ellipticity is 0·65, which agrees best with Solution II. The mass of the secondary component in Solution II corresponds to a spectral type about G0. The assumption that the secondary spectrum arises from a limited region close to the primary star thus serves to reconcile the deduced masses of both components with the general mass-spectral type relationship.

12. *The nature of the asymmetric terms.*—Asymmetric terms of the form $A_3 \sin\theta$ and $A_4 \sin 2\theta$ are frequently found in the variation of light between eclipses with close eclipsing binaries. The $\sin\theta$ term is the most easily recognized

from the light-curve, since it produces a difference in the heights of the two maxima. O'Connell (**28**) has made a statistical analysis of the occurrence of differences in the heights of maxima of light-curves of the β Lyrae and W Ursae Majoris types. The difference of magnitude in the yellow curve of the present observations is taken to be $+0{\cdot}015$, following O'Connell's sign convention, where Δm is taken to be positive if the maximum following the primary minimum is the brighter. (A value of Δm taken directly from the light-curve is used in preference to one deduced from the size of the coefficient A_3, since the expression of the variation of light between eclipses as a Fourier series is entirely arbitrary.) In Table V the deviations of the observed Δm from O'Connell's regression lines are given, together with the probable errors of Δm given by O'Connell.

TABLE V

Difference of magnitude of maxima (yellow obsns.) compared with O'Connell's statistics

	Δm (obs) $-$ Δm (O'C)	p.e.(O'C)
Ellipticity, ϵ	$-0{\cdot}016$	$\pm 0{\cdot}016$
Separation, a (soln. II)	$+0{\cdot}006$	$\pm 0{\cdot}014$
Ratio of radii, k	$-0{\cdot}040$	$\pm 0{\cdot}016$
Mass of primary, M_1 (soln. II)	$-0{\cdot}017$	$\pm 0{\cdot}016$
Ratio of densities, $\frac{\rho_1}{\rho_2}$ (soln. II)	$-0{\cdot}011$	$\pm 0{\cdot}019$

The agreement is satisfactory except for the ratio of the radii. The failure of the observed asymmetry to agree with the regression line for the ratio of the radii may be related to the conclusion arrived at above that the radiation of the secondary is from a limited area close to the primary star. The adopted value of $k = 0{\cdot}65$ was found from the relative intensities of the two spectra on the assumption that the secondary radiated uniformly; a failure of this assumption will cause the radius of the secondary to be underestimated. A ratio of about 0·80 would suffice to bring the observed difference in the heights of the maxima into agreement with O'Connell's statistics.

O'Connell also examined the variation of Δm with wave-length, and concluded that Δm decreases with increasing wave-length, and may become negative for photovisual and photored observations. Of the stars used in arriving at this conclusion, GO Cygni is included with observations by Payne-Gaposchkin (**10**). The present observations are inconsistent with those of Payne-Gaposchkin, although it should be pointed out that Liau's photographic observations do show an appreciable positive Δm. The present observations are rather in agreement with Mergantaler's conclusion that Δm increases with increasing wave-length. In any case, the relationship may well be obscured by other asymmetries, and it is significant that one of the exceptions to his rule cited by O'Connell is RS CVn, where other asymmetries are marked. The possibility that the magnitudes of the asymmetries of GO Cygni vary with time is strongly suggested by a comparison of the various series of observations at widely separated epochs.

The correlation of deviations from a mean curve with the asymmetric terms shows that the processes giving rise to these terms suffer intrinsic variations even during a single period. The significance of these observations has been discussed by the present author elsewhere (**29**). Following Mergantaler (**30**), the $\sin\theta$ variation is attributed to absorption in a system of gaseous envelopes surrounding the binary, and the $\sin 2\theta$ term is attributed to a similar cause. The asymmetry which increases with increasing wave-length (in this case the $\sin\theta$ variation) is supposed due to absorption by H^- ions (cf. Mergantaler,

loc. cit.). If a model similar to that of Kuiper (**31**) for β Lyrae is adopted for GO Cygni the H^- absorption is important in the expanding shell system. For the close shell which constitutes a common envelope of the two stars, absorption by hydrogen atoms on the Balmer level will be the more important process. Since a few per cent of the radiation received in the blue system of the photoelectric photometer used in the present investigation has a wave-length less than that of the Balmer series limit, this may explain the importance of the sin 2θ variation in the blue curve and its absence in the yellow curve. It would be of value to make photometric observations of a system like GO Cygni in two restricted wave-length regions, one on each side of the Balmer discontinuity. It may be remarked that the flare-like variation found by Huruhata for U Pegasi (**32**) shows a strong wave-length dependence of this type.

Acknowledgments.—My thanks are due to Professor R. O. Redman for providing facilities for this research; to Professor W. M. Smart, in whose department some of the work of reduction has been performed; to Dr A. Beer and Mr G. G. Yates for many valuable discussions on photometric problems; and to my wife and my colleagues at the Cambridge Observatories for assistance in the recording of the observations. I am also indebted to Dr F. B. Wood of the Flower Observatory for the loan of some unpublished manuscripts of the late Dr N. L. Pierce.

The Observatory,
Glasgow University:
1954 *July* 1.

References

(1) N. L. Pierce, *Astr. Journ.*, **48**, 113, 1939.
(2) H. Schneller, *Astr. Nach.*, **235**, 85, 1928.
(3) B. W. Kukarkin, *N.N.V.S.*, **2**, 26, 1929.
(4) S. Szczyrbak, *S.A.C.*, **10**, 44, 1931.
(5) B. W. Kukarkin, *N.N.V.S.*, **4**, 19, 1932.
(6) Z. Kopal, *Astr. Nach.*, **247**, 120, 1932.
(7) K. Kordylewski, *Acta Astr.* C, **2**, 46, 1933.
(8) M. Beyer, *Astr. Nach.*, **258**, 281, 1935.
(9) W. Iwanowska and W. Dziewulski, *Wilno Bull.*, **13**, 30, 1932.
(10) C. Payne-Gaposchkin, *Harvard Bull.* 898, 3, 1935.
(11) S. P. Liau, *Publ. de l'Obs. de Lyon*, Ser. I, I, Fasc. 13, 1935.
(12) N. L. Pierce, *Princeton Contr.* No. 25, 53, 1951.
(13) J. A. Pearce, *J.R.A.S. Canada*, **27**, 62, 1933.
(14) G. G. Yates, *M.N.*, **108**, 476, 1948.
(15) A. Danjon et A. Couder, *Lunettes et Telescopes*, pp. 565, 567, 1935.
(16) R. Prager, *Kleinere Veröff. Berlin-Babelsberg* Nr. 12, 1932.
(17) Z. Kopal, *Harvard Obs. Monographs* No. 8, 1950.
(18) H. N. Russell, *Ap. J.*, **108**, 388, 1948.
(19) H. N. Russell, *Ap. J.*, **104**, 153, 1946.
(20) R. S. Dugan, *Princeton Contr.* No. 5, 1920.
(21) J. E. Merrill, *Princeton Contr.* No. 23, 1950.
(22) W. Zessewitsch, *Bull. Astr. Inst. Acad. Sci. U.S.S.R.*, Nr. 45, 1938 and Nr. 50, 1940.
(23) H. N. Russell, *Ap. J.*, **102**, 1, 1945.
(24) G. Münch and S. Chandrasekhar, *Harvard Circ.* 453, 1949.
(25) A. S. Eddington, *M.N.*, **86**, 320, 1926.
(26) P. Pismis, *Ap. J.*, **104**, 141, 1946.
(27) H. N. Russell and C. E. Moore, *The Masses of the Stars*, Chicago, 1940.
(28) D. J. K. O'Connell, *Riverview Coll. Obs. Publ.* No. 10, 1951.
(29) M. W. Ovenden, *Vistas in Astronomy*, ed. A. Beer, Pergamon Press, in press.
(30) J. Mergantaler, *Wroclaw Obs. Contr.* No. 4, 1950.
(31) G. P. Kuiper, *Ap. J.*, **93**, 133, 1941.
(32) M. Huruhata, *Publ. Astr. Soc. Pacific*, **64**, 200, 1952.

COLOUR–MAGNITUDE ARRAYS IN THE CLUSTERS TOMBAUGH 5, NGC 7789, NGC 1528 AND NGC 2682

V. C. Reddish

(Communicated by the Director, University of London Observatory)

(Received 1954 September 25)

Summary

Magnitudes and colours of stars in four clusters have been obtained from simultaneous photographs on blue- and red-sensitive plates, using the twin refractor of the University of London Observatory at Mill Hill. The magnitudes have been reduced to the (B, V) system of Johnson and Morgan.

The colour–magnitude arrays show the cluster Tombaugh 5 to be of similar type to Praesepe. NGC 7789, previously classified as a galactic cluster, is found to be a globular cluster. Trumpler's classification of NGC 1528, a normal galactic cluster, is confirmed. NGC 2682 is known to be peculiar. The author considers it to be a transition type, between the normal Population I and Population II types. It is tentatively classified as of Population I on the basis of the existence of a narrow Hertzsprung Gap, a basis which the author suggests should be used as the main criterion to differentiate between clusters of the two types of population.

A continuous sequence of types of colour–magnitude arrays of clusters is arranged, in which the main variation along the sequence (apart from the brightness of the stars) is the width of the Hertzsprung Gap. This variation is probably a result of differences in the proportions of the stars' masses contained within their convective cores.

During the years 1953 and 1954, observations were made with the Radcliffe twin refractor of the University of London Observatory, Mill Hill, to determine colours and magnitudes of stars in four clusters.

Because of difficulties in guiding for long periods near the pole, and the well-known disadvantages of using the stars in that region as a standard system, the (B, V) system of Johnson and Morgan (1) was adopted as the standard. The $B-V$ colours in which the results are expressed were determined from colours (denoted $B-R$) obtained from the difference between blue and red magnitudes, the longer base-line of the latter resulting in smaller proportionate random errors.

Equipment.—The 18-inch visual refractor attached to the 24-inch photographic refractor was adapted for photography in 1953 September. It thus became possible to photograph simultaneously on red-sensitive and blue-sensitive plates. Guiding was done by means of an eyepiece attached at the side of the plate-holder on the 24-inch refractor. Photographs were taken on Ilford Astronomical Zenith (and in some cases on Kodak Oa–O) plates on the 24-inch refractor, which was stopped down to 18 inches to make the images of comparable density to those on the red-sensitive plates. Red-sensitive Kodak Oa–F plates were used, together with a Chance OR2 red glass filter, on the 18-inch "visual" refractor.

Exposure and development.—All exposures were of one hour's duration, the limiting visual magnitude being 15·2. Plates were developed for three minutes, in the pairs as exposed, in Kodak D 19b developer at 18 deg. C.

Measurement and reduction.—No photometer being available, diameter measurements of the images were used to obtain magnitudes, and a Hilger "Spectrum Plate" measuring machine was adapted for the purpose. All plates were measured twice—in the north–south and east–west directions. Magnitudes were estimated in the case of images which were too faint for diameter measurements. The colour–magnitude diagrams therefore extend to the limiting magnitude of the equipment. Satisfactory relations were found between magnitude and square root of image diameter.

Extinction.—It was not possible to make satisfactory measurements of atmospheric extinction and estimated extinction coefficients were employed.

The standard system

Visual magnitudes.—All visual magnitudes were standardized by comparison with plates of one-hour exposure on the clusters Praesepe and IC 4665, for which magnitudes on the (B, V) system have been given by Johnson (**2, 3**). A linear relation between red magnitude and square root of image diameter was found and is represented by the equation

$$R = -2{\cdot}23\sqrt{d_r} + 22{\cdot}74. \qquad (1)$$

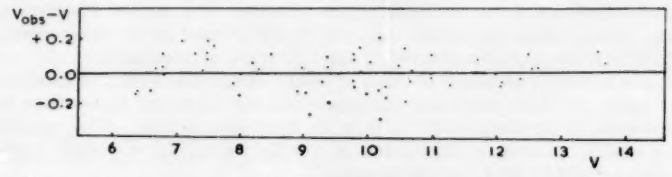

FIG. 1.—*Observed minus standard visual magnitudes, against visual magnitude. Each dot represents a magnitude determined from a single plate.*

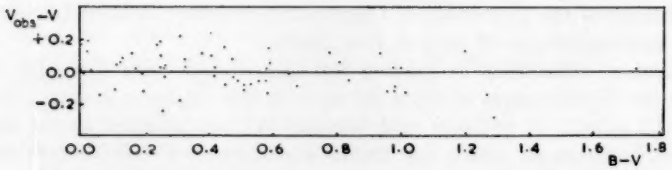

FIG. 2.—*Observed minus standard visual magnitudes, against colour index. Each dot represents a magnitude determined from a single plate.*

The relation between the colours was then found to be

$$B - V = 0{\cdot}70(B - R) \qquad (2)$$

and hence the visual magnitudes are given by

$$V = -2{\cdot}23\sqrt{d_r} + 0{\cdot}42(B - V) + 22{\cdot}74, \qquad (3)$$

where d_r is in units of 0·01 mm, and corrections for extinction have been made. Values of "observed *minus* standard" visual magnitudes are plotted against magnitude and colour in Figs. 1 and 2. There is a slight non-linearity in the plot against colour, of the order of a few hundredths of a magnitude. The use of non-linear relations to eliminate this would have greatly increased the labour of reduction, and was not considered worth while in view of the very small increase in accuracy which would result.

Blue magnitudes.—Because of a misunderstanding regarding supplies of photographic plates, no Kodak Oa–O plates were available to continue the programme after photographs had been obtained on the clusters Tombaugh 5 and NGC 7789. At that time, no exposures had been made on the standard (*B*, *V*) system, and previous work had to be adapted for the reductions, as explained in the next paragraph. The remainder of the programme was carried out using Ilford Astronomical Zenith plates.

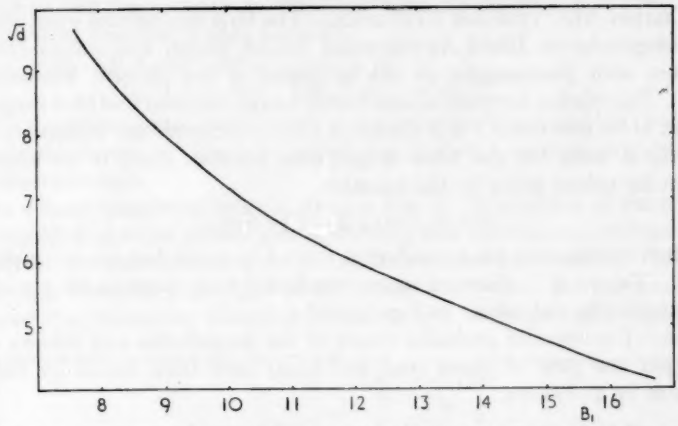

FIG. 3.—*Square root of image diameter against blue magnitude (corrected for extinction). The units of d are 0·01 mm. In addition to the curve, equation (5) is used for magnitude determinations.*

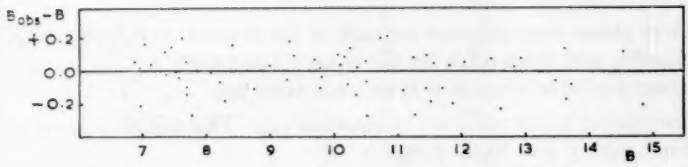

FIG. 4.—*Observed minus standard blue magnitudes, against blue magnitude. Each dot represents a magnitude determined from a single plate.*

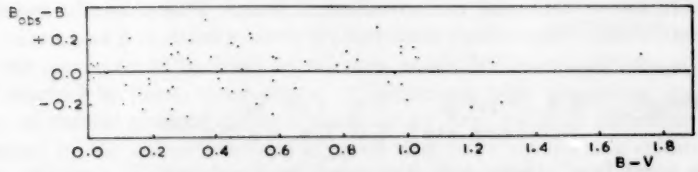

FIG. 5.—*Observed minus standard blue magnitudes, against colour index. Each dot represents a magnitude determined from a single plate.*

(*a*) *Clusters Tombaugh 5 and NGC 7789.*—The blue magnitudes were obtained from photographs on Kodak Oa–O plates, using an equation derived from a simple relation between square root of image diameter and magnitude. This relation, based on the (*P*, *V*) system and obtained from photographs of the North Polar Sequence, also on Kodak Oa–O plates, was found in earlier work (4).

The equation, corrected for extinction, is

$$B = -1{\cdot}25\sqrt{(d-10)} + 0{\cdot}03(B-V) + 19{\cdot}17, \qquad (4)$$

where d is in units of 0·01 mm. The equation holds down to $d = 0{\cdot}15$ mm (about $B = 16{\cdot}5$). The details of the manner in which this equation was obtained are too long for publication in this paper, but because some approximations had to be made in its derivation it cannot be expected to give magnitudes as reliable as those in the following section (*b*).

(*b*) *Clusters NGC* 1528 *and NGC* 2682.—The blue magnitudes were obtained from photographs on Ilford Astronomical Zenith plates, and standardized by comparison with photographs on similar plates of the clusters Praesepe and IC 4665. The relation between square root of image diameter and blue magnitude was found to be non-linear; it is shown in Fig. 3, corrected for extinction. The symbol B_1 is used for the blue magnitudes because there is an additional correction for colour given by the equation

$$B = B_1 - 0{\cdot}14(B-V) + 0{\cdot}05. \qquad (5)$$

The method of reduction was to read off B_1 from Fig. 3 and then apply equation (5) to get B. Values of "observed *minus* standard" blue magnitudes are plotted against magnitude and colour in Figs. 4 and 5.

Errors.—The internal probable errors of the magnitudes and colours determined from one pair of plates (red and blue) have been found by repeated measures to be as follows:

V	10^m	12^m	14^m	15^m
Probable error in V	$\pm 0^m{\cdot}04$	$\pm 0^m{\cdot}06$	$\pm 0^m{\cdot}06$	$\pm 0^m{\cdot}07$
Probable error in $B-V$	$\pm 0^m{\cdot}07$	$\pm 0^m{\cdot}08$	$\pm 0^m{\cdot}08$	$\pm 0^m{\cdot}10$

Two pairs of plates were obtained for each of the clusters NGC 7789, NGC 1528 and NGC 2682, and three pairs for the cluster Tombaugh 5.

The main probable sources of systematic error are:

(1) Uncertainty in the accuracy of equation (4). This affects only the clusters Tombaugh 5 and NGC 7789.

(2) The use of a linear relation—equation (3)—for reducing the visual magnitudes; the true relation probably differs from linearity by a few hundredths of a magnitude.

(3) The use of estimated extinction coefficients. This probably makes the zero point of the colours uncertain by about a tenth of a magnitude.

The clusters

Tombaugh 5.—R.A. $3^h\ 42^m{\cdot}9$ Dec. $+58°\ 54'$
Gal. Long. 112° Gal. Lat. $+4°{\cdot}8$ } 1940

This small faint cluster was discovered by Tombaugh in 1941 (**5**). The colour–magnitude array is given in Fig. 6. It appears to be a normal galactic cluster of Population I, with a few yellow giants. The six brightest main-sequence stars are separated from the rest of the main sequence by a gap of about 0·4 magnitude. One of them, at $V = 11^m{\cdot}76$, $B-V = +0^m{\cdot}07$, must really be very blue if it is a cluster star, because comparison of the main sequence with that of Praesepe (**2**) and the position of the yellow giants indicate a colour excess of about 0·35 magnitude. This would give for the star a true colour $B-V = -0^m{\cdot}28$.

There is a very red star at $V = 11^{m}.76$, $B - V = 2^{m}.35$; correction for colour-excess gives the true $B - V = 2^{m}.00$. It is almost certainly a cluster member—if it were more distant than the cluster and its red colour were due to interstellar absorption behind the cluster it would be much fainter than it is.

If the absolute visual magnitude of the yellow giants is $+0.3$ (*cf.* Praesepe —a similar type of cluster), the distance modulus is $m - M = 12.30$. Total absorption $A_{vis} = 3E_{B-V}$ (**6**). Hence the total absorption for this cluster $A_{vis} = 1^{m}.05$ and the distance modulus corrected for absorption is $11^{m}.25$. The corresponding distance is 1800 parsecs.

NGC 7789.—R.A. $23^{h}\ 52^{m}.0$ Dec. $+56°\ 10'$
Gal. Long. $83°$ Gal. Lat. $-5°.2$ } 1900

This cluster was listed by Shapley (**7**) as a galactic cluster, and by Trumpler (**8**) as a galactic cluster of type 2–3a, signifying probably more yellow giants than main-sequence stars.

The colour–magnitude array is given in Fig. 7. It is typical of the bright red giant branch of globular cluster arrays, showing that the cluster is of Population II and that the previous classifications as a galactic cluster are incorrect. The cluster is unusually open for a globular cluster—indeed it is only for the faintest stars measured that clustering becomes obvious at all. It is probable that the stars

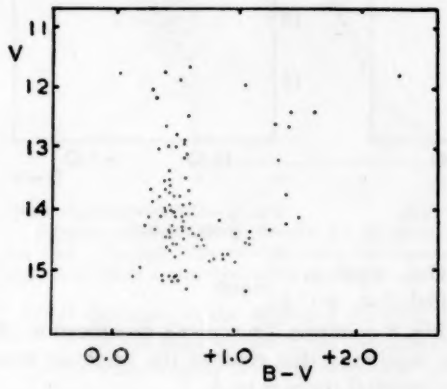

FIG. 6.—*Colour–magnitude array of Tombaugh 5.*

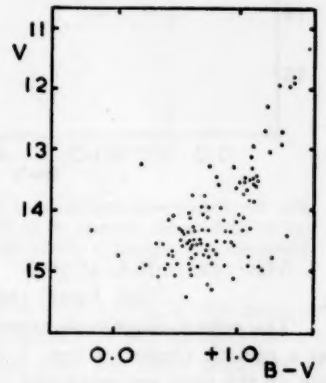

FIG. 7.—*Colour–magnitude array of NGC 7789.*

near the centre could be resolved down to much fainter magnitudes than have been reached in these observations. Comparison with the colour–magnitude arrays of various globular clusters obtained by Arp (**9**) (with allowance for the difference in the colour systems) suggests that NGC 7789 has a colour excess of about $0^{m}.2$; hence the total absorption $A_{vis} = 0^{m}.6$. Assuming that the brightest stars on the giant branch have an absolute visual magnitude of -3.5 (from which it follows that the horizontal branch, usually including the RR Lyrae variables, is just below the limiting magnitude of the diagram), the distance modulus is $m - M = 14^{m}.9$. The distance modulus corrected for absorption is $14^{m}.3$. The corresponding distance is 7200 parsecs, and hence the cluster is about 650 parsecs south of the galactic plane. The luminosity function for the giant branch is given in Fig. 10. It has been shown by Sandage (**10**) that the

luminosity function for stars between $M_{bol} = +1$ and $M_{bol} = +4$ in the globular cluster M3 is closely represented by the formula

$$\log_{10} \phi(M) = 0{\cdot}4 M_{bol} + \text{const.},$$

which would be expected from some evolutionary theories. Fig. 10 shows that the formula closely represents the luminosity function for the giant branch in NGC 7789 for stars brighter than $M_{bol} = -0{\cdot}5$.

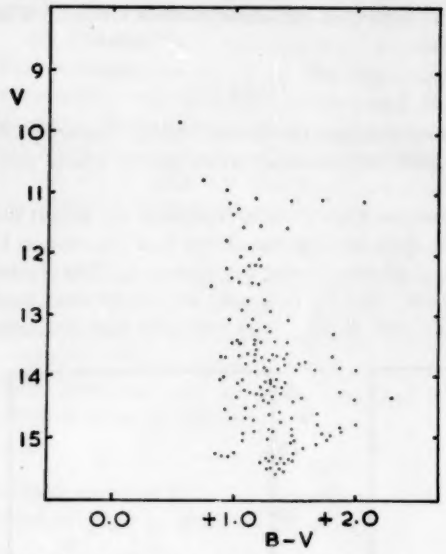

FIG. 8.—*Colour–magnitude array of NGC 1528.*

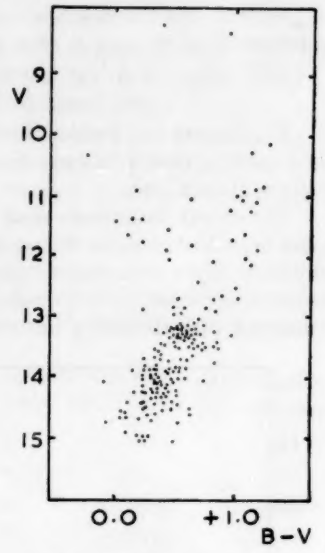

FIG. 9.—*Colour–magnitude array of NGC 2682 (= M67).*

NGC 1528.—R.A. $4^h\ 7^m{\cdot}6$ Dec. $+50°\ 59'$
Gal. Long. $120°$ Gal. Lat. $+1°{\cdot}2$ } 1900

The colour–magnitude array of Fig. 8 confirms Trumpler's classification (**8**) as a galactic cluster of type I–2b–a, signifying that most of the brightest stars are on the main sequence and are of spectral types B to A.

A colour excess of $1^m{\cdot}0$ is indicated by the position of the main sequence, giving a total absorption $A_{vis} = 3^m{\cdot}0$. Comparison of the main sequence with that of Praesepe suggests that the absolute magnitude zero corresponds to $V = 11^m{\cdot}1$. Hence the distance modulus corrected for absorption is $8^m{\cdot}1$ and the distance 420 parsecs.

The star at $V = 9^m{\cdot}82$, $B - V = 0^m{\cdot}54$, must be very blue if it is really a cluster member. Correction for colour excess gives a true colour $B - V = -0^m{\cdot}46$ at $M_v = -1{\cdot}3$.

NGC 2682.—R.A. $8^h\ 45^m{\cdot}8$ Dec. $+12°\ 11'$
(= M67) Gal. Long. $184°$ Gal. Lat. $+33°{\cdot}4$ } 1900

Listed by Shapley (**7**) as a galactic cluster, and by Trumpler (**8**) as a galactic cluster of type 2–3a, NGC 2682 was investigated by Ebbighausen (**11**) who pointed out that the Hertzsprung–Russell diagram bore some similarity to those of globular clusters. Further work on the cluster has been done by Vanderlinden (**12**) and by Becker and Stock (**13**) who classified it (on the basis of the

colours of the brightest cluster stars) as a Population I globular cluster. The present measures extend about a magnitude fainter than those of the latter investigations.

The colour–magnitude diagram, Fig. 9, is similar to those of globular clusters, but there are striking differences. These can be seen most easily by comparing a schematic diagram for NGC 2682 with one of a typical globular cluster, M3 (**14**). Since the absolute magnitudes of the stars in NGC 2682 are not known, the differences depend on how the clusters are compared.

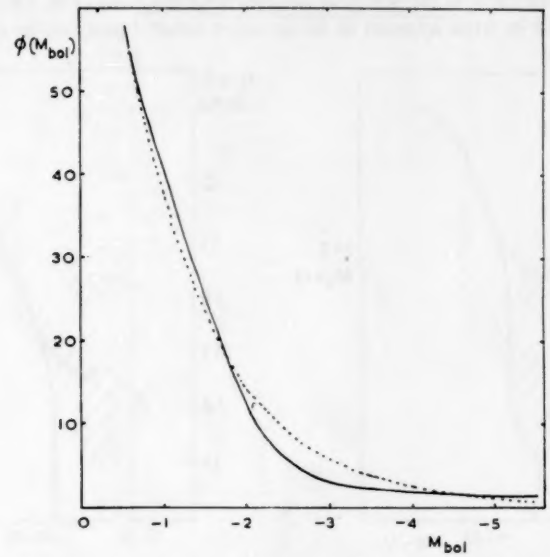

FIG. 10.—*The luminosity function for the giant branch of the globular cluster NGC 7789, full line. The dashed line gives the curve to be expected if the number of stars per unit luminosity range is inversely proportional to the luminosity.*

(1) If the stars in the region $V = 11^{m}\cdot5$, $B-V = +0^{m}\cdot3$ (Fig. 9) are assumed to be the same as those on the horizontal branch of M3 about $M_v = 0\cdot0$, the comparison is as in Fig. 11. In this case the main sequence of NGC 2682 has already been reached by these observations, but the "turn-off" of this main sequence takes place at about $M_v = +2\cdot5$, compared with $M_v = +3\cdot6$ in the case of M3. Also, the vertical giant branch in NGC 2682 would appear to be $0^{m}\cdot7$ redder than the main sequence at the "turn-off" point, the corresponding figure in M3 being about $0^{m}\cdot2$.

(2) If the brightest red giants in NGC 2682 are supposed to be equal in luminosity to the brightest in M3, the comparison is as in Fig. 12. Here, the "horizontal" branch in NGC 2682 is nearly two magnitudes brighter than in M3, and if the "turn-down" at $V = 14^{m}$ (Fig. 9) is supposed to be the start of the vertical giant branch, it is both fainter and bluer than the vertical branch in M3.

The first comparison appears more likely to be near the truth as regards comparing equivalent sequences. The author considers, however, that the cluster may represent a stage of transition from Population I to Population II. Despite the strong resemblance to colour–magnitude arrays of Population II, there are

characteristics typical of Population I—a narrow Hertzsprung Gap at $V = 13^{m}{\cdot}6$, the "bunching" of the red giants bordering the gap (at $V = 13^{m}{\cdot}3$) and the comparatively small number of red giants brighter than the bunching.

It is possible to arrange the colour–magnitude diagram of NGC 2682, together with diagrams of the clusters M3 (**14**), NGC 752 (**15**), Praesepe (**2**), M38 (**16**) (reduced to the (B, V) system (**4**)) and the cluster in Perseus (**17**) into a sequence in which the main variable along the sequence (apart from the brightness of the stars) is the width of the Hertzsprung Gap (Fig. 13). NGC 2682 has been placed in what appears to be its most natural position in the sequence.

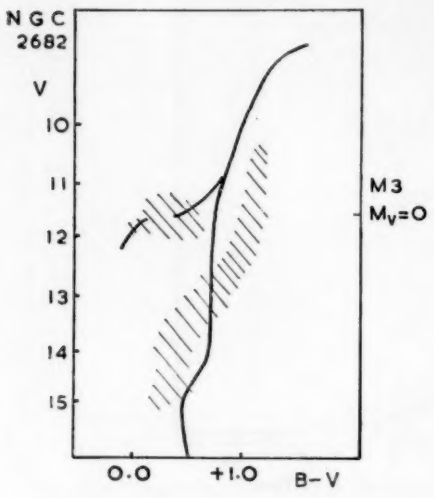

FIG. 11.—*Comparison of M3 (full line) and NGC 2682 (shaded). See the text.*

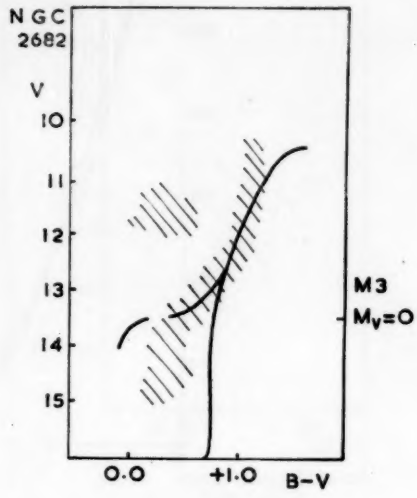

FIG. 12.—*Comparison of M3 (full line) and NGC 2682 (shaded). See the text.*

Comparison of the colours of the stars in NGC 2682 with those to be expected from the spectral types published by Ebbighausen (**11**) shows good agreement and indicates that there is no interstellar reddening of the cluster. This is not unexpected in view of the cluster's high galactic latitude. If the zero point of the absolute magnitudes indicated by Fig. 13 is correct, the distance modulus is $12^{m}{\cdot}0$ and the corresponding distance is 2500 parsecs.

The decreasing width of the Hertzsprung Gap along the sequence of diagrams in Fig. 13 may be expected from theoretical considerations. Along a sequence of stars of decreasing masses the proportion of the mass contained within the convective core decreases until finally it vanishes in stars of about the solar mass. This is because electron scattering becomes relatively less important in the opacity and the proton–proton reaction becomes relatively more important in the energy generation as the masses decrease. Both these changes act to reduce the proportion of mass contained within the convective core (**18, 19, 20**). It has been suggested by the author (**21**) that when the hydrogen in the core has been consumed in the nuclear reactions, evolution to the red-giant stage will be rapid and will thus cause a gap in the sequence of the stars on a colour–magnitude

array—the Hertzsprung Gap. The red-giant models of Sandage and Schwarzschild (**22**) show that as the proportion of mass contained within the hydrogen-exhausted core increases, the radius of the star increases, and its surface temperature falls. It is probable, therefore, that the width of the Hertzsprung Gap depends on the proportions of mass contained within the convective cores of the brightest main-sequence stars. Briefly, this is because the larger the core the more it must contract after hydrogen exhaustion—and hence the more the envelope expands

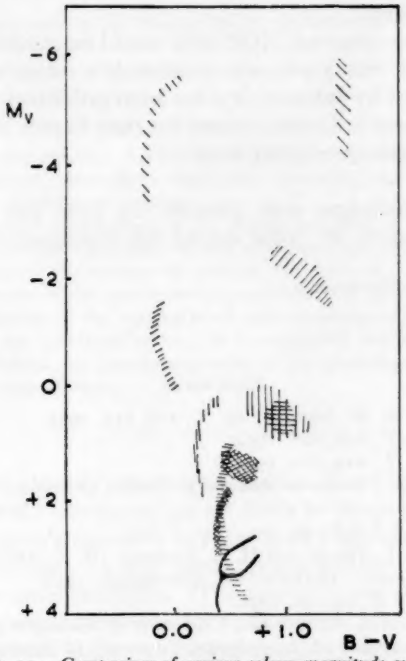

FIG. 13.—*Comparison of various colour–magnitude arrays, showing the narrowing of the Hertzsprung Gap.*

Cluster in Perseus.
$M38$.
Praesepe.
NGC 752.
NGC 2682.
$M3$, *outline only.*

Only those portions of the arrays bordering the Hertzsprung Gaps are given.

and the redder the star becomes—before the temperature at the surface of the core rises high enough for the carbon–nitrogen cycle to act there and slow down the rapid evolution. Thus the width of a Hertzsprung Gap on the colour–magnitude array of a cluster may depend on the masses of the brightest main-sequence stars in the cluster. Since the masses of the stars decrease with decreasing brightness, the width of the Hertzsprung Gap would, according to this theory, decrease with decreasing brightness as it does in Fig. 13. This explanation is of course tentative and requires further investigation.

The classification of clusters according to Population must be based on some easily recognizable criterion. The author suggests that the presence or absence of a Hertzsprung Gap is the best criterion to use. It suffers from the obvious disadvantage that the ability to detect narrow gaps depends on the accuracy of the colour measurements, but this difficulty will probably apply to any criterion based on the use of colour–magnitude arrays. One of its principal advantages is that it is closely connected with a structural characteristic of the stars—the presence or absence of convective cores—which is itself connected with the age of the stars.

On the basis of this criterion, NGC 2682 would be classified as Population I.

Addendum.—Since this paper was presented, a colour–magnitude array of NGC 2682 determined by Johnson (**23**) has been published. Fig. 9 appears to agree well with Johnson's diagram except for stars fainter than $V = 14^{m}$, where the colours of this paper are slightly bluer.

The author acknowledges with pleasure the help and encouragement he received from Professor C. W. Allen during this investigation.

University of London Observatory,
Mill Hill Park,
London, N.W.7:
1954 *September* 9.

References

(1) H. L. Johnson and W. W. Morgan, *Ap. J.*, **117,** 313, 1953.
(2) H. L. Johnson, *Ap. J.*, **116,** 640, 1952.
(3) H. L. Johnson, *Ap. J.*, **119,** 181, 1954.
(4) V. C. Reddish, *Star Clusters in Relation to Stellar Evolution*, Thesis, University of London, 1954.
(5) C. W. Tombaugh, *P.A.S.P.*, **53,** 219, 1941.
(6) W. W. Morgan, D. L. Harris and H. L. Johnson, *Ap. J.*, **118,** 92, 1953.
(7) H. Shapley, *Star Clusters*, Harvard Obs. Monograph, 1930.
(8) R. J. Trumpler, *L.O.B.* **14,** 154, 1930.
(9) W. Baade, *Symposium on Astrophysics*, University of Michigan, 1953.
(10) A. R. Sandage, *Symposium on Astrophysics*, University of Michigan, 1953.
(11) E. G. Ebbighausen, *Ap. J.*, **91,** 244, 1940.
(12) H. L. Vanderlinden, *Medd. Univ. Gent*, No. 10, 1945.
(13) W. Becker and J. Stock, *Zs. f. Ap.*, **31,** 316, 1953.
(14) A. R. Sandage, *A.J.*, **58,** 61, 1953.
(15) H. L. Johnson, *Ap. J.*, **117,** 356, 1953.
(16) J. Cuffey, *H.A.*, **105,** 403, 1937.
(17) W. P. Bidelman, *Ap. J.*, **105,** 492, 1947.
(18) L. R. Henrich, *Ap. J.*, **98,** 192, 1943; *Ap. J.*, **96,** 106, 1942.
(19) T. G. Cowling, *M.N.*, **98,** 528, 1938.
(20) I. Epstein, *Ap. J.*, **114,** 438, 1951.
(21) V. C. Reddish, *The Observatory*, **74,** 68, 1954.
(22) A. R. Sandage and M. Schwarzschild, *Ap. J.*, **116,** 463, 1952.
(23) H. L. Johnson, *Ap. J.*, **120,** 325, 1954.

STAR-STREAMING FROM THE PROPER MOTIONS OF THE A-TYPE STARS OF THE BOSS *GENERAL CATALOGUE*

T. R. Tannahill

(Communicated by the Director, University Observatory, Glasgow)

(Received 1954 November 4)

Summary

1. The proper motions of 8676 stars of spectral types B8–A3 in the Boss *General Catalogue* have been analysed, according to the two-streams hypothesis, by Eddington's method.

2. The galactic coordinates of the vertex are ($365°{\cdot}5$, $-0°{\cdot}5$).

3. The equatorial coordinates of the solar apex are ($264°{\cdot}8$, $+31°{\cdot}5$).

4. The ratio of the number of stars in the drifts is 1·54.

5. Comparison of the results with those from later types reveals large and irregular variations in the constants of star-streaming which are not to be accounted for by accidental error. It is suggested that inadequacy of the two-drift hypothesis, or non-homogeneity of the groupings of the data, may be the explanation of these.

---

1. In a previous paper (**1**) the proper motions of 22 374 stars of spectral types A5–M in the *General Catalogue of 33 342 Stars* by Benjamin Boss (**2**) have been analysed on Eddington's two-drift hypothesis in three spectral groups and four zones of galactic latitude. A later paper (**3**) analyses the motions of 1536 O- and B-type stars of the same catalogue. The present paper analyses the motions of 8676 stars in the spectral range B8–A3, and completes the determination, by this method, of the constants of the star streams, and the directions of the solar motion and the vertex of star-streaming, from the data of this catalogue.

2. The treatment of the observational data follows almost exactly that described (**1**) for the stars of types A5–M, and reference may be made to this paper for the system of assigning weights to the proper motions, for the systematic corrections applied and for the grouping into regions. Stars belonging to known clusters have been rejected—20 of the Pleiades group, 46 of the Ursa Major group and 9 of the Taurus cluster. As before, diametrically opposite regions have been combined, and (in cases where the precaution seemed necessary) corrections have been applied to the position angles of the proper motions to allow for the convergency of the meridians in regions of high declination.

The results of the analysis are given in Table VI.* In this table, hV_1 and hV_2 are the projections of the space-velocities of the drifts on the tangent-plane at the centre of the region, θ_1 and θ_2 the position angles of the directions towards the drift apices and N_1 and N_2 the numbers of stars allocated to the drifts. As with the A5–M stars, the regions round the Drift I apex offer difficulty in analysis, particularly in the determination of the Drift II constants. A further difficulty

* Tables VI to IX appear at the end of the paper.

in this investigation is the higher concentration of the stars in the galactic plane, the regions in the higher galactic latitudes being very sparsely populated—in Zone IV, comprising the six regions round the galactic pole, the total weight of stars does not exceed 100 in any region. Analysis has, however, been possible in all regions.

3. Solutions for the drift apices have been found for three groupings of the data—a solution for all the stars involved in the discussion, and solutions for low galactic latitude (obtained by combining the regions of Zones I and II of the previous paper) and for high galactic latitude (Zones III and IV). The mean galactic latitude for the low latitude group is 13°·7, and for the high latitude group 51°·6. The results are given in Table VII, in which X, Y and Z are the linear components of the space-velocity of a drift relative to the Sun, referred to the usual equatorial axes, hW is the resultant space-velocity and A and D are the equatorial coordinates of the apices. The decrease of hW_1 with increasing galactic latitude, already noted in the previous paper (**1**) on the A5–M stars, is quite apparent. In order to establish this variation without ambiguity, a further solution for the A5–M stars has been made, in galactic latitude groups similar to those used for the A-type stars (namely, combining Zones I and II and Zones III and IV). The results, given in Table I, show that this variation with galactic latitude holds for limited spectral ranges. It is not, therefore, a reflection of

TABLE I

Variation of hW_1 with galactic latitude

	B8–A3	A5–F5	F8–G5	K0–M	p.e.*
Zones I, II	1·742	1·934	1·756	1·491	±0·04
Zones III, IV	1·518	1·661	1·416	1·299	±0·04

any similar variation in spectral type. A comparison of the results from the spectral groups of the previous paper with those of the present paper (Table II) shows the surprising feature that the decrease of hW_1 with advancing spectral type, which is so clearly marked in the A5–M types, is not maintained in the A-stars of the present paper. A systematic change in the Drift II apex is now, however, apparent, the right ascension decreasing, the declination increasing, with advancing spectral type. In noting these apparently systematic trends it is desirable to emphasize that there occur also large and apparently irregular variations in some

TABLE II

Variation of drift constants with spectral type

	B8–A3	A5–F5	F8–G5	K0–M	p.e.
A_1	91°·4	91°·1	92°·9	96°·0	±1°
D_1	−16°·6	−8°·9	−10°·3	−10°·8	±1°
hW_1	1·628	1·770	1·564	1·385	±0·03
A_2	309°·4	301°·0	273°·5	265°·8	±6°
D_2	−55°·8	−63°·4	−71°·0	−74°·4	±3°
hW_2	0·695	0·735	0·889	0·770	±0·03

* The probable errors quoted in Tables I to IV are approximate values roughly applicable to all the quantities in the same line. The computed probable errors are given in the main tables of this and of the previous paper.

of the quantities determined—variations which, judged by the probable errors involved, are statistically significant, and yet indicate no systematic trend. The variation of hW_2 with spectral type (Table II) is one such case, the value of D_1 for the A-type group another. (It should be mentioned that the probable errors are derived from the residuals obtained from the separate regions, and measure the degree of accordance of the regional results with the results of the final solutions). Two possible reasons for these curious discrepancies may be tentatively suggested: firstly, that the two-drift hypothesis is merely a first approximation to the representation of proper motion data, and that the data are now sufficient to indicate the short-comings of the hypothesis; secondly, it is possible that the traditional grouping into spectral classes and zones of galactic latitude is not the grouping which best exhibits the variations in the constants involved; for example, a division of the data into giants and dwarfs rather than into spectral types, or a distance grouping of the material, might produce more homogeneous groups and more regular and systematic variations in the drift-constants derived therefrom.

4. The theoretical values of hV and θ, calculated for each region from the constants of the final solutions, are given in Tables VIII A to VIII C under the headings hV_c and θ_c, with the residuals hV_c–hV and θ_c–θ. The residuals are, on the whole, rather higher than those obtained for the A5–M stars. The values of λ—the distance of the region from the apex—and of β—the distance of the calculated apex from the great circle defined in each region by the observed direction of the apex—are also shown. The values of β_1 are satisfactory, only four in each table exceeding 10°; those of β_2 are rather high, usually exceeding 10° and attaining nearly 40° in Table VIII A. A noticeable improvement occurs in Tables VIII B and VIII C, where the observed regional values are compared with the zonal constants.

5. The linear components ξ, η, ζ of relative motion of the drifts, with the resultant Ω, and the corresponding right ascension α_v and declination δ_v of the vertex of star-streaming are given in Table IX, together with the galactic co-ordinates l_v and b_v of the vertex nearest to the galactic centre. The outstanding feature of the results is the high value of the longitude of the vertex, which exceeds that of the galactic centre by 31°. This value agrees substantially with the value 351°·5 obtained by Delhaye (4) from his analysis of A-type stars on the ellipsoidal hypothesis. Table III shows the variation of the longitude of the vertex and of the relative speed Ω of the drifts with spectral type, the results for the later types being obtained from the previous paper (1). The decrease in the

TABLE III

Variation of l_v and Ω with spectral type

	B8–A3	A5–F5	F8–G5	K0–M	p.e.
l_v	356°·5	348°·6	341°·7	342°·4	±1°·5
Ω	1·887	2·075	1·912	1·638	±0·04

longitude with advancing spectral type is clearly shown for the first three groups. The value of Ω follows the same trend as hW_1 (Table II), and the same remarks are apposite.

The variation of Ω with galactic latitude is shown in Table IV for the same groups of stars, in limited spectral ranges, as are used in Table I. It is somewhat perplexing to note that while the later types show a well-marked decrease with increasing galactic latitude (a result which was suggested by the results of the previous paper), the A-type stars reverse this tendency, and show an equally well-marked increase. It may be noted in Table IV that in the non-galactic zones the values of Ω suggest that this quantity decreases with advancing spectral type. This is not true of the zones of low galactic latitude, nor is it true of the values for the whole sky (Table III). The anomalies in Tables III and IV may therefore be summarized in the statement that, for the B8–A3 stars, the value of Ω is abnormally low in regions of low galactic latitude.

TABLE IV

Variation of Ω with galactic latitude

	B8–A3	A5–F5	F8–G5	K0–M	p.e.
Zones I, II	1·775	2·209	2·033	1·740	±0·06
Zones III, IV	1·987	1·981	1·838	1·578	±0·06

TABLE V

Solar motion with respect to spectral type

	B8–A3	A5–F5	F8–G5	K0–M
A_0	264°·8	266°·0	272°·8	277°·8
D_0	+31°·5	+28°·1	+37°·4	+40°·3
hU_0	0·973	0·948	0·883	0·770
n_1/n_2	1·54	1·22	1·18	1·02
		(1·17)	(1·04)	(1·08)

Table IX contains the results for the right ascension A_0 and declination D_0 of the solar apex, with the corresponding solar speed hU_0 and the ratio of the numbers of stars in the two drifts. The ratio n_1/n_2 is remarkably high. This is the only determination of the ratio for the A-type stars alone. Eddington's investigation (**5**) of the PGC stars (including the A-types) gave the value 1·48. Smart and Tannahill (**6, 7**) from the Cape photographic proper motions found the value 1·41 (including the A-stars) and the value 1·10 (excluding the A-stars). There is therefore some previous evidence for this high value of the ratio from the A-type stars. The variation of the elements of the solar motion with spectral type is shown in Table V. Two of the elements show a steady trend. The right ascension of the apex increases with advancing spectral type, and the solar speed decreases. The ratio n_1/n_2 is high for the early types, and reaches a minimum in the K-type. This feature is also shown by the Cape proper motions (**6**), the relevant values being shown in brackets in Table V.

University Observatory,
Glasgow, W.2:
1954 *October* 28.

References

(1) T. R. Tannahill, *M.N.*, **112**, 3, 1952.
(2) Benjamin Boss, *General Catalogue of 33 342 Stars*, Carnegie Institute of Washington, Publication 468, 1937.
(3) T. R. Tannahill, *M.N.*, **114**, 460, 1954.
(4) J. Delhaye, *Contribution à l'étude de la distribution des vitesses stellaires*, Paris, 1951.
(5) A. S. Eddington, *M.N.*, **71**, 4, 1910.
(6) W. M. Smart and T. R. Tannahill, *M.N.*, **100**, 30, 1939.
(7) W. M. Smart and T. R. Tannahill, *M.N.*, **100**, 688, 1940.

TABLE VI

Analysis of the drift curves

Region	No. of stars	Drift I hV_1	Drift I θ_1	Drift I N_1	Drift II hV_2	Drift II θ_2	Drift II N_2
1	445	0·4	260°	225	0·8	180°	141½
*2	571	1·0	280	250	0·3	200	181½
*3	440	1·3	265	180	0·45	175	150½
*4	427	1·7	130	207	0·5	200	106½
*5	388	1·4	147½	187	0·6	200	92
6	515	1·4	162½	222½	0·6	235	183
*7	318	1·0	280	136	0·45	190	123
*8	334	1·7	262½	174	0·75	180	86½
*9–15	323	1·8	100	146½	0·3	230	108
*10	241	1·9	175	93½	0·1	220	92
11	360	1·0	190	148	0·5	225	148
12	288	1·1	250	146	0·55	190	114
*13	320	0·9	340	120	0·5	200	132
*14	413	1·2	310	169	0·3	200	151
16	223	1·9	120	117½	0·8	215	53
17	334	1·85	132½	193	0·7	215	65
18	300	1·6	147½	144½	0·4	190	116
19	340	0·2	220	170	0·7	165	120
20	175	1·4	260	120	0·9	140	45½
21	110	1·5	265	65	0·8	140	30½
*22	84	1·5	235	43	0·2	300	28
*23	146	1·5	215	69	0·3	260	55½
*24	174	1·1	232½	110	0·5	90	29
*25	164	0·8	65	79	0·6	230	53
*26	196	1·1	55	100	0·65	240	55
*27–36	143	1·8	35	69	0·25	250	47
28	107	1·5	110	77	1·1	250	18½
29	94	1·4	112½	63	1·3	220	27
30	118	1·0	90	62	0·5	220	38
31	105	1·4	250	59½	0·7	130	33
32	96	1·7	260	57	0·9	150	36
*33	82	1·3	260	37	0·45	210	29
34	97	1·0	95	60	1·2	250	23½
*35	101	1·7	85	53½	0·65	245	27
37	104	1·4	102½	82	0·8	215	15½

* Position angles corrected for convergency of meridians.

TABLE VII

The drift constants

Drift I

	B8–A3	B8–A3, Zones I, II	B8–A3, Zones III, IV
X_1	-0.037 ± 0.029	-0.032 ± 0.040	-0.137 ± 0.041
Y_1	$+1.560$ 0.028	$+1.648$ 0.046	$+1.475$ 0.032
Z_1	-0.465 0.030	-0.562 0.046	-0.330 0.037
A_1	91°.4 1°.1	91°.1 1°.4	95°.3 1°.6
D_1	$-16°.6$ 1°.0	$-18°.8$ 1°.5	$-12°.6$ 1°.4
hW_1	1.628 0.028	1.742 0.044	1.518 0.033
n_1	4236	3030	1206

Drift II

X_2	$+0.248 \pm 0.035$	$+0.188 \pm 0.029$	$+0.341 \pm 0.068$
Y_2	-0.302 0.034	-0.113 0.033	-0.433 0.052
Z_2	-0.575 0.036	-0.558 0.033	-0.614 0.061
A_2	309°.4 5°.3	328°.9 8°.2	308°.3 6°.7
D_2	$-55°.8$ 2°.9	$-68°.5$ 2°.9	$-48°.1$ 4°.2
hW_2	0.695 0.035	0.600 0.031	0.825 0.049
n_2	2754	2163	591

TABLE VIII A

B8–A3 *stars—whole sky*

Region	Drift I						Drift II					
	θ_c	$\theta_c-\theta_1$	β_1	λ_1	hV_c	hV_c-hV_1	θ_c	$\theta_c-\theta_2$	β_2	λ_2	hV_c	hV_c-hV_2
	°	°	°	°			°	°	°	°		
1	240·1	−19·9	5·1	15·1	0.42	+0.02	194·5	+14·5	13·5	111·7	0.65	−0.15
2	298·2	+18·2	10·8	37·0	0.98	−0.02	182·5	−17·5	17·4	84·9	0.69	+0.39
3	275·1	+10·1	9·3	67·4	1.50	+0.20	158·3	−16·7	14·8	62·2	0.62	+0.17
4	122·7	− 7·3	7·3	90·8	1.63	−0.07	227·4	+27·4	20·3	131·1	0.52	+0.02
5	152·4	+ 4·9	4·5	67·1	1.50	+0.10	231·8	+31·8	19·9	139·8	0.45	−0.15
6	171·3	+ 8·8	6·2	45·0	1.15	−0.25	216·0	−19·0	12·7	138·0	0.46	−0.14
7	266·9	−13·1	8·7	41·4	1.08	+0.08	176·8	−13·2	12·8	104·4	0.67	+0.22
8	266·9	+ 4·4	4·1	67·0	1.50	−0.20	160·6	−19·4	19·1	80·3	0.69	−0.06
9–15	102·4	+ 2·4	2·3	104·0	1.58	−0.22	226·3	− 3·7	2·5	137·3	0.47	+0.17
10	183·5	+ 8·5	8·3	78·7	1.60	−0.30	273·9	+53·9	14·9	161·4	0.22	+0.12
11	198·1	+ 8·1	5·9	46·5	1.18	+0.18	205·4	−19·6	10·5	147·2	0.38	−0.12
12	232·1	−17·9	11·9	42·2	1.09	−0.01	183·4	− 6·6	4·8	133·5	0.50	−0.05
13	352·9	+12·9	6·4	29·6	0.80	−0.10	199·3	− 0·7	0·7	74·2	0.67	+0.17
14	315·1	+ 5·1	3·8	48·7	1.22	+0.02	182·7	−17·3	15·8	65·7	0.63	+0.33
16	114·6	− 5·4	5·4	86·8	1.62	−0.28	215·0	0·0	0·0	112·3	0.64	−0.16
17	129·0	− 3·5	3·1	63·3	1.46	−0.39	218·5	+ 3·5	3·2	115·9	0.63	−0.07
18	134·8	−12·7	7·6	36·9	0.98	−0.62	213·2	+23·2	21·4	112·0	0.64	+0.24
19	139·8	−80·2	9·4	9·5	0.27	+0.07	204·1	+39·1	37·5	105·1	0.67	−0.03
20	244·1	−15·9	13·6	59·1	1.40	0.00	168·3	+28·3	20·6	132·1	0.52	−0.38
21	257·7	− 7·3	7·0	74·1	1.56	+0·	158·3	+18·3	18·2	97·1	0.69	−0.11
22	235·9	+ 0·9	0·9	99·0	1.61	+0.11	32·6	+92·6	21·5	158·5	0.26	+0.06
23	226·2	+11·2	11·2	85·0	1.62	+0.12	68·7	+168·7	1·2	173·6	0.08	−0.22
24	229·1	− 3·4	3·2	72·0	1.55	+0.45	160·4	+70·4	16·9	162·1	0.21	−0.29
25	53·0	−12·0	6·4	32·3	0.87	+0.07	212·6	−17·4	16·4	70·4	0.65	+0.05
26	48·2	− 6·8	5·2	49·7	1.24	+0.14	224·0	−16·0	12·5	51·2	0.54	−0.11
27–36	29·2	− 5·8	5·1	60·9	1.42	−0.38	229·3	−20·7	13·7	42·0	0.47	+0.22
28	112·3	+ 2·3	2·3	78·9	1.60	+0.10	212·2	−37·8	37·6	95·9	0.69	−0.41
29	110·9	− 1·6	1·3	53·3	1.30	−0.10	214·2	− 5·8	5·8	90·3	0.70	−0.60
30	89·3	− 0·7	0·3	29·9	0.81	−0.19	211·9	− 8·1	8·1	84·7	0.69	+0.19
31	250·5	+ 0·5	0·5	85·3	1.62	+0.22	150·0	+20·0	14·5	132·9	0.51	−0.19
32	253·1	− 6·9	6·8	79·1	1.60	−0.10	156·1	+ 6·1	5·5	115·3	0.63	−0.27
33	253·9	− 6·1	6·0	97·6	1.61	+0.31	125·9	−84·1	29·6	150·3	0.34	−0.11
34	90·2	− 4·8	3·8	53·0	1.30	+0.30	218·3	−31·7	28·4	64·8	0.63	−0.57
35	92·2	+ 7·2	6·7	68·8	1.52	−0.18	231·5	−13·5	8·8	40·9	0.45	−0.20
37	104·7	+ 2·2	2·1	74·4	1.57	+0.17	213·4	− 1·6	1·5	68·6	0.65	−0.15

TABLE VIII B

B8–A3 *stars—galactic Zones I, II*

Region	Drift I						Drift II					
	θ_c	$\theta_c-\theta_1$	β_1	λ_1	hV_c	hV_c-hV_1	θ_c	$\theta_c-\theta_2$	β_2	λ_2	hV_c	hV_c-hV_2
	°	°	°	°			°	°	°	°		
1	233·5	−26·5	7·2	16·4	0·49	+0·09	194·8	+14·8	14·7	96·2	0·60	−0·20
2	295·1	+15·1	8·8	35·7	1·02	+0·02	189·0	−11·0	10·4	70·7	0·57	+0·27
3	273·5	+ 8·5	7·7	65·7	1·59	+0·29	172·7	− 2·3	1·8	52·4	0·48	+0·03
4	124·0	− 6·0	6·0	92·1	1·74	+0·04	206·7	+ 6·7	4·8	134·5	0·43	−0·07
5	153·5	+ 6·0	5·6	69·0	1·63	+0·23	210·4	+10·4	7·5	133·8	0·43	−0·17
6	172·1	+ 9·6	7·0	47·2	1·28	−0·12	203·8	−31·2	25·0	125·4	0·49	−0·11
7	263·5	−16·5	10·9	41·3	1·15	+0·15	186·0	− 4·0	4·0	91·2	0·60	+0·15
8	264·8	+ 2·3	2·1	66·0	1·59	−0·11	173·9	− 6·1	5·8	71·5	0·57	−0·18
9–15	103·3	+ 3·3	3·2	106·1	1·67	−0·13	206·0	−24·0	12·9	146·7	0·33	+0·03
10	183·7	+ 8·7	8·6	80·9	1·72	−0·18	230·3	+10·3	4·0	157·4	0·23	+0·13
11	197·6	+ 7·6	5·7	48·7	1·31	+0·21	200·0	−25·0	18·3	132·1	0·45	−0·05
12	229·8	−20·2	13·8	43·8	1·21	+0·11	189·6	− 0·4	0·4	118·8	0·53	−0·02
13	352·0	+12·0	5·5	27·4	0·80	−0·10	200·3	+ 0·3	0·3	58·7	0·51	+0·01
14	313·5	+ 3·5	2·5	46·8	1·27	+0·07	190·9	− 9·1	7·1	51·8	0·47	+0·17
16	116·4	− 3·6	3·6	88·1	1·74	−0·16	198·2	−16·8	15·3	114·3	0·55	−0·25
17	131·0	− 1·5	1·4	64·7	1·57	−0·28	202·4	−12·6	11·8	111·1	0·56	−0·14
18	137·7	− 9·8	6·1	38·2	1·08	−0·52	201·8	+11·8	11·6	101·0	0·59	+0·15
19	148·6	−71·4	10·5	11·1	0·33	+0·13	199·2	+34·2	34·2	90·4	0·60	−0·10

TABLE VIII C

B8–A3 *stars—galactic Zones III, IV*

Region	Drift I						Drift II					
	θ_c	$\theta_c-\theta_1$	β_1	λ_1	hV_c	hV_c-hV_1	θ_c	$\theta_c-\theta_2$	β_2	λ_2	hV_c	hV_c-hV_2
	°	°	°	°			°	°	°	°		
20	246·8	−13·2	10·7	54·0	1·23	−0·17	163·0	+23·0	14·9	138·8	0·54	−0·36
21	262·8	− 2·2	2·1	71·6	1·44	−0·06	152·9	+12·9	12·6	102·6	0·81	+0·01
22	233·0	− 2·0	2·0	94·2	1·51	+0·01	30·4	+90·4	29·2	150·8	0·40	+0·20
23	224·2	+ 9·2	9·1	79·9	1·49	−0·01	38·6	+138·6	8·2	167·5	0·18	−0·12
24	228·5	− 4·0	3·7	66·5	1·39	+0·29	140·2	+50·2	9·3	167·8	0·17	−0·33
25	53·5	−11·5	7·0	37·8	0·93	+0·13	217·9	−12·1	11·7	76·2	0·80	+0·20
26	50·5	− 4·5	3·7	55·0	1·24	+0·14	229·1	−10·9	9·2	57·6	0·70	+0·05
27–36	32·8	− 2·2	2·0	65·4	1·38	−0·42	231·6	−18·4	14·0	49·6	0·63	+0·38
28	107·0	− 3·0	3·0	80·8	1·50	0·00	219·4	−30·6	30·6	93·1	0·82	−0·28
29	105·2	− 7·3	6·1	56·3	1·26	−0·14	221·9	+ 1·9	1·9	91·1	0·82	−0·48
30	83·6	− 6·4	3·6	34·6	0·86	−0·14	218·3	− 1·7	1·7	88·9	0·82	+0·32
31	252·8	+ 2·8	2·8	80·3	1·50	+0·10	140·2	+10·2	7·1	136·1	0·57	−0·13
32	257·0	− 3·0	2·9	75·1	1·47	−0·23	149·2	− 0·8	0·7	119·9	0·72	−0·18
33	253·9	− 6·1	6·1	92·1	1·52	+0·22	111·0	−99·0	31·0	148·6	0·43	−0·02
34	87·7	− 7·3	6·2	58·1	1·29	+0·19	226·2	−23·8	21·8	67·4	0·76	−0·44
35	92·0	+ 7·0	6·7	74·3	1·46	−0·24	242·0	− 3·0	2·1	44·0	0·57	−0·08
37	101·1	− 1·4	1·4	78·6	1·49	+0·09	221·6	+ 6·6	6·1	67·5	0·76	−0·04

TABLE IX

The vertex of star-streaming and the solar motion

	B8–A3	B8–A3, Zones I, II	B8–A3, Zones III, IV
ξ	−0·285 ± 0·045	−0·220 ± 0·049	−0·478 ± 0·079
η	+1·862 0·044	+1·762 0·057	+1·908 0·061
ζ	+0·110 0·047	−0·004 0·057	+0·284 0·071
α_v	278°·7 1°·5	277°·1 2°·0	284°·1 2°·3
δ_v	−3°·4 1°·4	+0°·1 1°·8	−8°·2 2°·1
Ω	1·887 0·047	1·775 0·057	1·987 0·062
l_v	356°·5 1°·4	358°·5 1°·8	354°·6 2°·1
b_v	−0°·5 1°·4	+2°·6 1°·7	−7°·4 2°·3
A_0	264°·8	266°·3	268°·6
D_0	+31°·5	+31°·5	+26°·6
hU_0	0·973	1·074	0·948
n_1/n_2	1·54	1·40	2·04

ORBITAL ELEMENTS OF FOUR VISUAL BINARIES

W. D. Heintz

(Communicated by R. v. d. R. Woolley)

(Received 1954 September 17)

Summary

Provisional elements have been derived for Σ 3050 and OΣ 358, and the orbits of Σ 2 and Σ 228 have been recomputed in accordance with the new methods of W. Rabe.

---

1. Σ 3050 (ADS 17149; $23^h\,56^m{\cdot}9$, $+33°\,27'$). New orbit

This "beautiful pair" (37 Andromedae) has been measured very frequently since W. Struve's times. The distance decreased from 4″ to 1″·5, but the observed arc includes neither periastron nor apastron, so that the computation meets with some difficulties, even in the application of Rabe's method for short arcs (**1**).

The position angles P are expanded in the following power series:

$$P(\tau) = 219°{\cdot}14 + 6°{\cdot}58\tau + 0°{\cdot}730\tau^2 + 0°{\cdot}0629\tau^3 + 0°{\cdot}0021\tau^4,$$

where 1910·0 is taken as zero epoch (osculation) and 10 years as time unit, i.e. $\tau = (t - 1910)/10$. Generally, Rabe does not use second and higher differential quotients of the coordinates, but if the value $d\rho/dt$ is determined from the position-angle series, as in this case, it is advantageous to include the fourth power in the series, so that the second power coefficient can be fairly accurately derived.

The curvature of the apparent arc as given by the most recent normal places indicates high eccentricity, but this seems to be inconsistent with the older measurements. The computation, using Rabe's "solution B", was repeated several times under various assumptions about e and periastron time T. The final solution depends greatly on the accuracy of the 1831 normal place; the 1792·8 measurement 180° ± of Herschel gives O–C = −2°·5. The formulae of Russell and Moore (**2**) yield a dynamical parallax of 0″·065 and a total mass of the system of 1·8 solar masses. Table I gives the representation of the 23 normal places and an ephemeris. The change of position angle due to precession is negligibly small.

As the star is approaching periastron quickly now, it will be obvious in a few years whether the elements derived from the small arc approximate to the true orbit. But these elements will at least give a sufficient description of the motion of this interesting couple up to the present.

2. Σ 2 (ADS 102; $0^h\,06^m{\cdot}3$, $+79°\,26'$)

Recent observations give deviations up to +15° from van Arnam's orbit (**3**). As the components were too close for the observers in the years 1865–85, the observed arc consists of two separate parts, and the motion in periastron (1888) can hardly be determined with sufficient accuracy. The position angle ψ of the tangential velocity at periastron time, which is important for Rabe's improvement formulae, and which usually may be taken from the previous

orbit, had to be changed by nearly 7° in this case. Additionally to van Arnam's 17 smoothed normal places, there are 8 new ones, covering the time since 1930 (Table II). They were not smoothed out, for in such rapid angular motion the interpolation process may introduce some error. The resulting elements show little difference from those of van Arnam. Although the companion has moved more than 300° in position angle since 1830, the direction of the minor axis of the apparent ellipse is not yet determined, so that, owing to the high inclination, the values of eccentricity and period are still uncertain. From Russell's formulae, the orbit gives a parallax 0″·009 and a total mass 5·5 ☉.

Before finishing the computations, the writer was informed of a recent orbit published by van Biesbroeck, where the period is increased to 419 years. It will be seen in a few years whether the recent observations support this considerable change.

3. Σ228 (ADS 1709; $2^h\,10^m{\cdot}8$, +47° 15′)

Previous orbits of this pair showed that the older measurements could be hardly represented by the areal constant derived from the more recent observations. Rabe (1914) gave full credit to the position angles, while Kuiper's orbit (1930) satisfied the distances. The recent data now allow a solution which represents both coordinates fairly well. It should be a useful approximation to definitive elements as almost the full orbit is observed. Kuiper's orbit (**4**) was denoted "assez bon" in Baize's new catalogue (**5**), but gives residuals +6° recently. Using these elements as initial values, and adding 8 normal places (Table III), an improvement was easily obtained by means of Rabe's formulae of "variation of apsides". Period and eccentricity seem to be settled now, but an orbit of definitive accuracy will not be available before the companion has passed apastron, for the observations at the time after its last apastron passage are scanty and discordant. The dynamical parallax comes out to be 0″·023, giving a total mass of 3·0 ☉. Other parallax determinations, referred to by Baize (**5**), yielded values 0″·026 to 0″·047.

4. OΣ358 (ADS 11483; $18^h\,33^m{\cdot}6$, +16° 56′). New orbit

The numerous measurements, from which 14 normal places were formed (Table IV), cover 45° in position angle only, but with a distinct change in distance. The observed arc probably contains apastron; so 1930·0 was chosen as osculation and apastron epoch, and the position-angle series is (time unit = 25 years):

$$P(\tau) = 182^\circ{\cdot}95 - 9^\circ{\cdot}13\tau - 0^\circ{\cdot}403\tau^2 + 0^\circ{\cdot}056\tau^3 + 0^\circ{\cdot}010\tau^4.$$

As in the previous case, the observations seem to disagree with the law of areas somewhat; the distances were mainly represented. The companion will continue its slow motion towards the main star for a long time. The mass of the system, 3·3 solar masses, results from a dynamical parallax of 0″·021.

The writer wishes to thank Professor W. Rabe, Munich, for suggesting that computation of orbits of these binaries was worth undertaking, and also for communicating his unpublished measurements up to 1954·0.

Commonwealth Observatory,
Mt. Stromlo,
Canberra, A.C.T.:
1954 *September* 7.

References

(1) W. Rabe, *A.N.*, **280,** 1, 1951.
(2) H. N. Russell and G. E. Moore, *The masses of the stars*, Chicago, 1940.
(3) R. van Arnam, *A.J.*, **43,** 59, 1933.
(4) G. P. Kuiper, *B.A.N.*, **5,** 232, 1930.
(5) P. Baize, *J.O.*, **33,** 1, 1950.

TABLE I

Σ3050

P 320^y	e 0·62	i ± 73°·06	ω 65°·12
T 2044·0	a 3″·686	Ω 353°·68	μ 1·125

Normal places:

t	(n)	P_o	P_c	O–C	ρ_o	ρ_c	O–C
		°	°	°	″	″	″
1831·82	(11)	190·2	190·80	−0·60	4·02	3·962	+0·06
41·66	(5)	192·9	193·06	−0·16	3·90	3·834	+ 07
54·44	(15)	196·3	196·28	+0·02	3·59	3·620	− 03
66·58	(16)	200·0	199·76	+0·24	3·22	3·371	− 15
74·11	(21)	202·1	202·19	−0·09	3·04	3·206	− 17
82·83	(21)	205·8	205·35	+0·45	2·97	2·998	− 03
90·96	(29)	208·7	208·75	−0·05	2·78	2·794	− 01
96·94	(32)	212·0	211·60	+0·40	2·67	2·641	+ 03
1904·17	(26)	215·2	215·48	−0·28	2·49	2·454	+ 04
09·85	(37)	219·3	219·00	+0·30	2·32	2·308	+ 01
13·90	(51)	221·9	221·78	+0·12	2·19	2·206	− 02
17·65	(33)	224·7	224·58	+0·12	2·13	2·111	+ 02
21·19	(35)	227·6	227·50	+0·10	2·00	2·027	− 03
23·66	(33)	229·2	229·65	−0·45	1·93	1·971	− 04
26·22	(43)	231·6	232·03	−0·43	1·99	1·910	+ 08
30·19	(48)	235·9	236·03	−0·13	1·92	1·824	+ 10
35·05	(43)	241·3	241·57	−0·27	1·84	1·726	+ 11
38·20	(52)	244·8	245·24	−0·44	1·74	1·673	+ 07
40·66	(40)	248·4	248·37	+0·03	1·64	1·633	+ 01
42·48	(41)	251·2	250·81	+0·39	1·59	1·607	− 02
45·98	(33)	256·0	255·69	+0·31	1·57	1·561	+ 01
49·30	(33)	260·3	260·56	−0·26	1·45	1·528	− 08
52·24	(37)	265·0	265·05	−0·05	1·45	1·509	− 06

Ephemeris:

	P	ρ		P	ρ
	°	″		°	″
1954·0	267·8	1·50	1968·0	289·7	1·52
56·0	270·9	1·49	70·0	292·8	1·54
58·0	274·1	1·48	72·0	295·7	1·56
60·0	277·2	1·48	74·0	298·6	1·58
62·0	280·4	1·49	76·0	301·4	1·60
64·0	283·6	1·49	78·0	304·0	1·63
66·0	286·7	1·50	80·0	306·6	1·66

TABLE II

$\Sigma 2$

P 300^y	e 0·575	i ± 113°·2	ω 330°·1
T 1888·2	a 0″·686	Ω 169°·9	μ 1·200

Normal places:

t	(n)	P_o	P_c	O–C	ρ_o	ρ_c	O–C
		°	°	°	″	″	″
1829·00		343·4	343·91	−0·51	0·84	0·75	+0·09
1834·00		341·9	342·20	−0·30	0·80	0·71	+0·09
1839·00		340·2	340·22	−0·02	0·74	0·65	+0·06
1844·00		337·6	337·87	−0·27	0·64	0·59	+0·05
1849·00		335·4	334·94	+0·46	0·53	0·53	0
1854·00		332·4	331·13	+1·27	0·44	0·45	−0·01
1859·00		325·8	325·80	0	0·37	0·37	0
1864·00		316·4	317·93	−1·53	0·29	0·29	0
1889·00		181·5	180·57	+0·93	0·26	0·27	−0·01
1894·00		168·5	169·68	−1·18	0·30	0·31	−0·01
1899·00		160·5	160·49	+0·01	0·32	0·32	0
1904·00		151·3	151·30	0	0·32	0·31	+0·01
1909·00		140·8	141·13	−0·33	0·30	0·29	+0·01
1914·00		130·3	129·29	+0·71	0·27	0·27	0
1919·00		116·0	115·50	+0·50	0·24	0·25	−0·01
1924·00		99·3	100·31	−1·01	0·23	0·24	−0·01
1929·00		81·0	85·02	−4·02	0·23	0·25	−0·02
1931·47	(11)	77·7	77·95	−0·25	0·29	0·26	+0·03
1935·12	(13)	76·0	68·41	+7·59	0·28	0·27	+0·01
1937·46	(10)	64·6	62·94	+1·66	0·29	0·29	0
1939·34	(13)	54·3	58·92	−4·62	0·28	0·31	−0·03
1941·38	(16)	59·0	54·94	+4·06	0·28	0·32	−0·04
1944·81	(13)	50·4	49·03	+1·37	0·32	0·34	−0·02
1948·44	(18)	44·4	43·70	+0·70	0·35	0·37	−0·02
1952·22	(12)	38·9	39·00	−0·10	0·38	0·40	−0·02

Ephemeris:

	P	ρ
	°	″
1954·0	37·0	0·41
56·0	35·0	0·43
58·0	33·1	0·45
60·0	31·4	0·47
62·0	29·8	0·48
64·0	28·3	0·50

TABLE III

Σ 228

P 144ʸ·7	*e* 0·26	*i* ± 63°·4	ω 320°·95	
T 1898·2	*a* 0″·908	☊ 97°·6	μ 2·488	

(Equinox 1900)

Normal places:

t	(*n*)	P_o(1900)	P_c	O–C	ρ_o	ρ_c	O–C
		°	°	°	″	″	″
1831·46	(7)	262·4	262·81	−0·41	1·08	1·02	+0·06
43·55	(4)	273·9	272·37	+1·53	1·14	1·08	+ 06
56·54	(7)	284·1	282·73	+1·37	1·00	1·00	0
64·29	(10)	288·9	290·61	−1·71	0·93	0·87	+ 06
71·02	(8)	300·5	300·51	−0·01	0·72	0·69	+ 03
76·12	(16)	312·6	312·57	+0·03	0·59	0·54	+ 05
81·51	(9)	336·0	335·36	+0·64	0·38	0·39	− 01
84·52	(3)	356·2	356·13	+0·07	0·26	0·34	− 08
88·78	(14)	25·1	31·03	−5·93	0·40	0·34	+ 06
89·97	(10)	40·7	39·85	+0·85	0·39	0·36	+ 03
92·25	(7)	52·3	54·04	−1·74	0·34	0·40	− 06
95·18	(11)	66·0	67·57	−1·57	0·43	0·48	− 05
97·31	(20)	75·0	74·98	+0·02	0·60	0·53	+ 07
99·81	(14)	84·3	81·96	+2·34	0·60	0·59	+ 01
1901·13	(13)	87·6	85·16	+2·44	0·66	0·62	+ 04
03·25	(10)	90·1	89·74	+0·36	0·63	0·66	− 03
06·54	(19)	94·2	96·06	−1·86	0·60	0·70	− 10
10·01	(22)	104·4	102·20	+2·20	0·64	0·71	− 07
13·14	(17)	107·8	107·66	+0·14	0·72	0·71	+ 01
14·89	(15)	111·1	110·79	+0·31	0·69	0·70	− 01
17·34	(22)	114·4	115·37	−0·97	0·62	0·68	− 06
20·72	(20)	120·4	122·10	−1·70	0·61	0·64	− 03
22·62	(9)	123·9	126·69	−2·79	0·61	0·61	0
25·23	(12)	131·3	133·38	−2·08	0·64	0·57	+ 07
29·90	(6)	150·1	147·89	+2·21	0·46	0·50	− 04
1930·24	(21)	149·6	149·06	+0·54	0·56	0·50	+ 06
34·15	(23)	163·7	164·01	−0·31	0·53	0·46	+ 07
37·47	(24)	177·2	178·48	−1·28	0·45	0·45	0
39·41	(28)	187·5	186·96	+0·56	0·44	0·45	− 01
42·20	(29)	200·0	198·66	+1·34	0·47	0·47	0
46·64	(21)	214·7	214·82	−0·12	0·51	0·52	− 01
49·61	(19)	224·9	223·68	+1·22	0·60	0·57	+ 03
52·51	(26)	231·1	230·92	+0·18	0·60	0·62	− 02

Ephemeris (equinox of date):

	P	ρ		*P*	ρ
	°	″		°	″
1954·0	234·4	0·65	1968·0	255·3	0·91
56·0	238·4	0·69	70·0	257·4	0·94
58·0	241·9	0·73	72·0	259·4	0·97
60·0	245·1	0·77	74·0	261·2	0·99
62·0	248·0	0·80	76·0	263·0	1·01
64·0	250·6	0·84	78·0	264·7	1·03
66·0	253·0	0·87	80·0	266·3	1·05

TABLE IV

OΣ358

P 292^y	e 0·48	i ± 134°·23	ω 19°·43
T 1784·0	a 1″·358	Ω 16°·63	μ 1·233

(Equinox 1900)

Normal places:

t	(n)	P_o(1900)	P_c	O–C	ρ_o	ρ_c	O–C
		°	°	°	″	″	″
1845·30	(6)	220·4	219·78	+0·62	1·19	1·39	−0·20
65·27	(14)	207·5	208·02	−0·52	1·73	1·68	+ 05
74·05	(22)	202·3	203·93	−1·63	1·75	1·78	− 03
81·47	(45)	200·9	200·78	+0·12	1·85	1·84	+ 01
86·92	(53)	198·6	198·58	+0·02	1·88	1·88	0
96·73	(50)	194·8	194·84	−0·04	1·84	1·94	− 10
1905·78	(73)	190·9	191·52	−0·62	1·93	1·96	− 03
15·01	(52)	188·1	188·20	−0·10	1·91	1·97	− 06
20·45	(52)	185·9	186·26	−0·36	2·03	1·98	+ 05
25·07	(77)	184·8	184·59	+0·21	2·02	1·98	+ 04
30·28	(58)	183·2	182·70	+0·50	1·98	1·97	+ 01
38·04	(82)	180·0	179·83	+0·17	1·93	1·95	− 02
44·36	(53)	178·0	177·41	+0·59	1·92	1·89	+ 03
51·03	(54)	174·8	174·76	+0·04	1·87	1·85	+ 02

Ephemeris (equinox of date):

	P	ρ		P	ρ
	°	″		°	″
1954·0	173·2	1·83	1968·0	166·9	1·71
56·0	172·4	1·81	70·0	166·0	1·69
58·0	171·5	1·80	72·0	164·9	1·67
60·0	170·6	1·78	74·0	163·9	1·64
62·0	169·7	1·76	76·0	162·9	1·62
64·0	168·8	1·74	78·0	161·8	1·60
66·0	167·9	1·73	80·0	160·7	1·58

MEAN DAILY AREAS AND HELIOGRAPHIC LATITUDES OF SUNSPOTS IN THE YEARS 1951 AND 1952

Royal Greenwich Observatory

(Communicated by the Astronomer Royal)

(Received 1954 July 27)

The following results are in continuation of those given in *M.N.*, **114**, 134, 1954, and are derived from the measurement at Herstmonceux of photographs taken at the Royal Observatories of Greenwich and the Cape and at the Kodaikanal Observatory, India.

Table I gives the mean daily areas of umbrae, whole spots and faculae for each synodic rotation of the Sun included in the years 1951 and 1952; the means for the two years as a whole are included in Table II, which summarizes the yearly values since the last sunspot minimum of 1944.

TABLE I

No. of rotation	Rotation commenced U.T. 1950–52	Days photographed	Mean daily areas: Projected* Umbrae	Projected* Whole spots	Projected* Faculae	Corrected for foreshortening† Umbrae	Corrected for foreshortening† Whole spots	Corrected for foreshortening† Faculae
1301	Dec. 9·74	27	80	538	749	51	341	911
1302	Jan. 6·07	28	225	1344	842	154	911	1024
1303	Feb. 2·41	27	117	731	944	89	556	1173
1304	Mar. 1·75	27	233	1170	935	172	888	1179
1305	Mar. 29·06	28	337	2030	1081	237	1449	1314
1306	Apr. 25·33	27	650	3882	1176	479	2885	1457
1307	May 22·56	27	607	3678	1387	450	2724	1687
1308	June 18·76	27	292	1853	1449	213	1385	1712
1309	July 15·96	27	181	1038	1497	130	742	1797
1310	Aug. 12·18	28	118	669	1222	90	520	1445
1311	Sept. 8·43	27	236	1386	1282	165	953	1508
1312	Oct. 5·70	27	179	1073	1256	132	807	1455
1313	Nov. 1·99	27	148	885	1035	111	664	1196
1314	Nov. 29·30	28	121	845	882	86	614	1084
1315	Dec. 26·63	27	148	840	949	99	566	1128
1316	Jan. 22·96	28	76	475	749	51	322	880
1317	Feb. 19·30	27	32	165	519	25	132	633
1318	Mar. 17·63	27	67	402	540	46	280	670
1319	Apr. 13·92	27	58	338	660	55	329	794
1320	May 11·16	28	48	254	599	36	194	704
1321	June 7·37	27	136	727	652	95	522	773
1322	July 4·57	27	136	861	757	100	639	932
1323	July 31·78	27	126	709	641	94	543	772
1324	Aug. 28·01	27	116	664	602	90	510	735
1325	Sept. 24·28	27	70	390	476	49	280	559
1326	Oct. 21·56	28	77	456	439	56	318	520
1327	Nov. 17·87	27	138	799	352	100	589	421

* Expressed in millionths of the Sun's disk.

† Expressed in millionths of the Sun's hemisphere.

Table III gives for each rotation in the years 1951 and 1952 the mean daily area of the whole spots (corrected for foreshortening) and the mean heliographic latitude of the spotted areas for both northern and southern hemispheres.

The mean heliographic latitude of the entire spotted area and the mean distance from the equator of all spots are also tabulated. The mean values for the years 1951 and 1952 are included in Table IV.

TABLE II

	No. of days		Mean daily areas					
			Projected*			Corrected for foreshortening†		
Year	Photographed	Without spots	Umbrae	Whole spots	Faculae	Umbrae	Whole spots	Faculae
1944	366	157	30	160	284	23	126	344
1945	365	14	102	560	774	78	429	940
1946	365	0	389	2381	1794	291	1817	2188
1947	365	0	558	3559	2326	405	2637	2894
1948	366	0	419	2618	1849	314	1977	2331
1949	365	0	485	2873	2140	356	2129	2597
1950	365	3	274	1638	1421	203	1222	1754
1951	365	2	259	1552	1145	188	1136	1379
1952	366	24	96	548	594	70	404	711

* Expressed in millionths of the Sun's disk.
† Expressed in millionths of the Sun's hemisphere.

Tables II and IV are in continuation of similar tables in *Monthly Notices:* for the years *1874* to *1888*, **49,** 381, 1889: *1889* to *1902*, **63,** 465, 1903: *1901* to *1914*, **76,** 402, 1916: *1913* to *1924*, **85,** 1007, 1925: *1923* to *1933*, **94,** 870, 1934: and *1933* to *1945*, **110,** 501, 1950.

The rotations in Tables I and III are numbered in continuation of Carrington's series.

The chief features of the record for the years 1951 and 1952 are as follows:—

(1) Both years are of the descending phase of the sunspot cycle, but in 1951 the decreasing sunspot activity is largely obscured by the superposition of a considerable peak of activity included in Rotations 1306 and 1307 (see Table I). In the former rotation, the mean daily area of sunspots was 2885 millionths of the Sun's hemisphere and in the latter 2724 millionths. A giant sunspot (a late-comer after the four great spots of 1946–47) with its central meridian passage on May 16·0 contributed 1757 units to the mean daily area for Rotation 1306.

Another notable spot, the predecessor of that in May, with its C.M.P. on April 18·7, had a mean area during its disk passage of 2064 millionths. A third spot crossing the central meridian on June 18·4 was of nearly the same area, viz. 2100 millionths.

The mean daily area of faculae for each rotation in 1951 rose fairly steadily to maximum values in Rotations 1307–09.

In the following year (1952) there were no large excursions in the sunspot or facula values which for the year as a whole gave greatly reduced values as compared with the year 1951, viz. 64½ per cent for spots and 48½ per cent for faculae (see Table II).

TABLE III

No. of rotation	Rotation commenced U.T.	Spots north of the equator: Mean daily area	Spots north of the equator: Mean heliographic latitude	Spots south of the equator: Mean daily area	Spots south of the equator: Mean heliographic latitude	Mean latitude of entire spotted area	Mean distance from equator of all spots
	1950–52		°		°	°	°
1301	Dec. 9·74	268	14·94	73	12·10	+9·13	14·33
1302	Jan. 6·07	671	9·17	240	10·56	+3·98	9·54
1303	Feb. 2·41	482	10·31	74	11·33	+7·43	10·44
1304	Mar. 1·75	753	10·65	134	9·07	+7·66	10·41
1305	Mar. 29·06	1183	12·41	266	9·79	+8·34	11·93
1306	Apr. 25·33	2350	13·14	535	12·90	+8·31	13·10
1307	May 22·56	1660	13·37	1064	13·37	+2·92	13·37
1308	June 18·76	302	11·68	1084	10·97	−6·04	11·13
1309	July 15·96	239	7·82	503	8·32	−3·11	8·16
1310	Aug. 12·18	236	9·52	284	10·96	−1·65	10·31
1311	Sept. 8·43	729	10·64	223	6·25	+6·68	9·62
1312	Oct. 5·70	234	10·52	574	9·03	−3·37	9·46
1313	Nov. 1·99	282	13·62	382	9·75	+0·17	11·39
1314	Nov. 29·30	549	8·59	65	9·79	+6·64	8·72
1315	Dec. 26·63	543	5·66	23	12·61	+4·90	5·95
1316	Jan. 22·96	35	14·36	287	11·13	−8·38	11·48
1317	Feb. 19·30	20	15·45	112	11·56	−7·38	12·16
1318	Mar. 17·63	164	5·37	116	5·66	+0·81	5·49
1319	Apr. 13·92	75	10·55	254	7·53	−3·42	8·22
1320	May 11·16	10	10·48	184	6·28	−5·43	6·49
1321	June 7·37	60	15·67	462	11·00	−7·93	11·54
1322	July 4·57	120	10·40	519	5·07	−2·17	6·07
1323	July 31·78	335	10·50	207	9·47	+2·87	10·11
1324	Aug. 28·01	209	5·81	301	6·29	−1·34	6·10
1325	Sept. 24·28	221	9·57	59	6·34	+6·22	8·89
1326	Oct. 21·56	278	5·16	40	13·38	+2·80	6·21
1327	Nov. 17·87	528	6·09	61	10·30	+4·40	6·53

TABLE IV

Year	Days photographed	Spots north of the equator: Mean daily area	Spots north of the equator: Mean heliographic latitude	Spots south of the equator: Mean daily area	Spots south of the equator: Mean heliographic latitude	Mean latitude of entire spotted area	Mean distance from equator of all spots
			°		°	°	°
1944	366	42	19·00	83	22·81	−8·70	21·53
1944	366 Old Cycle	7	4·17	6	7·61	−1·14	5·72
	366 New Cycle	35	22·18	77	24·02	−9·63	23·45
1945	365	121	20·13	309	20·26	−8·92	20·22
1946	365	1127	20·74	690	18·79	+5·73	20·00
1947	365	992	16·58	1645	17·86	−4·91	17·38
1948	366	936	14·92	1041	13·53	−0·06	14·19
1949	365	1178	14·30	951	12·14	+2·49	13·33
1950	365	771	13·62	452	13·05	+3·77	13·41
1951	365	730	11·62	406	10·78	+3·62	11·32
1952	366	195	7·60	208	8·37	−0·64	8·00

The ratio of mean corrected areas of faculae/sunspots for 1951 is 1·21 and for 1952, 1·76. (See comments, *Monthly Notices*, **112**, 572, 1952.)

For other characteristics of the years 1951 and 1952 see *Monthly Notices*, **112**, 332, 1952, and **113**, 382, 1953.

(2) There were two days without spots in 1951 and 24 days in 1952.

(3) The mean weighted latitude of all spots in 1951 (Table IV) crept 2°·1 nearer the equator as compared with 1950. A further decrease of 3°·3 followed in 1952. The latitudes of the three giant spots of 1951 in order of date were +12°, +13° and −12°.

The northern hemisphere in 1951 had much the greater mean spotted area but this was largely due to the great spot in May which itself contributed 130 units to the mean for the year.

(4) The number and distribution, northern and southern hemispheres, of spot groups of (*a*) two days' duration or longer; (*b*) one day only, are as follows:

	1951		1952	
	(*a*)	(*b*)	(*a*)	(*b*)
Northern spots	142	39	56	26
Southern spots	115	29	73	20
Total	257	68	129	46

The range in latitude for the longer-lived spots in 1951 was from 1° to 25°. In 1952 the range was from 1° to 23°. The latitudes of the 1-day spots ranged from 2° to 26° in 1951 and from 2° to 22° in 1952.

An appended table gives the mean daily areas of sunspots and of faculae (corrected for foreshortening and expressed in millionths of the Sun's hemisphere) for each calendar month of the years 1951 and 1952.

	1951		1952	
Month	Spots	Faculae	Spots	Faculae
Jan.	746	1005	464	1034
Feb.	627	1173	305	774
Mar.	845	1210	142	639
Apr.	1600	1347	354	782
May	2899	1422	257	703
June	2477	1628	393	800
July	780	1942	654	906
Aug.	664	1534	689	768
Sept.	960	1548	307	720
Oct.	757	1427	339	518
Nov.	666	1205	455	421
Dec.	602	1091	477	470

Royal Greenwich Observatory,
Herstmonceux Castle,
Sussex:

1954 *July* 15.

STELLAR PARALLAXES DETERMINED PHOTOGRAPHICALLY AT THE CAPE OBSERVATORY (NINETEENTH LIST)

Royal Observatory, Cape of Good Hope

(Communicated by H.M. Astronomer)

(Received 1954 October 4)

This list is in the same form as the previous lists beginning in *M.N.*, **89**, 497, 1929.

The units in the last five columns are 0″·001. Two values of the proper motion in R.A. are given. The first (as also the proper motion in Dec.) is derived from meridian observations or other sources; the second is the relative value obtained from the parallax plates. The two values of probable error entered in the last column refer respectively to the parallax and to the photographic proper motion in R.A.

Nearly one-half of the stars in the present list are faint stars with a proper motion exceeding 0″·5 annually, given by Luyten in Vol. III, No. 1 of the *Publications of the Astronomical Observatory of the University of Minnesota*. Approximately one-third are stars selected from the *General Catalogue* or from the Cape Astrographic Zone as having an annual proper motion in excess of 0″·2. A few stars of considerably smaller proper motion—relatively bright stars of early and late spectral types—are also included, but none of these has a noteworthy parallax. The remainder of the list includes stars of interest derived from various sources, particularly Vyssotsky, *Ap. J.*, **97**, 381 and **104**, 234; while three faint stars, Nos. 1729, 1752 and 1792 appear on account of their relative proximity to Nos. 1730, 1753 and 1791 respectively, and the consequent original uncertainty as to the identity of the proper-motion star in each case.

Where possible, the magnitudes given are taken from the Henry Draper Catalogue; otherwise these are generally as given by the authority quoted for the proper motion.

Nine of the stars have parallaxes exceeding 0″·1. Of these, six are stars given by Luyten. The other three are BD + 4°4048 (No. 1773) and BD + 1°4774 (No. 1799)—two of Vyssotsky's dwarf M stars—and CoD −32°16135 (No. 1778), a star with only moderately large proper motion.

No.	Name and D.M. No.	Mag. Vis. Phot.	Type	R.A., Dec. (1900·0)	Proper Motion R.A.	Proper Motion Dec.	P.E. Unit Weight	Parallax	P.E.
				h m s					
1701	LPM 6	...	m	0 03 53	+ 660	+130	±21	+ 83	± 8
	−27° 16	12·0		−27° 41′·0	+ 692				± 4
1702	GC 452	6·44	Go	0 17 44	+ 388	+ 66	±27	+ 48	± 9
	9 Ceti	7·00		−12° 46′·0	+ 407				± 3
1703	LPM 26	...	m	0 27 36	+ 560	−100	±24	+ 21	± 7
	−63° 51	11·1		−63° 38′·3	+ 506				± 4
1704	LPM 29	9·4	G5	0 30 21	+ 920	−580	±26	+ 59	± 9
	−64° 51	10·1		−64° 13′·7	+ 868				± 5
1705	GC 721	8·58	G5	0 31 16	+ 372	−142	±23	+ 74	± 7
	−49° 138	9·2		−49° 40′·5	+ 378				± 2

No.	Name and D.M. No.	Mag. Vis. Phot.	Type	R.A., Dec. (1900·0)	Proper Motion R.A.	Proper Motion Dec.	P.E. Unit Weight	Parallax	P.E.
				h m s					
1706	GC 865	2·24	Ko	0 38 34	+ 231	+ 40	±25	+ 44	± 8
	β Ceti	3·24		−18° 32′·1	+ 221				± 3
707	GC 922	5·62	Ko	0 41 14	+ 198	− 1	±29	+ 29	±10
	−23° 293	6·9		−23° 04′·1	+ 184				± 3
1708	LPM 53	...	K5	0 56 57	− 200	−480	±31	+ 52	± 9
	−10° 216	11·2		−10° 24′·7	− 213				± 4
1709	GC 1296	6·86	Ma	0 59 56	+ 70	+ 20	±47	+ 6	±15
	−48° 259	8·6		−48° 28′·6	+ 72				± 8
1710	LPM 81	8·2	F8	1 38 20	+ 310	−480	±19	+ 20	± 6
	−68° 77	8·7		−68° 10′·2	+ 332				± 2
1711	GC 7127	8·0	G5	5 37 22	+ 220	−105	±25	+ 77	± 7
	−15° 1126	8·8		−15° 40′·6	+ 231				± 4
1712	LPM 248	...	M5	6 54 56	−1134	−119	±24	+112	± 6
	−44° 3045	12·4		−44° 09′·2	−1144				± 1
1713	GC 9264	6·70	G5	6 58 50	− 175	+249	±29	+ 59	± 8
	−61° 754	8·3		−61° 12′·0	− 171				± 4
1714	GC 9280	5·08	K2	7 00 01	− 38	+236	±22	+ 48	± 5
	−67° 686	6·6		−67° 46′·7	− 29				± 3
1715	LPM 257	...	K5	7 12 15	− 290	+590	±21	+ 46	± 6
	−63° 703	11·8		−63° 11′·2	− 238				± 4
1716	FS 3446	...	Ko	7 46 34	− 91	+116	±31	+ 11	± 8
	−44° 3764	9·9		−44° 20′·9	− 78				± 4
1717	GC 11306	7·6	G5	8 12 48	− 72	−233	±32	+ 4	± 9
	−1° 2005	8·4		−01° 29′·3	− 64				± 7
1718	GC 11398	8·89	G5	8 19 07	+ 79	+235	±22	+ 21	± 6
	−68° 771	8·8		−68° 40′·9	+ 90				± 3
1719	GC 11837	6·73	Go	8 32 57	− 277	+ 27	±23	+ 39	± 7
	−6° 2664	7·29		−06° 27′·5	− 285				± 4
1720	GC 11906	7·04	Mb	8 35 18	+ 9	−160	±26	− 11	± 7
	−16° 2541	8·39		−16° 56′·7	0				± 5
1721	GC 12307	6·01	Go	8 49 22	− 418	+ 27	±24	+ 95	± 6
	−4° 2490	6·57		−05° 03′·3	− 402				± 3
1722	GC 12554	7·41	Go	9 01 23	+ 40	−166	±30	+ 8	± 7
	−52° 1904	8·4		−52° 06′·6	+ 7				± 4
1723	GC 12996	6·45	Mb	9 21 22	− 60	+ 40	±28	− 1	± 8
	−43° 5262	7·8		−43° 32′·8	− 31				± 5
1724	GC 13043	4·94	Ko	9 22 44	+ 181	−164	±29	+ 29	± 9
	−21° 2802	6·5		−21° 54′·3	+ 182				± 3
1725	GC 13168	7·5	Ko	9 27 36	− 269	+ 28	±27	+ 77	± 8
	−10° 2857	8·5		−10° 44′·6	− 218				± 5
1726	LPM 322	...	k	9 34 37	+ 410	−350	±28	+ 14	± 8
	−38° 5760	12·6		−38° 55′·4	+ 416				± 5

No.	Name and D.M. No.	Mag. Vis. Phot.	Type	R.A., Dec. (1900·0)	Proper Motion R.A.	Proper Motion Dec.	P.E. Unit Weight	Parallax	P.E.
				h m s					
1727	LPM 336	...	m	10 06 54	+ 480	−640	±22	+118	± 7
		12·2		−02° 10′·0	+ 528				± 4
1728	LPM 341	...	k	10 11 53	− 400	−600	±20	+106	± 6
		12·4		−11° 26′·8	− 388				± 3
1729	N.p. No. 1730	...	...	10 18 44	...	...	±22	− 15	± 7
		12		−59° 37′·9	+ 8				± 3
1730p	LPM 345	...	m	10 18 48	+ 370	−440	±17	+ 58	± 6
		11·5		−59° 39′·0	+ 357				± 3
1730f	LPM 346	...	m	10 18 50	+ 370	−440	±29	+ 57	±12
		13·5		−59° 38′·9	+ 357				± 6
	Mean							+ 58	± 5
					+ 357				± 3
1731	LPM 361	...	g5	10 47 33	− 240	−750	±21	+ 45	± 6
	−1° 2457	11·0		−01° 33′·5	− 378				± 4
1732	LPM 366	...	K2	11 02 28	+ 350	−360	±26	+ 14	± 7
	−30° 8970	11·4		−30° 16′·2	+ 331				± 5
1733	LPM 368	...	...	11 04 44	− 790	−470	±23	+106	± 7
	−23° 9765	11·8		−24° 02′·6	− 769				± 4
1734	LPM 386	...	m	11 22 52	+ 510	−820	±32	+ 45	± 9
		13·0		−08° 36′·7	+ 565				± 5
1735	GC 15886	5·63	Ma	11 30 24	− 79	− 16	±32	+ 5	±11
	−46° 7199	7·1		−46° 49′·2	− 78				± 9
1736	ZC 9655	8·3	Ma	11 30 47	− 54	+ 5	±35	+ 34	±12
	−46° 7203	9·6		−46° 36′·9	− 24				± 7
1737	LPM 398	...	m	11 41 35	+ 760	−780	±24	+ 79	± 7
		12·6		−13° 26′·0	+ 727				± 3
1738	LPM 402	11·9	M4+	11 48 10	− 150	−520	±17	+ 79	± 5
		13·8		−06° 48′·3	− 157				± 2
1739	Ross 925	...	...	12 02 09	− 490	−220	±22	+ 10	± 6
	− 4° 3208	9·4		−05° 10′·3	− 246				± 2
1740	GC 16584	2·88	B3p	12 03 10	− 37	− 20	±23	+ 23	± 6
	δ Centauri	3·05		−50° 09′·9	− 24				± 3
1741	Ross 931	9·91	Ko	12 07 18	− 250	−260	±28	+ 36	± 9
	−5° 3450	10·91		−05° 47′·7	− 221				± 4
1742	GC 16724	3·08	B3	12 09 50	− 37	− 17	±25	0	± 7
	δ Crucis	2·91		−58° 11′·6	− 13				± 5
1743	LPM 430	...	G5	12 23 11	− 500	− 30	±26	+ 34	± 7
	−16° 3469	10·5		−16° 21′·5	− 544				± 2
1744	Ross 974	...	...	12 56 53	− 10	−570	±17	+ 75	± 6
		12		−01° 32′·8	+ 34				± 2
1745	LPM 475	...	m	13 20 19	− 510	−100	±23	+116	± 6
	−27° 9225	12·0		−27° 51′·1	− 493				± 3

No.	Name and D.M. No.	Mag. Vis. Phot.	Type	R.A., Dec. (1900·0)	Proper Motion R.A.	Proper Motion Dec.	P.E. Unit Weight	Parallax	P.E.
				h m s					
1746	LPM 477	...	k	13 22 26	− 480	−120	±28	+ 10	± 7
	−27° 9236	11·3		−27° 45′·9	− 472				± 3
1747	LPM 478	...	M4	13 23 11	+ 160	−470	±21	+ 60	± 6
	Ross 486	11·8		−01° 50′·1	+ 161				± 2
1748	FS 11167	...	...	13 29 33	− 358	+ 11	±25	− 1	± 7
	CAZ −47° 951	13·6		−46° 11′·2	− 341				± 3
1749	FS 11346	...	G5	13 39 03	− 223	+ 30	±27	+ 5	± 7
	−47° 8579	10·9		−47° 34′·0	− 209				± 4
1750	GC 18666	4·40	Mb	13 43 39	− 46	− 55	±26	+ 4	± 7
	−33° 9358	6·3		−33° 57′·1	− 48				± 6
1751	LPM 509	...	m	14 03 41	− 470	−230	±21	+ 37	± 6
	−30° 11195	12·4		−30° 27′·4	− 472				± 3
1752	S.p. No. 1753	...	...	14 13 51	...	...	±28	+ 38	±11
		13·5		−06° 50′·2	− 10				± 1
1753	LPM 519	...	M4	14 13 55	−1000	−930	±38	+ 62	±12
	Wolf 534	14·5		−06° 50′·0	−1114				± 3
1754	LPM 521	12·7	M5	14 14 50	− 710	−820	±21	+ 88	± 8
	Ci 20 851	14·4		−09° 08′·8	− 617				± 2
1755	ZC 12226	8·1	G5	14 15 04	− 283	− 31	±20	+ 16	± 5
	−42° 9252	8·7		−43° 01′·7	− 269				± 2
1756	ZC 12336	9·1	Go	14 22 35	− 267	+146	±25	+ 16	± 7
	−46° 9347	9·5		−46° 17′·8	− 153				± 3
1757	LPM 530	...	m	14 26 50	− 440	−330	±21	+ 27	± 6
	−27° 9894	11.7		−27° 48′·6	− 446				± 3
1758	LPM 554	...	k	15 03 42	− 450	−250	±23	+ 12	± 7
		12·2		−19° 35′·0	− 490				± 4
1759	LPM 557	...	g	15 07 25	− 700	− 90	±25	+ 18	± 7
		11·8		−21° 35′·9	− 706				± 4
1760p	GC 20537	7·95	G5	15 11 32	− 94	−238	±24	+ 42	± 7
	−7° 3992 S.p.	8·73		−07° 54′·6	− 70				± 3
1760f	−7° 3992 N.f.	9·4	G4	15 11 33			±36	− 15	±14
		...		−07° 54′·5	− 85				± 6
	Mean							+ 31	± 6
					− 73				± 3
1761	LPM 569	...	Ko	15 20 06	− 780	− 30	±30	− 11	± 7
	−26° 10870	10·2		−26° 21′·2	− 809				± 4
1762	LPM 595	...	Go	16 10 23	− 500	−420	±23	+ 35	± 7
	−70° 2196	11·0		−71° 02′·2	− 476				± 4
1763	LPM 601	...	m	16 17 10	− 510	−730	±22	+ 50	± 7
		13·4		−46° 28′·9	− 494				± 3
1764	LPM 612	...	f–g	16 30 38	− 560	−150	±21	+ 24	± 5
	−14° 4454	12·0		−14° 57′·6	− 557				± 3

No.	Name and D.M. No.	Mag. Vis. Phot.	Type	R.A., Dec. (1900·0)	Proper Motion R.A.	Proper Motion Dec.	P.E. Unit Weight	Parallax	P.E.
				h m s					
1765	GC 23708	2·97	B3p	17 24 07	− 32	− 77	±27	+ 4	± 7
	α Arae	2·80		−49° 47′·8	− 28				± 3
1766	FS 17263	10·0	Ko	17 38 33	− 231	−209	±24	− 8	± 6
	−40° 11804	...		−40° 45′·3	− 206				± 2
1767	− 1° 3474	8·8	Mo	18 14 39	− 26	+ 68	±22	+ 89	± 6
		...		−01° 58′·8	+ 8				± 3
1768	LPM 676	...	k	18 18 27	+ 290	−420	±21	+ 35	± 6
		12·4		−05° 11′·5	+ 311				± 4
1769	FS 18061	...	K7	18 19 45	− 122	+150	±18	+ 21	± 5
	−51° 11572	10·8		−51° 07′·3	− 119				± 2
1770	GC 25488	5·36	Mb	18 32 24	− 36	− 51	±30	+ 4	± 8
	−43° 12699	6·7		−43° 16′·3	− 46				± 6
1771	Ross 142	10·0	M2	18 45 01	− 120	−440	±22	+ 58	± 7
	Ci 20 1111	...		+02° 59′·2	− 169				± 5
1772	ZC 18044	9·9	Go	19 08 22	+ 187	−194	±26	+ 22	± 7
	−50° 12397	10·0		−50° 21′·7	+ 175				± 2
1773	Wolf 1055	9·5	M2	19 12 03	− 590	−1330	±19	+208	± 5
	+ 4° 4048	10·9		+05° 01′·8	− 602				± 2
1774p	FS 18978	...	G5	19 56 57	− 24	−185	±17	+ 7	± 4
	−46° 13364	11·0		−46° 04′·4	− 39				± 2
1774f	FS 18979	...	...	19 56 57	− 22	−163	±16	+ 13	± 4
	−46° 13365	11·4		−46° 04′·0	− 39				± 2
	Mean							+ 10	± 3
					− 39				± 1
1775	LPM 724	...	k	20 01 19	− 380	−560	±20	+ 19	± 6
		12·7		−19° 41′·6	− 426				± 4
1776	LPM 736	...	k	20 15 58	+ 200	−490	±25	+ 27	± 7
		12·5		−06° 44′·3	+ 192				± 4
1777	GC 28425	6·26	Ko	20 20 24	− 244	−114	±29	+ 27	± 7
	−37° 13741	7·4		−37° 43′·6	− 260				± 3
1778	−32° 16135	...	M	20 35 36	+ 269	−329	±21	+130	± 5
		11·2		−32° 46′·9	+ 266				± 2
1779	ZC 19181	9·1	Go	20 59 54	+ 12	−235	±37	− 13	± 8
	−46° 13835	9·2		−46° 40′·3	+ 19				± 4
1780	GC 29782	6·90	G5	21 11 54	+ 224	+ 27	±24	+ 43	± 6
	−43° 14464	6·9		−43° 45′·3	+ 221				± 2
1781	FS 19554	...	K7	21 27 59	+ 175	− 96	±27	+ 12	± 8
	CAZ −51° 61	12·6		−50° 00′·1	+ 169				± 3
1782	FS 19595	...	...	21 35 07	− 48	−238	±25	+ 26	± 6
	CAZ −48° 346	12·3		−47° 28′·9	− 108				± 2
1783	LPM 806	...	m	21 55 43	+ 620	− 80	±22	+ 70	± 6
		12·0		−70° 24′·3	+ 610				± 2

No.	Name and D.M. No.	Mag. Vis. Phot.	Type	R.A., Dec. (1900·0)	Proper Motion R.A.	Proper Motion Dec.	P.E. Unit Weight	Parallax	P.E.
				h m s					
1784	LPM 808	...	m	21 56 22	+ 920	+ 50	±13	+ 78	± 4
		13·0		−19° 58′·0	+ 924				± 2
1785	LPM 817	...	k	22 09 07	− 80	−620	±19	+ 62	± 6
	Wolf 1332	12·0		−09° 13′·4	− 106				± 3
1786	LPM 831	...	m	22 20 36	− 470	−600	±21	+ 67	± 7
		13·6		−21° 19′·7	− 494				± 3
1787	FS 19954	...	K	22 25 27	+ 2	−270	±24	− 4	± 7
	CAZ −51° 35	12·2		−51° 44′·1	− 22				± 2
1788	LPM 837	12·3	M6+	22 32 56	+2350	+2270	±31	+329	±10
		14·3		−15° 53′·3	+2335				± 4
1789	LPM 840	...	m	22 42 32	+ 740	−300	±26	+ 54	± 8
		12·8		−37° 18′·6	+ 758				± 4
1790	GC 31913	6·32	G5	22 47 43	+ 197	− 78	±23	+ 56	± 6
	−49° 13988	6·7		−49° 07′·7	+ 230				± 2
1791	LPM 847	...	g	22 55 31	+ 580	−470	±22	+ 22	± 7
		13·2		−55° 02′·0	+ 453				± 2
1792	S.f. No. 1791	...	...	22 55 32	...	...	±23	+ 19	± 7
		13		−55° 02′·2	− 20				± 2
1793	LPM 854	...	k–m	23 04 48	+ 690	0	±18	+ 88	± 5
	−26° 16501	12·2		−26° 28′·5	+ 698				± 2
1794p	LPM 859	8·3	F5	23 08 52	+ 551	− 35	±29	+ 36	± 6
	−9° 6149	8·9		−09° 28′·1	+ 558				± 3
1794f	LPM 860	8·8	G2	23 08 53	+ 552	− 7	±20	+ 11	± 5
	−9° 6150	9·4		−09° 28·5	+ 553				± 2
	Mean							+ 21	± 4
					+ 554				± 2
1795	FS 20274	...	...	23 11 15	0	−263	±26	+ 45	± 9
	CAZ −42° 96	13·3		−41° 19′·7	− 17				± 3
1796	−2° 5958	...	M2	23 21 55	+ 385	+249	±26	+ 51	± 7
		11·1		−01° 50′·1	+ 370				± 3
1797	LPM 875	...	M4	23 29 03	−1060	−920	±22	+ 97	± 7
	Ci 20 1433	12·2		−00° 20′·7	− 994				± 3
1798p	LPM 881	...	m	23 37 50	+1270	−2200	±29	+ 42	±10
	−24° 17814	12·9		−24° 39′·4	+1282				± 4
1798f	LPM 882	...	m	23 37 53	+1270	−2200	±31	+ 46	±10
		13·4		−24° 40′·8	+1282				± 4
	Mean							+ 44	± 7
					+1282				± 3
1799	GC 33053	8·7	M2	23 43 59	+ 980	−962	±29	+218	± 7
	+1° 4774	...		+01° 52′·3	+ 971				± 3
1800	LPM 895	...	m	23 50 35	− 440	−340	±25	+ 84	± 8
	−6° 6318	12·5		−06° 41′·5	− 525				± 4

NOTES

1703. This star was originally selected as a reference star for β Tucanae (No. 1401).

1705. This star has common proper motion with No. 4.

1712. A difficult double, of which the mass was measured. The observations extend over 18 years.

1759. This is CPD -21° 5912.

1760. This is ADS 9564.

1778. This star, which is itself a close double, has common proper motion with No. 1189.

CONTENTS

PAGE

Meeting of 1954 May 14:

Fellows elected ... 501

Presents announced ... 501

Presentation of the Gold Medal ... 501

Meeting of 1954 October 8:

Fellows elected ... 502

Presents announced ... 502

M. J. Smyth, Photoelectric investigations of solar corpuscular radiation. II ... 503

R. v. d. R. Woolley, Relaxation of stellar velocities ... 514

R. O. Redman and Z. Suemoto, Temperature and turbulence in the chromosphere ... 524

R. J. Bray, The apparatus function of the Oxford solar spectroscope ... 540

P. A. Sweet, Field reversal in magnetic variable stars ... 549

Anne B. Underhill, On the development of the Fe I chromospheric lines during the 1951 eclipse of 31 Cygni ... 558

M. W. Ovenden, Two-colour photoelectric photometry of GO Cygni ... 569

V. C. Reddish, Colour–magnitude arrays in the clusters Tombaugh 5, NGC 7789, NGC 1528 and NGC 2682 ... 583

T. R. Tannahill, Star-streaming from the proper motions of the A-type stars of the Boss *General Catalogue* ... 593

W. D. Heintz, Orbital elements of four visual binaries ... 600

Royal Greenwich Observatory, Mean daily areas and heliographic latitudes of sunspots in the years 1951 and 1952 ... 606

Royal Observatory, Cape of Good Hope, Stellar parallaxes determined photographically at the Cape Observatory (nineteenth list) ... 610

Printed in London by Taylor & Francis, Ltd., 1955 *April*